Biomechanics of human ascending aorta and aneurysm rupture risk assessment

Siyu Lin

THESE DE DOCTORAT DE L'ETABLISSEMENT UNIVERSITE BOURGOGNE FRANCHE-COMTE

PREPAREE au Laboratoire ImViA

Ecole doctorale n°37

Sciences Pour l'Ingénieur et Microtechniques (SPIM)

Doctorat de Instrumentation, Informatique de l'image

Par

LIN Siyu

Biomechanics of Human Ascending Aorta and Aneurysm Rupture Risk Assessment

Thèse présentée et soutenue à Dijon, le 7 Décembre 2021

Composition du Jury :

Pr. AVRIL Stéphane	Directeur de recherche, Université Claude-Bernard Lyon-I	Président
Pr. DEPLANO Valérie	Directeur de recherche, Université d'Aix-Marseille	Rapporteur
Pr. VERHOYE Jean-philippe	PU-PH, Université de Rennes	Rapporteur
Dr. ROCHETTE Michel	Directeur de recherche, ANSYS, Inc.	Examinateur
Dr. LALANDE Alain	MCU-PH, Université de Bourgogne Franche-Comté	Examinateur
Pr. BOUCHOT Olivier	PU-PH, Université de Bourgogne Franche-Comté	Directeur de thèse

Titre : Biomécanique de l'aorte ascendante humaine et évaluation du risque de rupture d'anévrisme

Mots clés: propriétés biomécaniques, test d'étirement biaxiale, anévrisme de l'aorte ascendante, dissection aortique, valve aortique quadricuspide, impresson 3D de l'aorte

Résumé: Les anévrismes de l'aorte ascendante et les dissections aortiques sont des maladies cardiovasculaires potentiellement mortelles. Les critères majeurs pour décider d'une intervention chirurgicale d'un anévrisme de l'aorte ascendante est le diamètre maximal ou le taux annuel d'evolution de l'anévrisme. La mortalité de la dissection aortique non traitée peut être de 21% à 74%, selon le delai de l'admission à l'hôpital.
L'objectif de nos travaux est de caractériser les propriétés biomécaniques de l'aorte ascendante et de proposer une approche spécifique à chaque patient pour évaluer les risques de rupture. L'objectif de notre travail est doc multiple.
D'une part, des tests de traction biaxiaux ont été réalisés sur des prélèvements d'anévrisme de l'aorte ascendante obtenus au cours de remplacement chirurgical de l'aorte ascendante. L'effet de différents paramètres cliniques et de facteurs de risque a été étudié. Nous avons montré que le sexe, l'âge, le diamètre et les pathologies associées à la valve aortique ont les impacts majeurs sur la rigidité d'anévrisme de l'aorte ascendante. D'autre part, onze échantillons de dissection aortique de type A ont été collectés. Nous avons confirmé que l'adventice présente une rigidité significativement supérieure par rapport à la couche intimo-médiale. De plus, on a montré qu'un cas d'anévrisme de l'aorte ascendante associé à une valve aortique quadricuspide possède des propriétés biomécaniques plus similaires à celles d'anévrismes de l'aorte ascendante associé à une valve aortique bicuspide comparé à un valve aortique tricuspide. Afin de réaliser des impressions 3D de l'aorte pour des études de flux 4D en Imagerie par Résonance Magnétique (IRM), trois matériaux imprimables en trois dimensions ont été testés pour les comparer avec une paroi de l'aorte non-dilatée. Les propriétés biomécaniques du 50 SH (shore stiffness) RDG450+TangoPlus sont les plus semblables à l'aorte non-dilatée.
Pour conclure, à partir de nos resultats sur une centaine de patients, le sexe, l'âge, le diamètre et les pathologies associées à la valve aortique sont les parametres clés de la rigidité de l'aorte.

Title: Biomechanics of human ascending aorta and aneurysm rupture risk assessment

Keywords: biomechanical properties, biaxial tensile test, ascending aortic aneurysm, aortic dissection, quadricuspid aortic valve, 3D printed aorta

Abstract: Ascending aortic aneurysms (AsAA) and aortic dissections are life-threatening cardiovascular diseases. The main criteria for determining surgical intervention of AsAA are the maximum diameter or the increasing annual rate of the aneurysm. The mortality of the untreated aortic dissection can be 21% to 74%, depending on the delay of hospital admission.
Our study aims to characterize the biomechanical properties of the ascending aorta and propose a patient-specific approach to assess the risks of rupture. The purpose of this PhD work is multifold.
On the one hand, biaxial tensile tests were performed on AsAA samples obtained from one hundred patients with surgery of AsAA. The impact on the different characteristics and risks was evaluated and cross-compared. We have shown that the risk factors of gender, age, diameter, and aortic valve disorders have a major impact on the stiffness of AsAA. On the other hand, eleven acute Type A aortic dissection samples were collected. We have confirmed that the adventitia shows a significant stiffness than the intimomedial layer. Meanwhile, a rare case of AsAA associated with the quadricuspid aortic valve displayed similar biomechanical properties to AsAA associated with the bicuspid aortic valve than with the tricuspid aortic valve. In order to make synthetic modeling from 3D printed aorta in 4D flow magnetic resonance imaging (MRI) study, three three-dimensional printable materials were tested to compare with an undilated aortic wall. The biomechanical properties of the 50 SH (shore stiffness) RGD450+TangoPlus is the most aorta-alike material.
To conclude, from our result from one hundred patients, gender, age, diameter, and aortic valve disorders are the key to aortic stiffness.

UBFC UNIVERSITE BOURGOGNE FRANCHE-COMTE
Université Bourgogne Franche-Comté
Bâtiment I3M, 64b rue Sully 21000
Dijon, France

What doesn't kill you, makes you stronger.

Friedrich Nietzsche

Acknowledgment

I would like to thank Pr. Olivier Bouchot, who first gave me the opportunity to work with him in my master internship, and then offered me the position as a Ph.D. candidate. He continually conveyed a spirit of adventure regarding research. He was the one showing a great model of hard work. Thanks to him, I became a braver and stronger person.

Secondly, I would give my great thanks to Dr. Alain Lalande. He helped me all the way, from small details to big decisions. It is my great pleasure to have Alain in the project. He is very patient, thoughtful, and professional. Officially, he was not my supervisor, but practically, he is and will always be my supervisor.

Next, I would like to thank my boyfriend, Dr. Andranik Petrosyan, who was supporting and helping me to go through the terrible moment during my Ph.D. He was the one who witness my tires millions of times on dark nights. And he was the one always saying: “It is not a big deal.”

Then, many thanks to my college, Diana Marin. She is not only a college but a very good friend of mine. I am appreciating the time we spend together, for good and also for bad.

Meanwhile, I would like to thank Serge Aho and Louis Legrand. They are the one who supported selflessly with their professional point of view in my Ph.D. program.

Many thanks to Ivan Porcherot and Catherine Vergely. They sincerely helped me during from the beginning of my arriving of “UFR science de sante”.

Also, thanks to my colleges in ImViA, and staff in CCVT, also the nurses in the OR.

I cannot ignore a very important person: Paul Michel Walker. However, he named his middle name as “perfect”, which might be the truth. Indeed, he brings the laugh and jokes in my daily lab life.

Finally, I also admire the support from my friends: Dr. Meiling Yue, Yuedi Fang, Dr. Tingting Wang, Fangmin Wang, and those whom I don’t have space to mention here. Their encouragement is the power to guide me to start my Ph.D. and to finalize it.

Last but not the least, thanks to my parents, they are the greatest parents in the world. I am thankful for their support and understanding that I couldn't go back to China for two years due to my work and the Covid-19.

CONTENTS

LIST OF FIGURES

LIST OF TABLES

GLOSSARY

3D = Three Dimensional
ACTA2 = Actin Alpha 2
AD = Aortic Dissection
AD-FD = Fully Dissected Aortic Dissection
AD-PD = Partially Dissected
AI = Aortic Insufficiency
ANT = Anterior
AR = Aortic Regurgitation
AS = Aortic Stenosis
AsAA = Ascending Aortic Aneurysms
AsAA-BAV = Ascending Aortic Aneurysm associated with Bicuspid Aortic Valve
AsAA-QAV = Ascending Aortic Aneurysm associated with Quadricuspid Aortic Valve
AsAA-TAV = Ascending Aortic Aneurysm associated with Tricuspid Aortic Valve
ASVD = Atherosclerotic Vascular Disease
ATA = Ascending Thoracic Aorta
AV = Aortic Valve
BAV = Bicuspid Aortic Valve
BMI = Body Mass Index
CAD = Coronary Artery Disease
CDC = Centers for Disease Control and Prevention
CHU = University Hospital
CIR = Circumferential
CT = Computed Tomography
DTA = Descending Thoracic Aorta
DYS = Dyslipidemia
ESC = European Society of Cardiology
FDM = Fused Deposition Modeling
HTA = Arterial Hypertension
HU = Hounsfield Unit
LAT = Lateral

Layer A = Adventitia Aortic Wall Layer
Layer MI = Intimomedial Aortic Wall Layer
LCC = Left Coronary Cusp
LON = Longitudinal
MED = Medial
MHY11 = Myosin Heavy Chain 11
MRI = Magnetic Resonance Imaging
NCC = Non-Coronary Cusp
PA = Pulmonary Artery
PBS = Phosphate-Buffered
POST = Posterior
QAV = Quadricuspid Aortic Valve
RCC = Right Coronary Cusp
SD = Standard Deviation
SH = Shore Hardness
SLA = Selective Laser Assimilation
SLS = Selective Laser Sintering
STL = Standard Tessellation Language
TES = Thermoplastic Polystyrene.
TGF-B = Transforming Growth Factor Beta
TAV = Tricuspid Aortic Valve
TPA = Thermoplastic Polyamide
TPE = Thermoplastic Elastomers
TPU = Thermoplastic Polyurethane

Introduction

Ascending aortic aneurysm (AsAA) is a life-threatening cardiovascular disease. Over 90% of the cases are reported as asymptomatic.[1] The incidence of AsAA is between 5.6 to 10.4 cases per 100,000 per year[2]. An untreated AsAA can lead to an aortic rupture, with 26% of mortality[3]. Moreover, the surgical mortality of Stanford type A aortic dissection is as high as 18% to 25%[4]. The natural course of AsAA is the aortic dilation which can lead to tears of the aortic wall (dissection of the ascending aorta) or ruptures of the aneurysm. Both of the two complications are extremely serious because they carry a lethal risk, as high as 58%[5]. That is the main reason why it is essential to predict the risk of aortic or aortic dissection rupture and treated AsAA in time. Indeed, according to the European guidelines, the surgery of AsAA consists of the replacement of the aorta by a synthetic graft[6].

The surgical decision will be made primarily on the size of the aneurysm (generally larger than 55 mm), without taking into account other factors such as the symptomatic aneurysms, Marfan syndrome, aortic valve disorders, and the annual growth rate of the aorta, etc. In practice, it appears some difficulties in correctly assessing the risk of the rupture of the aneurysms. However, the risk of aortic dissection appears in 40% of cases for aorta with a diameter under 50 mm[7]. Other parameters influence fragility and the risk of dissection, such as atherosclerosis arterial hypertension, familial aortic aneurysms, connective tissue disorders (Marfan syndrome and Loyes Dietz syndrome)[8]. Therefore, it is necessary to understand the related characteristics of the aorta in the field of biomechanics, which can help improve the standard to some extent. Studies have been published in the uniaxial tensile test[9–13], budge inflation test[14], or biaxial tensile test[15]. However, due to different methods, the limited number of populations, and the heterogeneous pathology, there is no existing complete research on this subject. The main objective of our study is to use the biaxial tensile test to characterize the biomechanical properties of the human aorta on a relatively large population. Moreover, specify the influence of them on different pathology and risks. In the period of this thesis, we included more than one hundred aortic samples. All the samples in our study were obtained from the University Hospital of Dijon, France. The research was approved with the ethical agreement (2018-A02010-55) by French law.

In addition, another prospective project is the simulation of aortic movement controlled by the industrial pump. To achieve that, we are looking for a three-dimension (3D) printable material which can represent the undilated human aorta. It is expected that the 3D printed aorta can have similar biomechanical behavior as an undilated human aorta with a personalized geometry.

Chapter 1 presents the clinical background and the physiologic structure of ascending aortic aneurysms and aortic dissection covered in this thesis. Chapter 2 is about the current biomechanical research on the aorta as well as the main experimental methods used in this thesis. Chapter 3 is the key part of this thesis, representing the biomechanical studies based on one hundred AsAA samples collected from December 2018 till June 2021. This chapter mainly elaborates on the influence of more than ten kinds of different clinical risks and pathological conditions. Chapter 4 presents an extremely rare case; AsAA associated with the quadricuspid aortic valve. The aim is to compare the effectiveness of the quadricuspid aortic valve. Chapter 5 presents the impact of biomechanics on eleven ascending aortic samples of acute Stanford type A aortic dissection. This chapter will compare the difference between the aortic wall layers and between some specific aortic quadrants. Chapter 6 is a summary of an undergoing project on the 3D printed material. This part aims to describe the most similar 3D printed material identical to healthy human aorta so far.

Chapter 1 - Clinical context

This chapter mainly focuses on clinical background and the physiologic structure of the cardiovascular system, ascending aortic aneurysms, aortic valve disorder, and aortic dissection covered in this thesis.

1.1 Cardiovascular system

The heart and blood vessels form the network of blood transportation called the cardiovascular system. The cardiovascular system has two pathways: systemic circulation and pulmonary circulation. Systemic circulation (Fig. 1-1): blood is pumped out of the left ventricle through the aorta and its branches to the capillaries. Then it exchanges substances and gases with surrounding tissues and cells, passes through all levels of veins. Finally, blood returns to the right atrium through the superior and inferior vena cava and coronary sinus, from where the pulmonary circulation starts. The pulmonary circulation: blood leaves from the right ventricle through the pulmonary trunk and its branches to the alveolar capillaries for gas exchange (O_2 to CO_2). Then blood transfers through the pulmonary vein into the left atrium. Systemic and pulmonary circulation occurs simultaneously. The systemic circulation has a long-distance and wide range. It nourishes all body parts with arterial blood and carries the metabolites and carbon dioxide from all parts of the body back to the heart.

Each contraction of the heart pumps blood to the systemic circulation and to the pulmonary circulation. After the contraction, blood exists from the heart, creating a certain pressure on the blood vessels. It is so-called systolic blood pressure. Normally, the systolic blood pressure is less than 120 mmHg. During cardiac relaxation, when the heart is at rest between two contractions, there is residual pressure in the blood vessels. It is so-called diastolic blood pressure. Normally the diastolic blood pressure is less than 80 mm Hg.

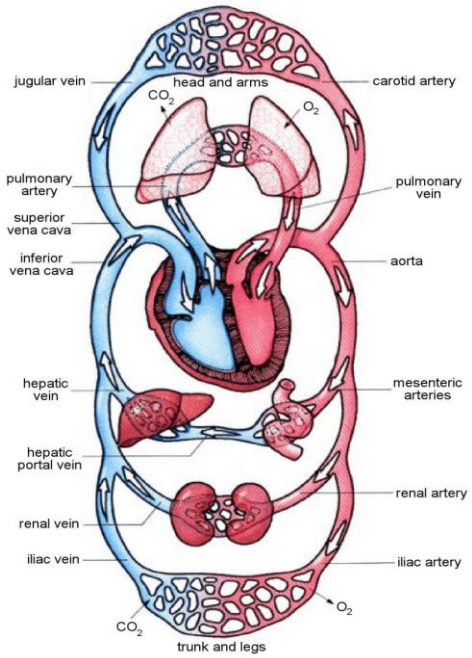

Figure 1-1. An overview of the cardiovascular system with the heart as the driving force. (From https://www.daviddarling.info/encyclopedia/C/circulatory_system.html, viewed 14.09.2021)

1.1.1 The heart and aortic valve

The heart is an organ mainly composed of cardiac muscle known as the "power pump" of the cardiovascular circulatory system (Fig. 1-2).

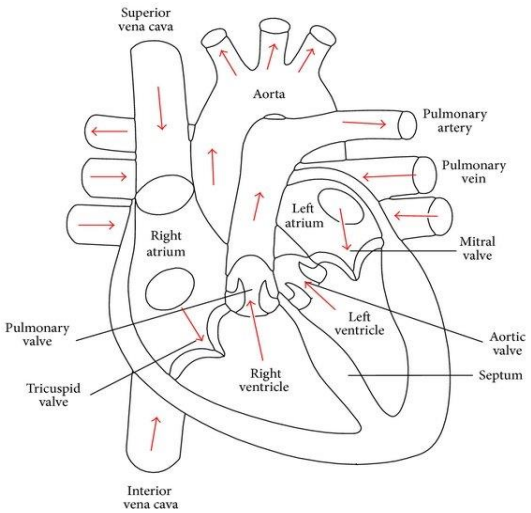

Figure 1-2. Sagittal section of the human heart. (From Sahu et al., 2015 [16])

Anatomically, the heart can be divided into two parts (right and left), separated by the septum, which forms a wall to separate the left and right heart. It is in the center of the chest, surrounded by lungs. The heart has four hollow chambers, divided into the upper

chambers (two atria) and the lower chambers (two ventricles). These two unilateral chambers are communicated by atrioventricular orifices where heart valves ensure that the blood keeps flowing in the one direction. The valve in the right atrioventricular orifice is the so-called tricuspid aortic valve (TAV) because of its three cusps: anterior, posterior, and septal. The valve in the left atrioventricular orifice has two leaflets and is called mitral: anterior and posterior. At the exits of each ventricle, there is a valve to assure the unilateral flow of the blood. The valve at the exit of the right ventricle is called the pulmonary valve, and at the left ventricle, the exit is called the aortic valve. They both have three leaflets. The deoxygenated blood and waste products are coming out through the pulmonary valve to the pulmonary artery, communicating the heart with the lungs (pulmonary circulation). The oxygenated blood flows through the four pulmonary veins into the left atrium. It then passes through the mitral valve into the left ventricle. Blood in the left ventricle is shot into the aorta passing through the aortic valve and the systemic circulation when the heart contracts.

1.1.1.1 Anatomy of the heart

The heart base can be identified after sectioning the aorta and pulmonary artery at the origins and after removing the atriums (Fig.1-3). The aortic and pulmonary valves are in the open position in Fig. 1-3, and mitral with tricuspid valves are in the closed position[17,18].

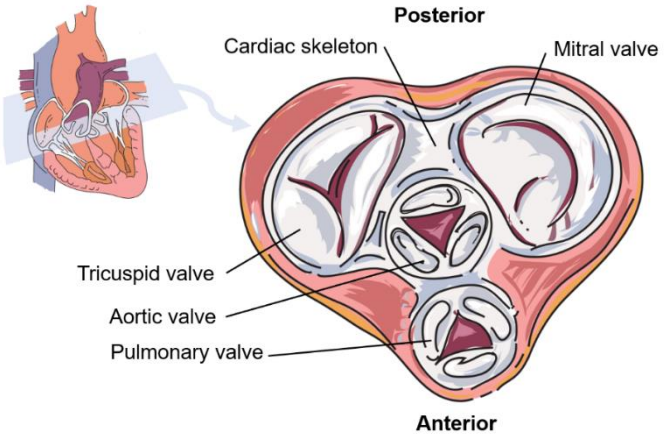

Figure 1-3. Schematic illustration of the transversal section of the heart. (https://med.libretexts.org/@go/page/22375, viewed 31.07.2021)

The pulmonary valve has three sigmoid valves, each presenting in the middle of its free edge, the Morgagni nodule. The tricuspid valve is located below and to the right of the aortic valve. The tricuspid orifice is circumscribed by the right coronary artery. The aortic valve has three leaves: the right below the origin of the right coronary artery, the left below the origin of the left coronary artery, and the posterior one. Below and to the left from the aorta, it is possible to observe the mitral orifice circumscribed by the

circumflex artery. The mitral valve has two leaflets: the anterior and posterior leaflets, separated by the anterior and posterior commissures.

At the junction of the three orifices, aortic, mitral, and tricuspid, and the three fibrous rings that constructing them, a thick fibrous nucleus is formed, the trigone (cardiac skeleton, Fig. 1-3) [19,20].

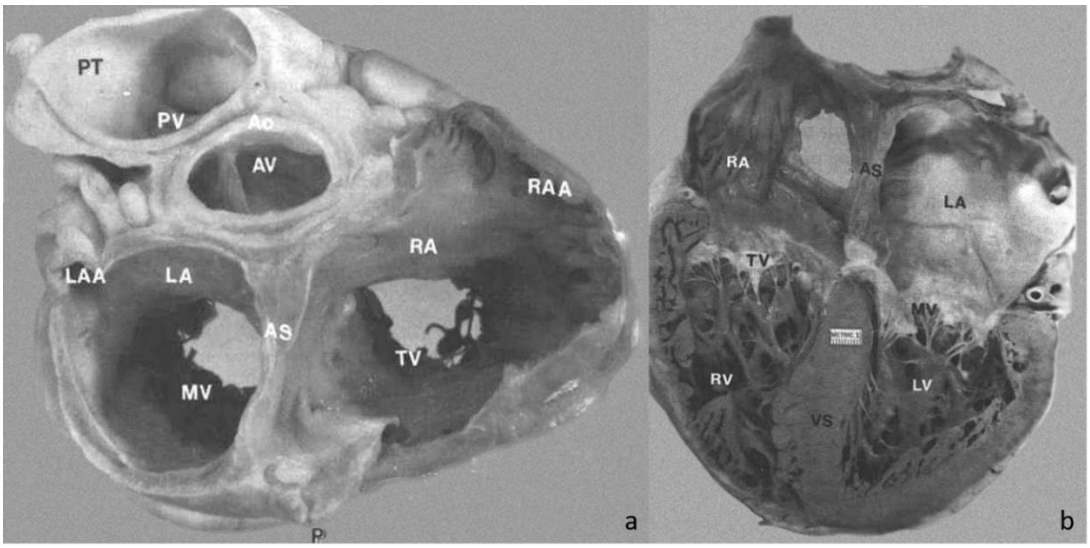

Figure 1-4. Anatomy of the heart. a) transversal cut of the heart, b) sagittal cut of the heart. p = posterior, PT = pulmonary trunk, PV = pulmonary artery, AV = aortic valve, LAA = left atrial appendage, LA = left atrium, MV = the mitral valve, AS = atrial septum, Ao = aorta, TV = tricuspid valve, RA = right atrium, RAA = right atrial appendage, RV = right ventricle, LV = left ventricle. (From Hurst's, The Heart, Eighth edition, page 61 and 66, 1998 [21])

The sagittal section shows the four heart chambers (Fig. 1-4). The left atrium is the upper posterior chamber, while the right atrium is the anterior upper chamber. The right ventricle is called the anterior cavity, while the left ventricle is the so-called left cavity[17,22]. The sectional view also shows the floor of the four cavities with the valves: mitral and tricuspid apparatus. The attachment of the tricuspid valve separates the membranous portion into two parts: an interventricular portion and another portion that can separate the right atrium from the left ventricle [20,22,23].

The wall of the heart is made up of three layers of unequal thickness. From the view of superficial to deep, these are the epicardium, myocardium, and endocardium[20,22]. As well as being the outermost layer of the heart wall, the epicardium is covered by the visceral pericardium.

The middle and thickest layer is the myocardium, which is largely made up of heart muscle cells. It is built on a framework of collagen fibers and blood vessels that supply the myocardium and nerve fibers that help regulate the heart. During contractions of the myocardium, blood is pumped through the heart and major arteries, the so-called

systole. The muscle pattern is complex because the muscle cells swirl and spiral around the heart's chambers, resembling the heart skeleton. They form around the atria and the bases of the large vessels. The deeper ventricular muscles also form a spin around both ventricles and move towards the apex (Fig. 1-5). Both ventricles are surrounded by more superficial layers of ventricular muscle.

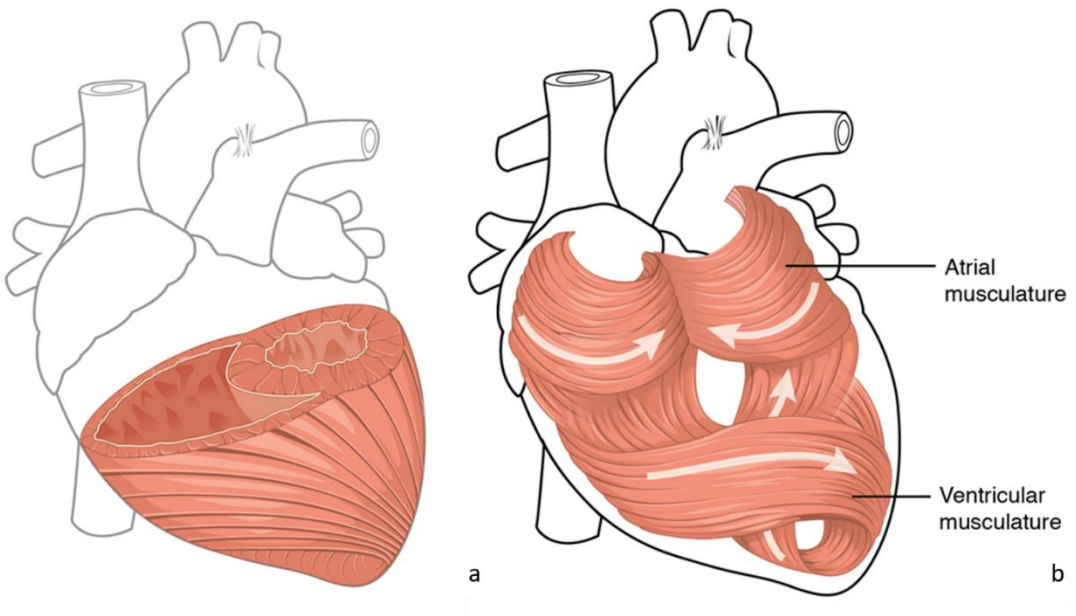

Figure 1-5. Illustration of the muscular in the heart. *a) the relaxed ventricular muscle (https://open.oregonstate.education/aandp/chapter/19-1-heart-anatomy/, view 01.09.2021), b) the swirling musculature of the heart ensures effective pumping of blood. (http://www.clipartbest.com/clipart-KinM4qyiq, viewed 01.09.2021)*

1.1.1.2 The left ventricle

During diastole, when heart muscles are relaxed, blood enters the left ventricle from the left atrium, and during systole, blood flows to the systemic circulation. The left ventricle is roughly ball-shaped with the blunt tip pointing forward, down, and to the left, where it contributes, along with the lower ventricular septum, to the apex of the heart. The left ventricle is positioned at posterior and to the left of the right ventricle, anterior and the left to the left atrium. The left ventricular chamber is roughly elliptical, surrounded by thick muscle walls measuring 8 to 12 millimeters in thickness (up to 13 to 16 mm in the athletic population[24]). Normally, left ventricular wall thickness is about three to four times thicker compared with the right ventricular wall. The ventricular septum is located on the medial wall of the left ventricle and is shared with the right ventricle. The septum is a roughly triangular shape, which is entirely muscular except for the small membranous septum. This membranous septum is located below the right coronary cusps. The upper third of the septum is a smooth endocardium. Intertwined muscles, the trabeculae carinae striate the remaining two-thirds of the septum and the

remaining ventricular walls. The ventricular wall excluding the septum is often referred to as the free wall of the left ventricle[19,22].

1.1.1.3 The aortic valve

The aortic valve is a semilunar valve (Fig. 1-6). Usually, it has three leaflets (sometimes, in world literature, leaflets are called cusps), but the valve can be unicuspid, bicuspid, or quadricuspid due to some congenital changes. These leaflets are the moving parts of the valve. Each has a wrinkled surface that faces the aorta and a smoother surface that faces the ventricle. Each leaflet comprises a free margin that is slightly thicker than the basal portion and participates in valve closure during the heart beating (systole and diastole). The apposition zones, the so-called lunulae, are on the ventricular surface, below the free margin, where each leaflet meets the adjacent leaflets during aortic valve closure. At the mid-portion of the "lunulae," a further thickening is called the "nodule of Arantius." Recognition of these anatomical parts, "lunulae" and "nodule of Arantius," is important to understand the physiology of the valve function and the physiopathology of valve dysfonction[25].

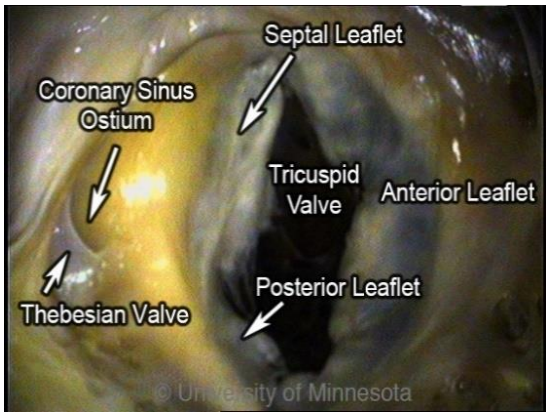

Figure 1-6. A human tricuspid valve viewed from the right atrium. (From Iaizzo, 2015 [26])

The leaflets of the aortic valve are fixed on their base (the aortic annulus). The valve annulus is the end of the left ventricular outflow tract, and at the same time, it is the beginning of the aorta, making it the border of these two parts. Fibrous structures called commissures keep them suspended in the aorta. There is a corresponding sinus for each leaflet, and the orifices of the coronary arteries names them (left coronary, right coronary, and non-coronary). The anatomical descriptions of the aortic valve are a little different from surgical descriptions: the left posterior sinus (or leaflet) corresponds to the left coronary, the anterior sinus (or leaflet) corresponds to the right coronary and the right posterior to non-coronary. The leaflets do not have the same surface. Compared to the aortic root, the leaflets' total area is approximately 40% greater, with the largest area measured in the non-coronary leaflet and the smallest in the left coronary leaflet in most cases[27].

- **Interleaflet Fibrous Triangles**

Aranzio's nodules (interleaflet fibrous triangles, interleaflet triangles, intervalvular trigones, fibrous trigones, or inter-annular trigones) are between the bases of the sinuses and attached to the left ventricular wall. These triangles extend to the level of the sinotubular junction boundary between the extracardiac space and the left ventricular cavity[27]. The septal part of the right ventricular outflow tract (facing the pulmonary valve) is the interleaflet fibrous triangle between the right and left coronary sinuses. The bundle of His comes in through the ventricular septum, where the interleaflet fibrous triangle lays between the non-coronary sinuses the right coronary sinus[28].

- **Aortic valve function**

The leaflets of the aortic valve open once the pressure in the ventricle is greater than that in the aorta, allowing blood to flow from the ventricle to the ascending aorta. It happens during the heart contraction and is called the systole or systole phase. When left ventricular pressure decreases and the aortic pressure raises, the leaflets of the aortic valve close. It occurs during cardiac relaxation and is called the diastole or diastole phase.

- **Aortic valve blood and lymphatic supply**

The aortic valve cusps are made up of three layers: ventricular, spongy, and fibrosis. The aortic valve contains microcirculation with arterioles, venules capillaries, and a certain number of lymphatic vessels to provide metabolic activity, immunological protection, and repair damaged valve tissue. The vessels start from the base (annulus) and move towards the free edge of the leaflet. For the distribution of oxygen in the cusps, the relationship between the thickness of the valves and the tension of the ventricle versus aorta is very important[29].

Limited information was concerned about the involvement of nerves in the valve. However, the cusps receive innervation from the autonomic system, where sympathetic stimulation increases the cusps' tone, shown in the animal model. Ventricular endocardial plexuses are the origin of innervation of the aortic valve. Some nerves may originate from the adventitial aortic wall. The most innervated layer of the cusps is the ventricular[30–32].

- **The aortic annulus**

The definition of the aortic annulus is controversial in different literatures[25,33–38]. From the surgeons' point of view, the aortic annulus is where the cusp communicates with the aortic wall[33]. However, from the cardiologists' or radiologists' point of view[35–38], the aortic ring is the virtual basal line, which communicates the nadir of each leaflet joining in a circular shape. The aortic annulus certainly has a three-dimensional shape and an extremely complex function (Fig.1-6).

The aortic valve annulus can be viewed as a functional unit from a three-dimensional perspective. It is composed of the virtual line that joins each leaflet nadir and the respective inter-leaflet triangles in the bottom part of this annulus. They are attached by the semilunar and the aortic leaflets. The main body of the annulus suspends from the sinotubular junction as an upper board (Fig. 1-7). The entire system is integrated with the Sinus of Valsalva, making it unique.

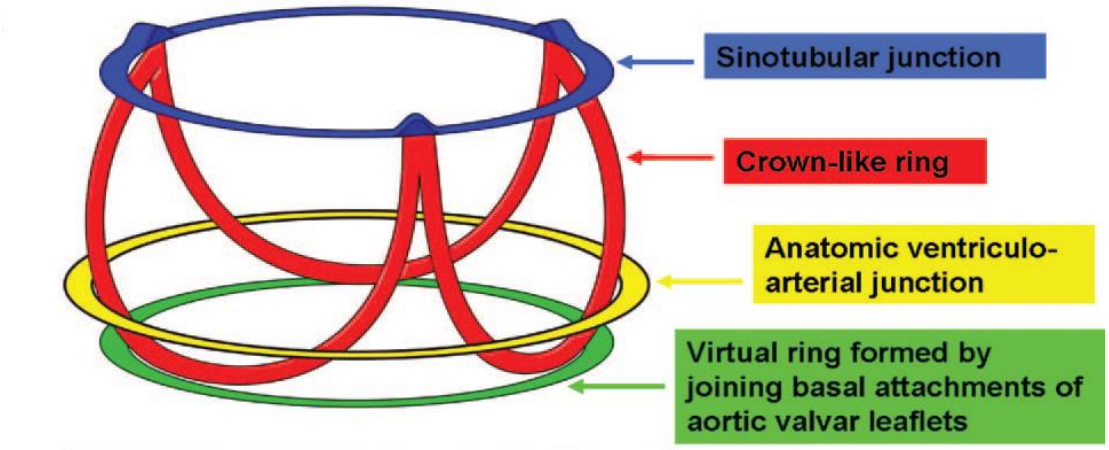

Figure 1-7. Three-dimensional illustration of the aortic functional unit. (From De Paulis and Salica, 2019 [25]*)*

1.1.1.4 The sinotubular junction

The supra-aortic ridge, also known as the sinotubular junction, is different from other parts of the aortic valve annulus. Sinotublar junction can be regarded as a hemodynamic annulus with a high ability to move with systole and diastole.

The sinotubular junction is in direct continuity with the aortic valves and limits upwards the lower tubular part of the aorta and downwards the sinuses of Valsalva. It is a marginally raised ridge of the thickened aortic wall. From its appearance, it is smooth and generally recognizable. The sinotubular junction is not perfectly circular and has a slight trefoil or scalloped outline.

The sinotubular junction is one of the key components of aortic root architecture and aortic valve function[39] (Fig. 1-8). The sinotubular junction increases in diameter over time with age and hypertensive cardiomyopathy[40]. A healthy, normal heart has sinotubular junction diameters of about 75% of the maximum sinus of Valsalva`s diameter[41]. The sino tubular junction is larger than the aortic ring, with a ratio of 1.3. This shift in this ratio between the sinotubular junction and the virtual basal ring may cause aortic dysfunction (insufficiency).

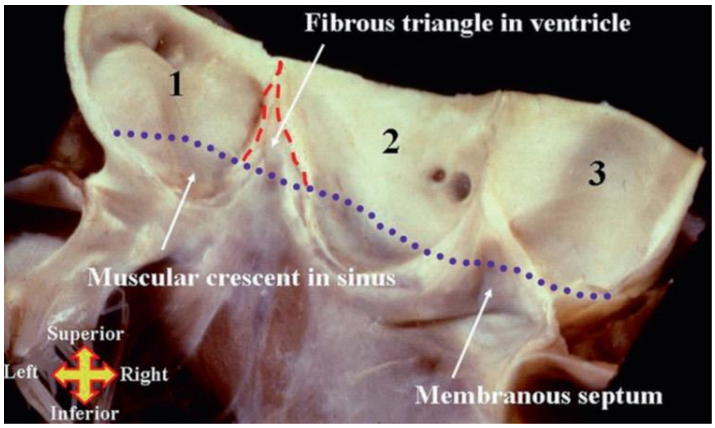

*Figure 1-8. Unfold aorta (opening is on the left and non-*commissure*). 1: the left sinus, 2: the right sinus, 3: non-coronary sinus. The blue line is the radiological annulus. The red line is the border of the fibrous triangle. (From De Paulis and Salica, 2019 [25])*

Another hypothesis of the aortic insufficiency can be the lack of apposition of "lunulae" and "nodule of Arantius," which can be caused either by tissue retraction or by enlargement of the skeleton of the root. It happens mainly at the level of the annulus or of the sinotubular junction, including the sinus of Valsalva.

1.1.2 The aorta

The biggest artery coming out right from the left heart is the aorta. The start is the aortic annulus, and it finishes with the bifurcation of iliac arteries at the L4 vertebral level. The aorta is divided into the thoracic and abdominal parts with a division level of the diaphragm. In the thoracic part, we identify the ascending aorta, the aortic arch, and the descending aorta[42,43].

The division line is the sinotubular junction. Anatomopathologists defined the numbers of classification to the entire ascending aorta: the sinus of Valsalva as part “0”, the ascending aorta as part “1“, the aortic arch as part “2”, the descending aorta as part “3”, and abdominal aorta as part “4”. The transaction from part “1” to part “3” is right the innominate artery. The aortic arch can be so-called the part between the innominate artery and the left sub-clavier artery.

The first branches coming out from the aorta are coronary arteries. The orifices are in the sinus of Valsalva[27]. There is no artery branch from part “0” and part “1” (Fig. 1-9). From the aortic arch brachiocephalic (innominate), the left common carotid and left subclavian arteries are coming out[44,45].

During contraction, if the volume is high, systolic pressure can be elevated. That is the reason why in pressure regulation, aortic compliance plays a key role. Due to its elasticity (more elastic fibers and less smooth muscle with less collagen), the aorta has very high compliance, which softens the pressure on the aortic wall and on the peripheral vessels by expanding with each blood ejection. If the aorta is less compliant,

it will be more difficult to control blood pressure. So with each ejection, there is an expansion of the aorta, and there is a return to the initial position of the aorta during cardiac relaxation[46].

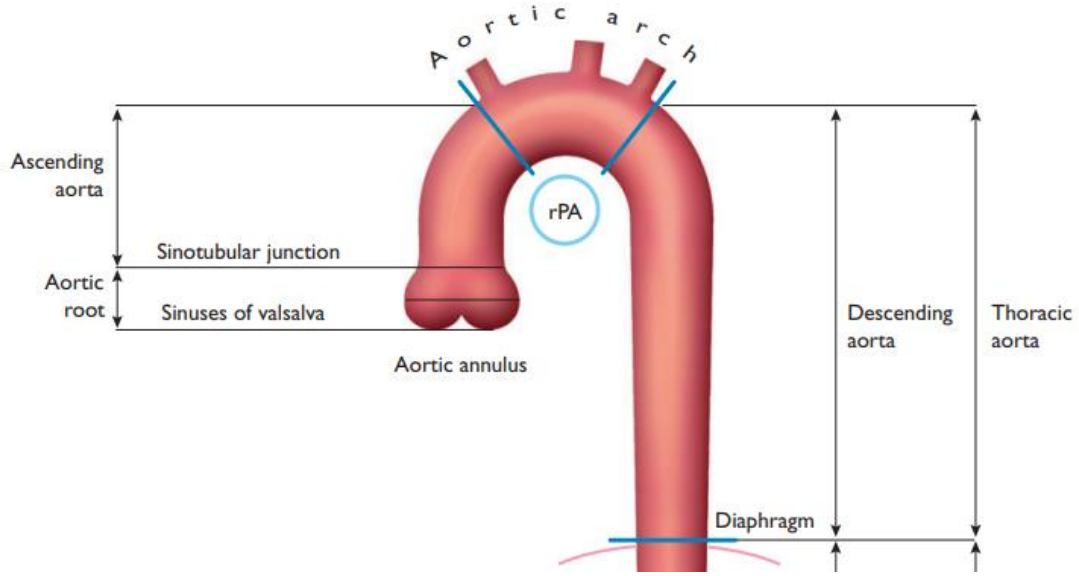

Figure 1-9. Illustration of the aorta in its different portions. (From Erbel et al., 2014 [47])

1.1.2.1 The Sinus of Valsalva

The sinus of Valsalva can be defined as the three-dimensional space surrounding the aortic leaflets in the aortic root[25]. A cross-section of the three bulges resembles a clover. The root has a significantly greater diameter at the sinuses' midpoint than the basal attachment of the leaflets or the sinotubular junction. According to theory, each of the three sinuses is identical. Two of them give rise to coronary arteries and are therefore called the right and left coronary sinuses, respectively. This third sinus, also known as the non-coronary aortic sinus, has an exclusively arterial wall. Interestingly, the basal part of the sinus is made up of a portion of the mitro-aortic curtain.

The Sinus of Valsalva can be characterized by a pear-shaped presentation with a certain level of asymmetrical shape. The internal height and volume of each sinus can differ for a variety of reasons. As a rule, the left coronary sinus is the smallest, while the right coronary sinus is similar to the non-coronary sinus, which can be the tallest and largest one, in many cases[25,48]. The aortic root naturally follows the ascending aorta's curvature, with a tilt angle of 5.5°–11° between the virtual basal ring and sinotubular junction plane.

The sinuses of Valsalva have a complex structure. As shown in Fig. 1-8, it is one of the unique elements of the aortic valve structure.

Leonardo da Vinci[49] has spoken about the sinuses of Valsalva hundreds of years ago (Fig. 1-10). He described a movement of the sinus of Valsalva with extension during the systole. This extension continues to the supra junctional part. This aortic root expansion probably reduces shear stress on the leaflets during the valve opening at the commissural level. Some hypotheses described that this expansion was initiated before ejection[50,51].

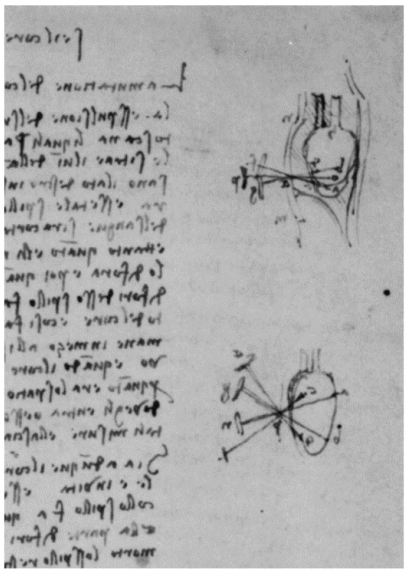

Figure 1-10. Leonardo da Vinci's drawing of sinuses of Valsalva. (From Robicsek, 1991 [49])

Lansac et al. proved with sonomicrometry, with a data acquisition rate of 200 Hz, that the root increased its volume by 37.7 +/- 2.7%, with 36.7 +/-3.3% of it occurring during the isovolumic contraction[52] (Fig. 1-11). During systole, the most significant changes occurred at the commissural level. They also found that the commissures and the sinotubular junctions showed some differences during contractions and diastoles.

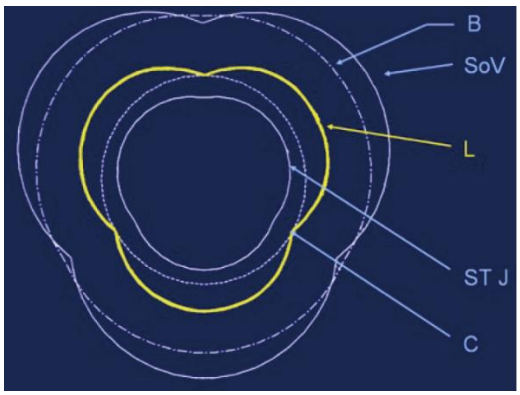

Figure 1-11. Cross-sectional area diagram of the aortic root at maximum expansion during ejection. B = the base of the ascending aorta; C = commissures; STJ = sinotubular junction; L = leaflets; SoV = sinus of Valsalva. (From Lansac et al., 2019 [52])

1.1.2.2 The aortic wall

The aorta is rich in elastin and having less vascular smooth muscle. Histologically it has three layers (Fig. 1-12): the first of those three layers is the intima which is the thin inner layer of the aorta covered by endothelium. The middle elastic, or media, is the second layer composed of sheets of elastic and collagen fibers with the border zone of the lamina elastic internal and external and smooth muscle cells. The outer fibrous layer, or adventitia, contains collagen, vasa vasorum, and lymphatic vessels[53,54]. The inner part of the aorta, the most elastic layer, participates in the blood pumping during diastole. It is known as the Windkessel function[55].

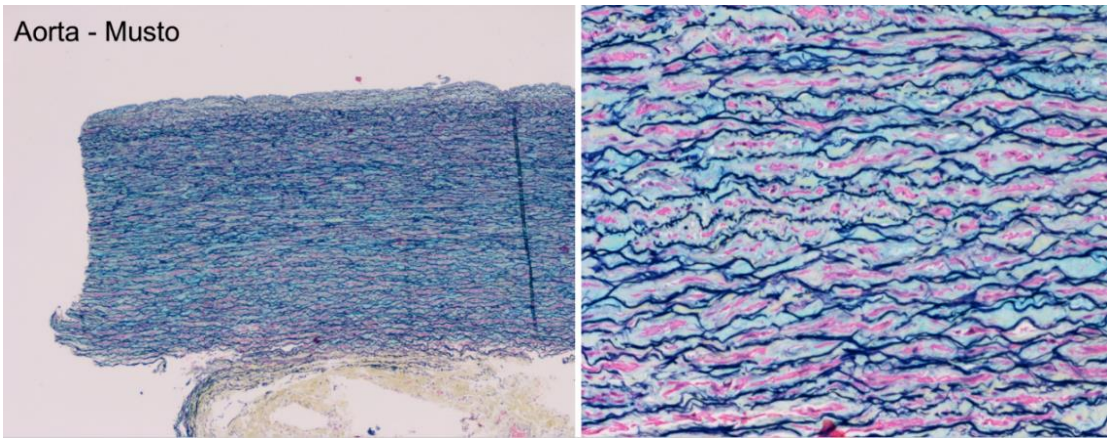

Figure 1-12. Movat's Pentachrome (Musto) stain of a healthy aorta: *nuclei and elastic fibers (black), collagen and reticular fibers (green), mucin (bleu), fibrin (red), muscle (pink). (From Bromley, 2015* [56]*)*

The vasa vasorum network is the vascularisation of the aortic wall, which is always accompanied by lymphatic vessels[57,58]. Sympathetic and parasympathetic nerves tie the aorta. At the same time, the aorta has an autonomic nervous system[59]. Ascending aorta and aortic arch receptors in the ascending aorta act jointly to control systemic vascular resistance and blood pressure. As aortic pressure increases, heart rate and systemic vascular resistance decrease, whereas aortic pressure decreases, heart rate and systemic vascular resistance increase[54].

Over the years, the aorta is getting larger with the rate of 0.9 mm in men and 0.7 mm in women for every ten years of life[60]. Vasoreactivity is diminished with age[61]. Intima fibroblasts show increased collagen deposition and show a disoriented appearance[62]. In the media, smooth muscle cells have become deorganized, collagen has increased, and elastin has been fractured and crosslinked. The adventitia displays increased collagen deposition[63] (Fig. 1-13). Besides age, other factors such as gender, body size, and blood pressure are influencing on the aortic diameter[53,60].

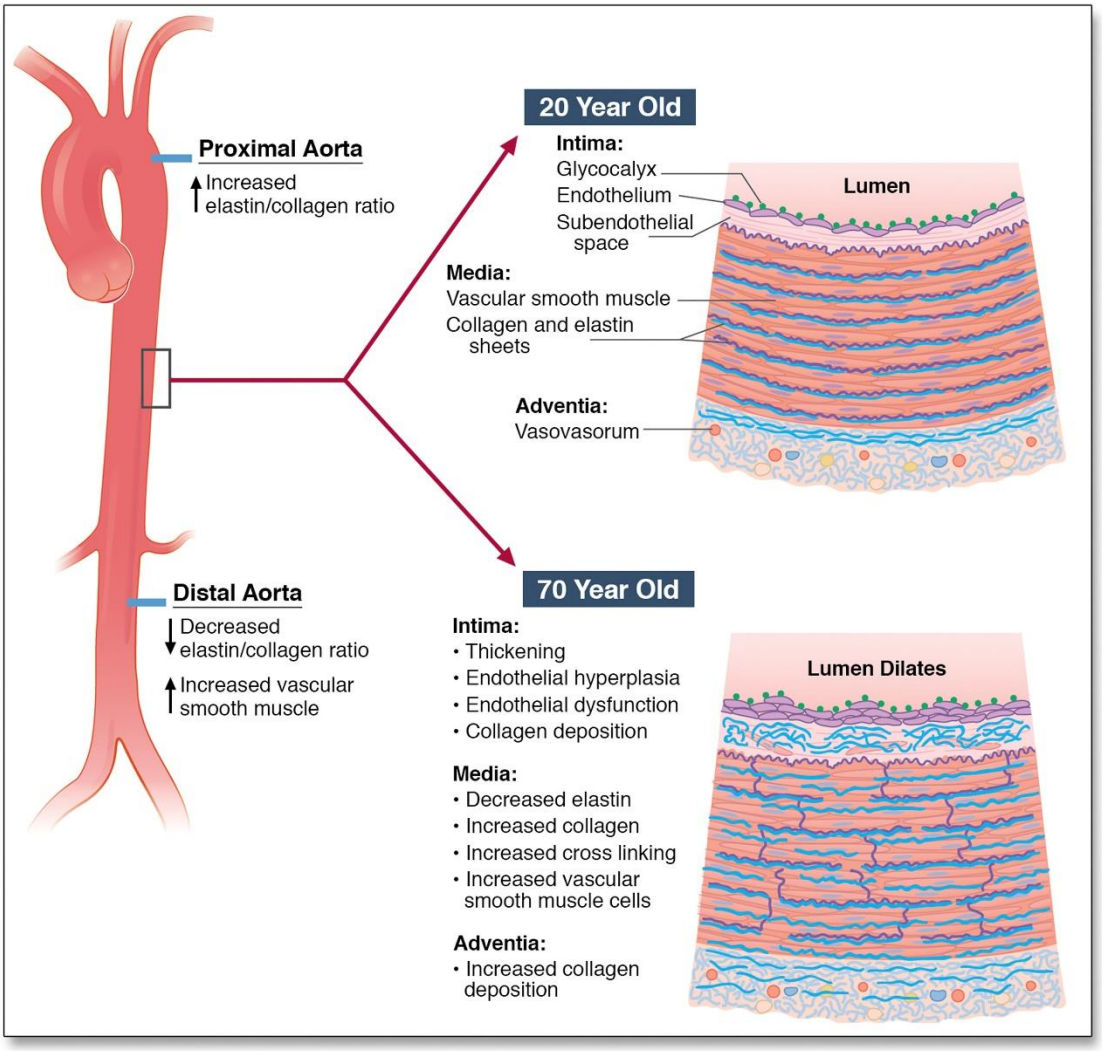

Figure 1-13. Diagram of the Aortic wall with the components of the three layers in a healthy young individual (20 years of age) and in an elderly individual (70 years of age) demonstrating aortic aging. (From Whitlock and Hundley, 2015 [63])

1.2 Ascending aortic aneurysms

Dilation of the aorta more than 50% of expected diameter (ratio of observed to expected diameter more than 1.5) can be called an aneurysm[64]. If it is less than 50%, it can be called ecstasy. Ascending aorta aneurysms may lead to dramatic consequences. As long as it is treated properly and on time, the prognosis is tremendous[65].

According to a report of CDC (Centers for Disease Control and Prevention, the USA)[66], the incidence of thoracic aortic aneurysms has been only 5.9 cases per 100,000 people per year in the early 1980s. Nevertheless, the detection of the AsAA increased. There are reasons to explain that: the advances in imaging modalities, population aging, increased use of transthoracic echocardiography, and routine screening with better diagnostic. According to a report published in 2005, more than half of the thoracic aortic aneurysms are localized in the ascending part[67]. The incidence of ascending aorta

aneurysms is estimated to be around 10 per 100,000 people per year[66]. There was an increase in the incidence rate from the 1980s to 2005. In general, women and men have similar incidences of thoracic aortic aneurysms. However, the age at diagnosis was a decade higher in women (in the 1970s) than in men (in the 1960s).

Studies have shown the relationship between the vascular wall stress of Laplace's law and the risk of vascular dilatation[68–70]. In an undilated aorta, the blood pressure is harmoniously distributed on the aortic wall with no pressure differences[71]. Once aortic diameter changes, the blood pressure can be distributed differently on the aortic wall. This distribution may be more obvious in the aortic aneurysms since the blood pressure difference is significant[72]. Continues blood pressure fluctuations in the aneurysms can provoke the dilatation of the aortic aneurysm. Laplace's law may explain the reason for the dilatation that, in given blood pressure, wall tension is proportional to the aortic radius. Laplace's law can be described as: $T = P \times r$ (where T is the circumferential wall tension, P is the pressure on the wall, and r is the average aortic radius)[71]. If the strength of the aortic wall is unevenly distributed, the dilatation would be the compensatory response to high blood pressure in the relative wake area, which might provocate a continuous dilatation of the aorta. Meanwhile, it can develop to the entire aorta because the radius of the spherical dilation of the aorta will increase the pressure on a given radius by half. However, this spheric dilatation is not enough to relieve the stress on the aortic wall and might continue to distend up to the moment where aortic elasticity reaches its peak. The next step of deterioration is the rupture of the aortic. The Laplace's law is adapted to the ascending aorta's aneurysm according to its cylindric shape in part "1" of the aorta[72].

An aortic aneurysm can accompany some familial syndromes. One of these syndromes is the Marfan syndrome. With Marfan syndrome, aortic enlargement mainly occurs at the sinuses of Valsalva, which cause annulo-aortic ectasia. The aneurysm can be associated with other syndromes or malformations. One of the malformations is the bicuspid aortic valve. There are three enlargement patterns described in patients with bicuspid valves, depending on whether the maximum aortic diameter occurs at the level of the sinuses of Valsalva, supracoronary ascending aorta, or sinotubular junction. The morphology of the ascending aorta is related to the pattern of valve fusion[65].

Familial thoracic aortic aneurysms grow faster, up to 2.1 mm per year (combined ascending and descending thoracic aorta aneurysms). The growth rate in thoracic aorta aneurysms varies from different syndromes. In patients with Marfan syndrome, the thoracic aorta aneurysm growth is on average at 0.5 to 1 mm per year. In contrast, thoracic aorta aneurysms in patients with Loeys-Dietz syndrome can grow even faster than 10 mm per year, resulting in death at a mean age of 26 years[73–77].

1.2.1 Pathology and symptoms

For a long period, the major hypothesis of the aortic aneurysmal development was atheroma or syphilis. Although atheromatous plaques were, as expected, common in the older patients in the series of the Pomerance et al.[78], only two aneurysms appeared to be actually due to atheroma, and only four were syphilitic. By far, the commonest pathology was cystic medionecrosis in almost three-quarters of the cases. Their study includes some patients with the dissected aorta, but even if these cases are excluded, 28 (62%) of the remaining 45 were due to cystic medionecrosis. They concluded that there are two distinct types of cystic medionecrosis. Localized, widely separated lesions were found in most of the patients with dissecting aneurysms, and the elastic abnormalities were largely confined to the foci of cystic medionecrosis. Aneurysmal dilatation in these cases affected the outer media only and, where dilatation was chronic, fragmentation of Elastica was seen in this site. However, the elastic pattern, in general, appeared normal, and, as this change appeared to be secondary to distension of the separated outer media, they regarded these cases as cystic medionecrosis without elastopathy (Fig. 1-14).

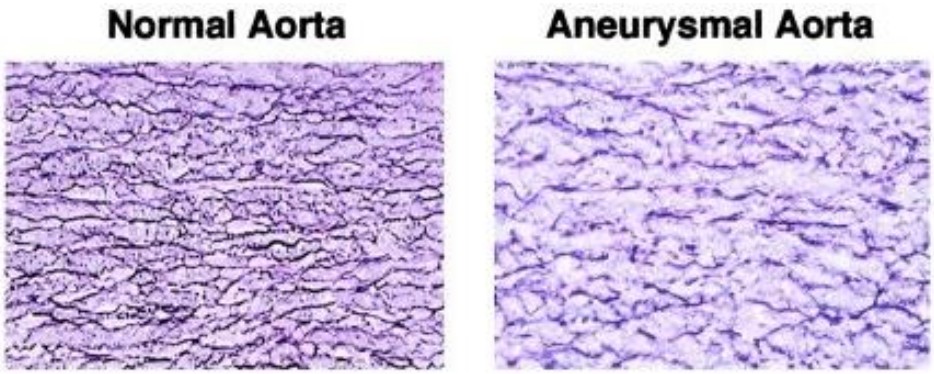

Figure 1-14. Histopathology of ascending aortic aneurysms (Verhoeff–van Geisen stain): *elastin in dark purple. (From Absi et al., 2003* [79]*)*

The second, more common, cystic medionecrosis was associated with widespread fragmentation and loss of elastica. It was seen in patients who were, on average, a decade younger than those without elastopathy and included most of the patients with Marfan syndrome.

Pomerance et al.[78] described the accumulation of mucoid material between elastic laminae, elastic tissue disappearing as the mucoid cysts expanded and became confluent, confirming that the initial changes are in the muscle and not the elastin. They published that some of the patients had areas of smooth muscle irregularity. The most striking example was in one of the syphilitic aneurysms. Adventitial fibrosis was present in almost all the cases with chronic aortic dilatation, including chronic dissections and aneurysms due to aortitis.

According to Erbel et al.[47], signs and symptoms of thoracic aortic aneurysms are dividing into two parties, knowing that most of the time, it stays without any signs and symptoms. Sharp, sudden pain in the chest or upper back can be a more common sign directly related to the aorta due to its expansion. The aneurysm may develop compression syndrome with subjacent organs such as the trachea or bronchus, provocating some cough, trouble breathing, shortness of breath, some pneumonia, and in the worst cases, aortobronchial fistula. In the same way, it can compress the esophagus, create some swallowing disorders, and even provoke a fistula between the oesophagus and the aorta. In sporadic cases, patients can have superior vein cave syndrome with the displacement of the heart by compressing the superior vena cave.

The ascending aorta can be dilated just in zone one, which is called the supracsoronary aneurysm. In the same way, the sinus of Valsalva can be dilated, which we call aortic root dilation. The aorta can be dilated in its all length. All these dilatations can be accompanied by aortic valve insufficiency depending on the aortic functional unit involvement degree[80].

1.2.2 Risk factors and causes of the ascending aortic aneurysm

A variety of etiologies and pathologies can lead to ascending aortic aneurysms. The leading causes are atherosclerosis aortic valve disorder. Connective tissue disorders like Marfan and Loeys-Dietz syndrome can also be a cause. Other factors like genetic risk, Erdheim–Gsell media degeneration, or aortitis can also trigger AsAA.

- Atherosclerosis

Atherosclerosis is one of the most common causes of aortic aneurysms. Study shows that hypertension, smoking, and advanced age are associated with aortic aneurysms[81]. Although there is a link between atherosclerosis and ascending aortic aneurysms, the specific pathogenesis remains unclear[82]. An important factor may be the increased activity of matrix metalloproteinases, which regulate tissue homeostasis. It is clear that atherosclerosis can deterge and create ulcers in the aortic wall, which can be seen as an ascending aortic aneurysms type[47].

- Aortic valve issue

The bicuspid aortic valve (BAV) is a congenital anomaly of the aortic valve. About 26% of bicuspid aortic valve patients develop ascending aortic aneurysms[83]. 50% of AsAA is associated with severe aortic stenosis. On the other hand, AsAA is present in 34% of patients with severe aortic stenosis and 33% of patients with severe aortic insufficiency[84].

- Connective tissue disorders

Marfan syndrome is one of the connective tissue disorders caused by a mutation in the fibrillin-1 gene[85]. The prevalence of Marfan syndrome is around 3.3 per 10,000 people. However, many patients remain undiagnosed[86]. The revision diagnostic criteria for Marfan syndrome (Ghent nosology, in 2010) account for the variable phenotype by simplifying it[87]. Almost all people with Marfan syndrome will develop at least one type of aortic disease (aortic aneurysm, aortic dissection, rupture) in their lifetime. With optimal treatment, the life expectancy is increased from 32 to 60 years[82,88]. The majority of aortic aneurysms occur at the aortic root. Aortic valve insufficiency is present mainly (15% to 44%) when the sinotubular junction is involved[85].

Loeys–Dietz syndrome results from a mutation of the transforming growth factor-beta (TGF-β) receptor. It is an autosomal dominant genetic aortic aneurysm syndrome. Phenotype 1 is the most common phenotype. The tortuosity (in 84% of the cases) and aneurysm (in 98% of the cases) of the great vessels, hypertelorism (in 90% of the cases), and bifid uvula (in 90% of the cases) are observed in this phenotype. The second phenotype is similar to the vascular Ehlers–Danlos syndrome. It is a connective tissue disorder in which collagen III synthesis is impaired, leading to arterial dissections and ruptures (in 65% of the cases) and rupture of hollow organs (in 21% of the cases) [89]. Despite the aggressive course in aortic aneurysms in Phenotype 2, Loeys–Dietz syndrome has lower operative mortality associated with aortic replacement (4.8% compared to 45% in vascular Ehlers–Danlos syndrome). The average life expectancy in patients with Loeys–Dietz syndrome is 37 years since aortic dissection occurs at a younger age and a smaller diameter[90].

In Marfan syndrome and Loeys–Dietz syndrome, vascular instability is attributed to higher TGF-β activity[85,90]. It was found that angiotensin-III-receptor type 1 (AT1) antagonists and TGF-* antibodies inhibit aneurysm growth[66,81(p2),91]. It does not mean that all aneurysms follow the same development mechanism as these since mechanisms vary between aneurysms[92].

Turner syndrome is a condition that affects only women. It is caused by one or part of one of the X chromosomes (sex chromosomes) is missing. Turner syndrome can result in a variety of medical and developmental problems, including short height, ovarian failure, and heart defects[43]. In recent years, there are reports showed that aortic dilatation rates are high at all ages in Turner syndrome[93–95]. The growth rate of the sinuses of Valsalva and ascending aorta can be 0.1 - 0.4 mm per year[96]. It was also reported that when the aorta is associated with BAV, the aortic growth rate can be 0.19 mm per year[97].

- Familial aortic aneurysms and genetic risk factors

Aortic aneurysms and aortic dissections occur in families, albeit without syndromes or connective tissues diseases. Several genetic mutations are responsible for these diseases (Myosin Heavy Chain 11 (MHY11), Actin Alpha 2(ACTA2), though the mechanism is only partially understood[82]. According to the results of a genome-wide association

study, the gene variant 15q21.1 is associated with a sporadic thoracic aortic aneurysm. This gene codes for fibrillin-1, which may explain the similarities in the pathogenesis of sporadic aneurysms and Marfan syndrome[98]

- Erdheim–Gsell media degeneration

Aneurysms are known histopathologically as medial cystic necrosis, characterized by necrosis of smooth vascular muscle cells, destruction of elastic fibers, and proliferation of basophilic ground substance in the cell-free areas[99]. Since neither cysts nor necrosis appears consistently, the term "media degeneration" is more appropriate today[48]. Due to this degeneration, the aortic vascular mechanics deteriorate as its distensibility diminishes with increasing diameter. Meanwhile, wall stress increases with rising blood pressure. All these are corresponding the Laplace's law[100].

- Aortitis

An aortic aneurysm is rarely caused by aortitis. However, aortic root dilatation and insufficiency are common in patients with manifest aortitis. Currently, syphilitic aortitis is a rare occurrence and should only be considered when syphilis is suspected clinically. Female patients under the age of 40 with Takayasu aortitis must be differentiated from the patients older than 75 years with giant cell aortitis[101].

1.2.3 The risk assessment

As aortic diameter increases with age, weight, and height, it is difficult to provide a standard aortic diameter[102]. In some studies, ratios of aortic diameter to body weight and height have been developed in place of individual values[93,103,104]. Even though there is a paucity of study evidence, it seems reasonable and practicable from a clinical perspective[105]. In particular, the risk of complications can be underestimated based on absolute values, e.g., in Turner syndrome in women and patients of small stature (body surface area less than 1.68 m^2). Studies showed that[93,106], in patients with Turner syndrome, aortic dilatation is p[47]resent when the maximum aortic diameter is greater than 20 mm/m^2. A high risk of aortic dissection can be detected when it is greater than 2.5 mm/m^2. Existing studies have used absolute values to identify threshold values for the general surgical indication (Fig. 1-15). The European guidelines[6] are based on the work of Coady and al., where the authors described the natural history of patients having different diameters of aortic aneurysm[107]. They described that the aorta could be dissected or ruptured in any diameter, but when the aorta reaches 60 mm, the risk of dissection or rupture is extremely high. That is why the European guidelines recommend treating the aorta whey before the 60 mm of the diameter when it is 55 mm or more.

However, apart from the diameter of the aorta, other specific risk factors also impact management decisions[33,108].

- A familial predisposition to aortic complications
- Growth rate (> 5 mm per year)

- Aortic valve morphology (unicuspid or bicuspid)
- Corrected or uncorrected aortic coarctation
- Arterial hypertension
- Connective tissue disorders

Recommendations	Class[a]	Level[b]
Surgery is indicated in patients who have aortic root aneurysm, with maximal aortic diameter[c] ≥50 mm for patients with Marfan syndrome.	I	C
Surgery should be considered in patients who have aortic root aneurysm, with maximal ascending aortic diameters: • ≥45 mm for patients with Marfan syndrome with risk factors.[d] • ≥50 mm for patients with bicuspid valve with risk factors.[e,f] • ≥55 mm for other patients with no elastopathy.[g,h]	IIa	C
Lower thresholds for intervention may be considered according to body surface area in patients of small stature or in the case of rapid progression, aortic valve regurgitation, planned pregnancy, and patient's preference.	IIb	C

Figure 1-15. Guidelines for elective surgery to replace the aorta. (From "2014 ESC Guidelines on the diagnosis and treatment of aortic diseases", 2014 [6])

1.2.4 The surgical strategies

The risk of surgical death associated with aortic replacement can be observed to be between 1% and 5% or higher. It depends on the age and comorbidities of the patient, the method of surgery, and the experience of the surgeons[109,110]. Aneurysm location plays a role in surgical correction. There exist different surgical procedures, depending on the localization of the aneurysm: ascending aorta +/-aortic root +/- associated with aortic valve disease (stenosis or insufficiency).

A tube graft can be implanted distally to the sinotubular junction when only AsAA is present. Aortic insufficiency is often present when aneurysms involve the aortic root. The aortic replacement by a prosthesis between the sino-tubular junction and the innominate artery stays the gold standard. This technique was proposed by Cooley and De Bakey back in 1966[111] (Fig. 1-16). They showed the solidity of the aortic tissue in anatomical landmarks out of the aortic aneurysm, such as sino-tubular junction and innominate artery. At that moment, the majority of the aneurysms were treated by Cooley and De Bakey technique[111].

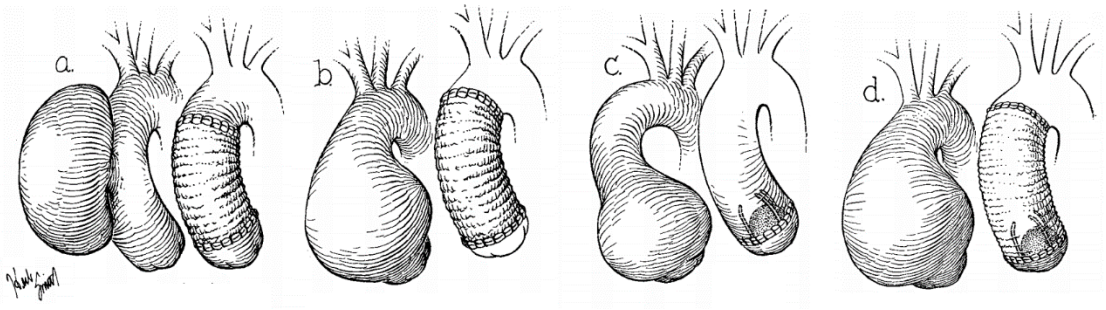

Figure 1-16. Cooley and De Bakey surgical procedure. a) resection of saccular aneurysm and segment of ascending aorta. b) replacement of ascending aorta when sinuses of Valsalva are uninvolved and aortic valve function is unaltered. c) direct anastomosis at base of ascending aorta and aortic valve replacement. d) replacement of ascending aorta and aortic valve replacement. (From Cooley and De Bakey [111])

- **Bentall surgery**

In 1968, Hugh Bentall and Antony De Bono presented their case report of a 33 years old patient who had total replacement of the aortic aneurysm with aortic valve replacement by Starr-Edwards prosthetic valve[112] reimplantation of the coronary arteries[113] (Fig. 1-17). They certify a thin aortic wall with a large aortic annulus without having aortic valve organic changes. Meanwhile, they resected all aorta creating buttons of the coronary orifices. They included Starr-Edwards mechanical valve in the prosthetic tube and sutured above mentioned complex to the aortic annulus by resecting the aortic valves. They created the halls on the prosthesis and reestablished the continuity of the coronary arteries. The patients do not have any dilatation on the horizontal aorta so that the distal anastomosis was underneath the innominate artery. This article changes the treatment strategy, giving another chance to patients with aortic aneurysms and aortic valve diseases.

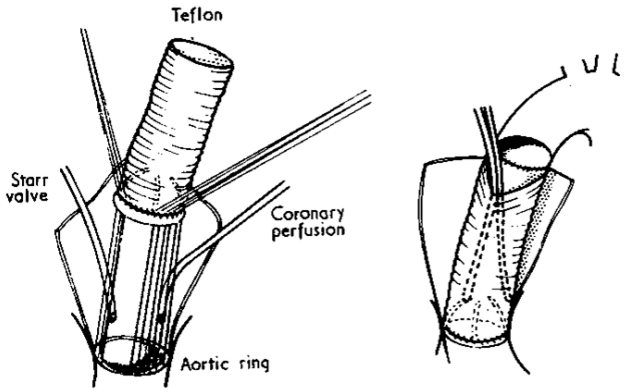

Figure 1-17. Bentall surgical procedure. (From Bentall et al., 1968 [113])

The short-term and long-term observation shows promising results: 85,9% of the patients' survival at ten years follow up without technique related complications[114], 60% at 20 years[115]. Another study[116] demonstrated a 14 years follow-up of patients with BAV initially. They were operated on an elective and emergency basis with no

complications detected. The patients under 60 years old who got Bentall surgery observed 94% of survival at 14 years follow up and 81 % of survival at 20 years follow up[79,80]. Left coronary ostia stenosis was published as a complication for long-term follow-up[115]. Other complications related to the technique and prosthetic material use were published[117]. This indication is now performed by all cardiac surgeons in elective or emergency cases, with mechanical or biological prosthesis, on the aortic valve replacement.

- **Yacoub Surgery**

In 1982, Yacoub published their experience with aortic aneurysm surgery, where replacement of the aorta was proposed with reimplantation of the coronary arteries. The main point of this strategy was preserving the aortic native valve, which was a huge advancement compared to Bentall surgery[113]. Yacoub surgery was applied when the aneurysm involves the aorta without having any aortic valve organic problems, then [118]. This type of surgery allows to keep in place the native valve and avoid the complications related to the aortic prosthetic valve (mechanical and biological) as in the short-term and long-term[114–117]. The indications were widened up to the correction of the aortic insufficiency due to the sinotubular junction's enlargement, expecting that the created sinotubular junction would decrease the dilatation consecutively of the aortic insufficiency. Fig. 1-18 shows the surgical steps of the Yacoub surgery: resection of the aorta from the innominate artery to the aortic annulus leaving 1 - 2 mm of the aortic tissue for suturing, creating the coronary buttons, tailoring the prosthetic tube, suturing the prosthetic tube to the aortic annulus with 1 - 2 mm aorta as reinforcement, reinstalling the coronary buttons in the created halls in corresponding newly fashioned sinuses.

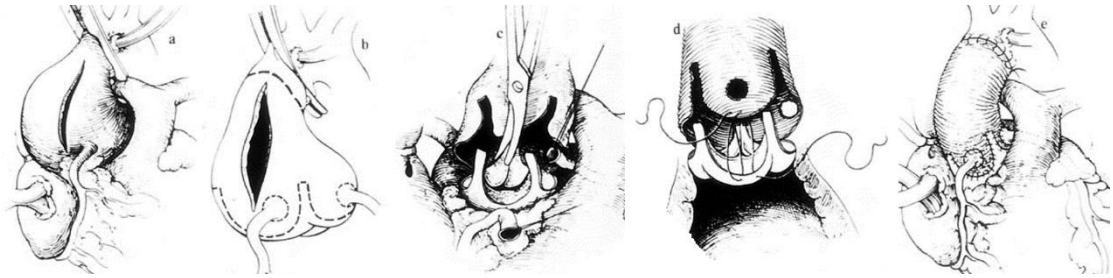

Figure 1-18. The Yacoub surgery in its different steps. a) opening of the AsAA; b) AsAA resection; c) preparation of the aortic cups; d) implantation of the tailored prosthesis; e) reconstruction of coronary ostias. (From Yacoub et al., 1998 [118])

The efficacy of this technique for patients with aortic dissections in the short term is reported with a high survival rate, while low survival rate in the long term[118]. It is the main reason that Yacoub surgery in the long term was not suggested. As a result of follow-up, they recorded 33.3% mild to moderate aortic insufficiency with 3.0 % severe aortic insufficiency. Even though the reoperation rate is 85% in 15 years follow-up and 86% in [84]10 years for patients with Marfan syndrome[118]. In practice, the critical of the

Yacoub technique is that the aortic annuls are not treated, which may present dilatation in long-term follow-up.

- **David surgery**

In 1992, Dr. David published a series study of ten patients with annuloaortic ectasia (aortic insufficiency and aortic root dilatation without any valvular organic changes)[119]. In this series, five patients had Marfan syndrome, and four patients had aortic dissections. Unfortunately, the result was not corresponding to the expectations in three patients: a mild degree of aortic insufficiency was detected. One patient kept significant aortic insufficiency with the requirement of the aortic valve replacement. After several modifications, the standard surgical technique was established as Fig. 1-19.

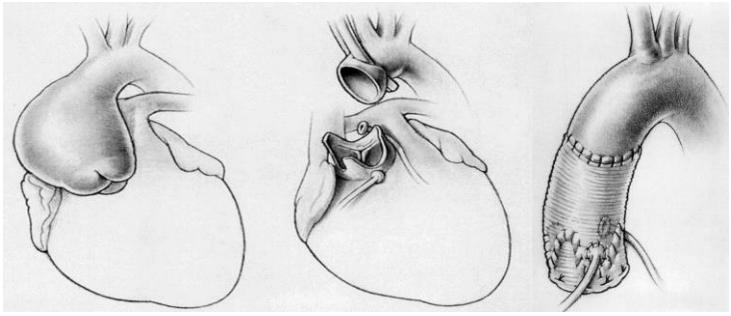

Figure 1-19. David surgery procedure. (From David et al., 1992 [119])

The resection of the aorta in the dilatated part and the creation of the coronary buttons was very similar to in Yacoub technique (keeping 1-2 mm of the aortic tissue for suturing). The difference was in stabilization or diminishing the aortic annulus to create the correct coaptation. For that reason, the soft heart tissues were dissected until the apparition of the aortic annulus from the outside. Once the aortic annulus was identified, the prosthesis was pulled until the aortic annulus by fixing sutures controlling from outside. This technique was widely used since the results are satisfactory in patients operated on an elective or emergency basis. A publication of 20 years follow-up concluded that the technique provided "excellent clinical results and stable aortic valve functioning." It is reported that the survival was 72.4% in 20 years and 77.9% in 15 years[120]. From the 15th year of follow-up until the 20th year, 96.2 % were free from moderate or severe aortic insufficiency, and 96.9 % were free from reoperation. David surgical procedure includes the aortic valve and the annulus, which can avoid the future dilation of the aortic annulus. However, it did not respect the physiology of the aortic root.

- **Lansac surgery**

In 2005, Dr. Lansac proposed another approach to replace the ascending aorta and repair the aortic valve. It is for patients with aortic aneurysms and aortic valve insufficiency without organic disoder[121]. The technique was proposed as an alternative to the David surgery and as a completion of the Yacoub technique with external aortic annuloplasty.

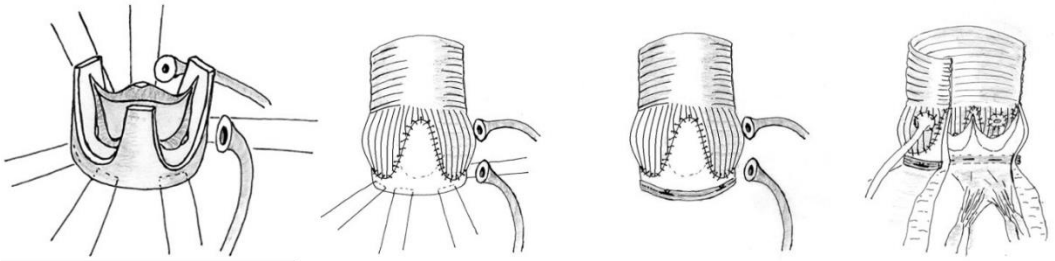

Figure 1-20. Lansac surgery procedure. (From Lansac et al., 2006 [121])

The resection of the aorta from the innominate artery to the aortic annulus was performed as described by Yacoub and David (Fig. 1-20). In addition, Lansac et al.[121] proposed cleaning the aortic annulus from the heart soft tissues and identifying the aortic annulus from the outside. In this step, they installed a ring from outside of the aortic annulus to reduce the diameter. According to them, it is easier and quicker than David procedure and assuring a better outcome than Yacoube surgery. Two hundred thirty-two patients were followed for seven years[122]. Freedom from significant aortic insufficiency was 90.6 %, with 85% of the survival rate. The technique is applicable for aortic dissections where the aortic valve is intact. A recent midterm study shows that it reduces the modality and the indications[123].

1.3 Aortic valve malformation

The aortic valve is a semilunar valve. Usually, it has three leaflets, but the valve can be unicuspid, bicuspid, and quadricuspid due to some congenital changes.

1.3.1 Bicuspid aortic valve

Bicuspid aortic valve, which can be present at birth in 1–2% of cases, is the most common congenital cardiac malformation. Males are more likely to be affected than females, with the ratio ranging from 2:1 to 4:1[124–127]. The bicuspid aortic valve is the result of the fusion of the left coronary cusp and right coronary cusp in > 70% of patients, of fusion of the right coronary cusp with the non-coronary cusp in 10 – 20%, and of fusion of left coronary cusp with a non-coronary cusp in 5 – 10%[128]. Another aortic valve malformation, the so-called unicuspid aortic valve, is an extremely rare condition with 0.02% prevalence in adults. There are two types of unicuspid valves: acommissural and unicommissural. The classification is based on the lateral attachment of the commissures. The unicommissural type is usually associated with aortic stenosis[129]. Aortic dilation is defined as an aorta diameter exceeding 40 mm regardless of body surface area[130–132]. Around 26% of patients with a bicuspid aortic valve can develop an aneurysm of the ascending aorta[83]. In patients with BAV, the risk of developing aortic dilation is probably much higher than in the general population[73]. However, there are no reliable population-based data on its incidence. There are some indications of racial differences in the extent of aortic dilation in BAV[133].

Three subtypes of BAV are associated with different forms of valve cusps[128], where Type 0 refers to the valve with no raphe; Type 1 to the valve with one raphe; and Type 2 to the valve with two raphes (Fig. 1-21). In patients with a left coronary cusp or right coronary cusp type BAV, ascending aorta dilation is common with aortic root dilation[134]. The aortic root was rarely affected in the right coronary cusp – non-coronary cusp type, and only dilation of the ascending aorta is seen[73]. Aortic dilation reaches the peak at the level of the tubular aorta, with a mean rate of 0.5 mm per year, similar to that seen in Marfan patients[77]. However, in this population, half of the patients do not present aortic dilation over three years, whereas other studies[77] do, emphasizing the heterogeneity of the population of patients with BAV. The aortic arch is rarely affected[135].

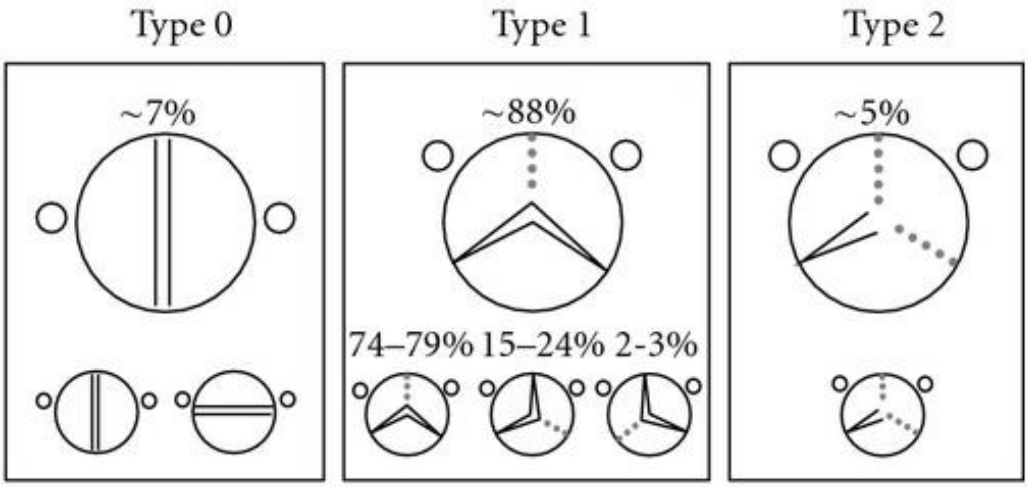

Figure 1-21. Different types of the bicuspid aortic valve (Sievers' classification). L = left; R = right; N = non-coronary. (From et al., 2019 [136])

Beyond aortic dilation and aneurysm formation, the bicuspid aortic valve is a risk factor for dissection and rupture[135]. Patients with BAV, including those with a hemodynamically normal valve, have dilated aortic roots and ascending aortas, compared with age and sex-matched control subjects[137]. Among those adults with BAV and no significant valve disease at baseline, 27% require cardiovascular surgery within 20 years[138]. The mean growth rate of proximal ascending aortic aneurysms in BAV and aortic stenosis patients is greater than that seen in tricuspid valves (1.9 vs. 1.3 mm per year, respectively)[97]. Another study reported an annual growth rate of 0.77 mm among patients with a normally functioning BAV[139]. In patients with BAV, the average annual change in the ascending aorta was reported from 0.2 to 1.2 mm[77,137,140]. The aortic dilation rate is higher in the tubular ascending aorta than in the sinuses of Valsalva, which differs from Marfan syndrome[77]. During the first 15 years after aortic valve replacement, 86% of patients with BAV without aortic dilation treatment experienced complications or aortic surgery when the initial aortic diameter was 40 mm, 81% with diameters from 40 - 44 mm, and only 43% for diameters from 45 - 49 mm, respectively[141]. There is another study showed that a low risk of adverse aortic events

after isolated valve replacement in patients with BAV stenosis and concomitant mild-to-moderate dilation of the ascending aorta (40 - 50 mm) with about 3% of patients requiring proximal aortic surgery at up to 15 years follow-up[142].

Notch1 gene mutations are associated with BAV[143(p1)]. There was a high incidence of familial clusters, which is consistent with autosomal dominant inheritance with reduced penetrance.

Different orientations of the leaflets (fusion of LCC to RCC or RCC to NCC) seem to have distinct aetiologies in the embryonic phase[144]. BAVs are associated with a variety of types of aortic pathology. However, the pathophysiology underlying these variations remains unknown. The cause may be genetic, with common genetic pathways for aortic dilation and BAV[145,146], or due to altered aortic flow patterns in BAV[147–149], or both.

As it is shown that BAV may lead to the aortic annulus dilatation being the reason for the aortic regurgitation and may lead to aortic valve stenosis. In the elderly population, when the patient is associated with BAV, the dilatation is mostly in part one of the ascending aorta. While, in the younger population, it is located in the aortic root. It is reported that 40% - 50% of the cases with BAV can develop the aortic aneurysm[150,151]. Yazdani et al. found out that 75% of the BAV patients had aortic stenosis, and 13% had aortic regurgitation[152]. The genetic changes and the aortic wall weakening is not the only existing hypothesis explaining the aortic dilatation. From a mechanobiology point of view, there is a couple of hypotheses to explain. Blood flow through BAV is a turbulent flow that directs mostly on one part of the aortic wall. The stroke volume during the systole is higher if BAV is associated with aortic regurgitant, which may bring higher stress on the aortic wall. The shear stress can be higher if the BAV presents with aortic stenosis, as a reason of the high velocity of the blood passing through the narrow orifice of the aorta[48].

1.3.2 Quadricuspid aortic valve

Quadricuspid aortic valve (QAV) is a congenital disorder with an extremely rare prevalence (0.0127 - 0.0133% in autopsy specimens)[153]. Approximately 0.0059 - 0.0065% of patients undergoing transthoracic echocardiography are affected by QAV[154]. The possibility is 0.05 - 1% in those receiving aortic valve replacements for aortic insufficiency (AI)[155,156]. QAVs are increasingly reported in the era of echocardiography and other imaging diagnostic techniques[157].

QAV development mechanisms remain unclear. The cause was believed to have been the abnormal septation of a conotruncus and an endocardial cushion, caused by an inflammatory episode[158]. Cusps may form abnormally due to abnormal fusion of the aorticopulmonary septum or abnormal mesenchymal proliferation in the truncus arteriosus[159].

There are two classification schemes. The Hurwitz & Roberts[160] classification, based on the relative size of the supranumerary cusp, divides QAVs into seven types from A to G (Fig. 1-21). More than 85% of the cases are reported as types A, B, or C, while the type D variant is extremely rare[161].

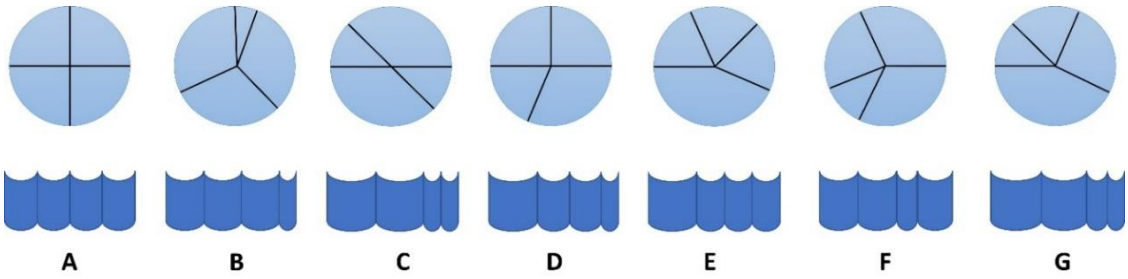

Figure 1-21. Hurwitz & Roberts classification of the quadricuspid aortic valve. A) Four equal-sized cusps; B) Three equal-sized cusps and one smaller cusp; C) Two equal larger cusps and two equal smaller cusps; D) Once large cusp, two intermediate-sized cusps and one smaller cusp; E) Three equal-sized cusps and one large cusp; F) Two equal larger cusps and two unequal smaller cusps; G) Four unequal cusps.

Another classification is designed by Nakamura et al. [162]. It is simplified by focusing on the position of the supernumerary cusp. (Fig. 1-20). They identify types A and B as being the same as Hurwitz & Roberts types A and B. Their study of 42 patients with a QAV revealed that 23.8%, 30.9%, 7.1%, and 4.9% were caused by these four types of QAV (I, II, III, IV, respectively). Additionally, they found that the location of the supernumerary cusp did not affect clinical outcomes. However, Pirundini et al. found that type II QAV account for 39%[156].

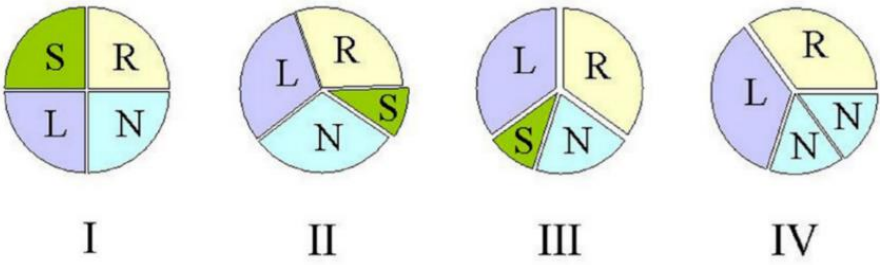

Figure 1-20. Simplified classification of the quadricuspid aortic valve. S = supernumerary cusp; L = left coronary cusp; N = non-coronary cusp; R = right coronary cusp. I) Supernumerary cusp between the right and left coronary cusps; II) Supernumerary cusp between the right and non-coronary cusps; III) Supernumerary cusp between the left and non-coronary cusps; IV) Unidentified supernumerary cusp as of two equal-sized smaller cusps (From Yuan, 2016 [153])

A patients' study found that the QAV was rarely associated with ascending aortic aneurysms, with only two documented cases[159]. Nevertheless, some studies reported three earlier cases of aortic root dilatation[163,164]. According to a recent report on

dysfunctional QAV surgery, 42% of patients had an ascending aortic diameter greater than 4 cm, and 53.8% of those patients underwent concomitant ascending aorta replacment[154]. They observed aortic dilation in 29% of patients, encompassing aortic root dilation in 36% and tubular ascending aorta dilation in 36%, as well as both root and ascending aortic dilation in 29% of patients. There were 79% mild and 21% moderate cases of aortic dilation. The aortic root dilation in QAV was attributed to elastic disruption of the aortic ring[163].

1.4 Aortic dissection

An untreated AsAA can lead to an aortic rupture, with 26% of mortality[3]. Moreover, the surgical mortality of Stanford type A aortic dissection is as high as 18% to 25%, associated with high morbidly like renal failure, cerebral damage, etc[4]. The rupture of the aortic inner membrane causes aortic dissection (AD) due to blood entering the aortic wall after the rupture of the medial layer[165] (Fig. 1-22). Aortic dissection develops as a tear in the intima of the aorta, resulting in the formation and spread of a hematoma. The result is that the aorta has both true and false cavities (lumens), often referred to as double-lumen aorta. Usually, the false lumen can have a bigger surface which may compress the true lumen[47]. The aortic dissection can progress along with the aorta and the collateral arteries, which may create malperfusion syndrome. Aortic dissection is one of the most complex and dangerous cardiovascular diseases[166]. Aortic dissection is characterized by acute onset, rapid progression, multiple clinical manifestations, high misdiagnosis, and fatality.

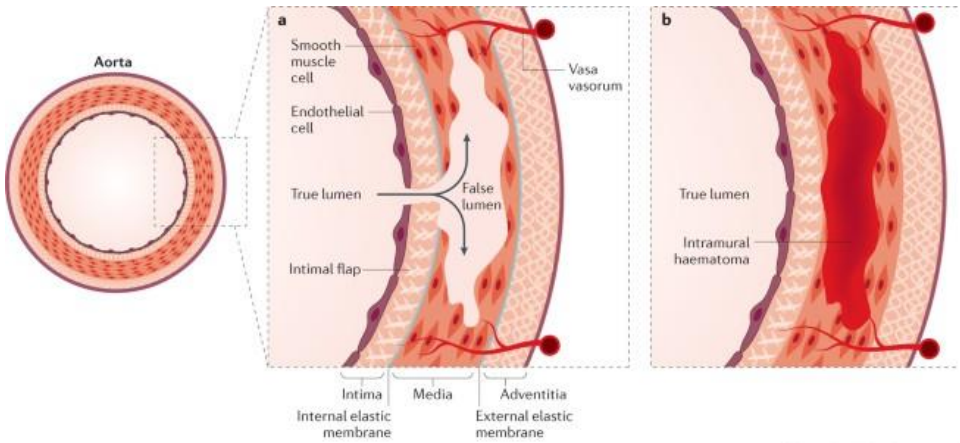

Figure 1-22. Microstructure of aortic dissection. (From Nienaber et al., 2016 [167])

In recent years, due to the aging population and the increasing incidence of hypertension, the incidence of aortic dissection has been increasing year by year[108,166,168]. Due to the complex clinical manifestations and high rate of missed diagnosis and misdiagnosis, the untreated acute aortic dissection mortality rate was 21% in the day, 37% on the second day, and 74% in the first week[169]. Meanwhile, the mortality is increased as 1 % per hour during the first 48 hours. According to statistics, the incidence of the disease can be as high as 10-29 cases per 1 million people every

year[170]. In the United States, there are about 10,000 new cases every year[171], and most of them occur in winter and spring. The incidence of the male is significantly higher than that of females, and the ratio of males to females is 2-3:1. However, the mortality rate in females is significantly higher than in males, which may be related to the older onset age, the gradual occurrence of pain, or the indiscernible pain leading to delayed treatment[172,173].

1.4.1 Aortic dissection classifications

Acute and chronic aortic dissection can be classified according to the time of occurrence, with acute active dissection occurring within 14 days and chronic aortic dissection lasting longer than 14 days[174]. Meanwhile, Giannakoulas et al.[175] put forward the concept of subacute phase, which refers to the subacute phase of dissection between 14 days and two months, and the chronic dissection after two months.

DeBakey [176] and Stanford[177] classification classifies the aortic dissections according to aortic dissection involvement and range. DeBakey classified aortic dissection into three types: Type I aortic dissection includes the entire aorta; Type II aortic dissection only involves the ascending aorta; Type III involves descending aorta starting from the subclavier artery, with type IIIba in the upper diaphragm and Type IIIb in the lower septum[178] (Fig. 1-23).

Stanford classification was divided AD into types: Type A refers to the aortic dissections which involve the ascending aorta +/- aortic arch; Type B refers to the aortic dissection, which is only located in the descending aorta, starting from the left subclavian artery. Stanford Type A corresponds to DeBakey Types I and II, and Stanford type B corresponds to DeBakey III (Fig. 1-22).

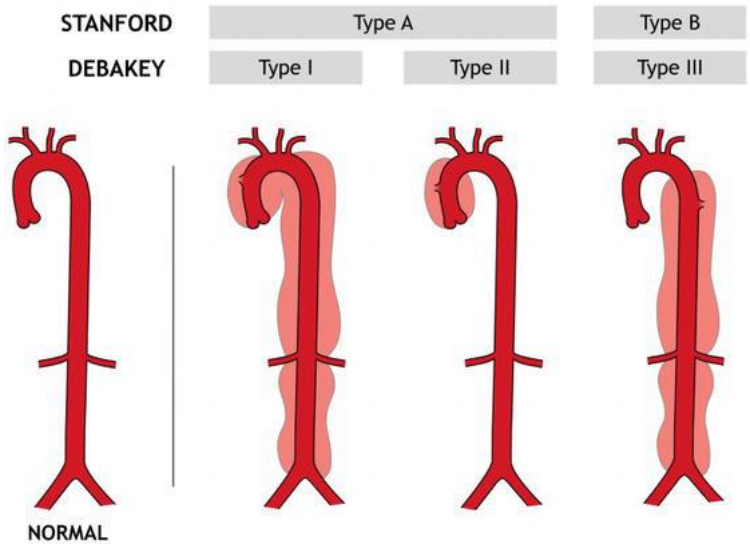

Figure 1-23. Stanford and De Bakey Classification for dissection. (https://www.intechopen.com/chapters/69460, viewed 31.08.2021)

In surgery, Stanford classification has largely replaced DeBakey classification because it is more practical in decision-making[179].

1.4.2 Pathology, symptoms, and treatment of aortic dissection

Aortic dissection is common in men over 50 years of age and presents as a sudden onset of severe splitting or laceration pain behind the sternum or between the scapulas. It can associate with syncope, sometimes with stroke, heart or kidney failure, abdominal or peripheral ischemia due to the malperfusion organ. If aortic dissection is suspected, it is obligated to consider diagnostic imaging tests, which include computed tomography (CT) scans, magnetic resonance imaging, and transthoracic or transesophageal echocardiography. Emergency surgical repair is necessary when the ascending aorta or aortic arch is involved.

- **Pathology**

The pathology of aortic dissection stays unknown, but it has been established that it is a multifactorial disease with a high mortality rate. Researchers show that hypertension and arteriosclerosis are the most common causes of aortic dissection, followed by aging, coronary heart disease, Marfan syndrome, and other inheritance disorder[8,180,181]. More than 80% of patients with aortic dissection are associated with hypertension. Many studies have shown that aortic dissection is more related to the amplitude of blood pressure fluctuations than the maximum blood pressure value[182,183]. Long-term hypertension leads to aortic fibrosis, calcification, or decreased aortic elasticity. If these pathological states are not controlled, the lumen of the aortic wall can be narrowed. The aortic wall is highly resistant to pressure for healthy adults. And the defects in the aortic wall (especially in the medial layer) are the primary condition for aortic wall rupture. Generally, in the elderly, degenerative lesions of the intermediate layer aortic wall are predominant. In young patients, the primary cause can be the reduction of elastic fiber. If there the patient is associated with atherosclerosis, the aorta can be less elastic, which can increase the incidence of aortic dissection. Other aortic dissection causes, such as Marfan syndrome with inherited connective tissue defects[184] risk and autoimmune diseases (systemic lupus erythematosus, iatrogenic factors, trauma, etc.), are also factors for aortic dissection. Some studies have found that aortic dissection can also occur during pregnancy[185], especially in women with Marfan syndrome and bicuspid aortic valve disorder.

Degenerative changes caused by cystic necrosis of the aortic medial layer are the prerequisite for forming aortic dissection[186]. The pathological basis of these changes of aortic dissection is the degeneration of collagen and elastic tissue. The main pathological changes were the local fracture or necrosis of elastic fibers in the medial layer of the aorta. Connective tissue diseases are genetically characterized by medial

layer cystic changes, which are common in patients with Marfan and Turner syndromes. Due to the high flow impact at the level of ascending aorta, it is more common that aortic dissection happens in the ascending aorta than in other aortic regions. However, it is less severe at the distal end of the aortic arch since the flow impact is reduced. Once the aortic wall is ruptured, blood and clots can accumulate in the false lumen of the aortic wall.

- **Symptoms**

Aortic dissection is a disease with complex and variable clinical symptoms. The particular symptoms are laceration pain and elevated blood pressure. Pain is the most common symptom, which is usually in the front or back of the chest[4]. More than 90% of ascending aortic dissections present with chest, neck, throat, and jaw pain. Most descending aortic dissections present with scapular pain[187]. Sometimes the migration of the aortic dissection in the descending aorta may also present with other pain symptoms, such as back pain, low back pain, and lower limb pain. However, in elderly patients, the pain symptoms are not typical, leading to missed diagnosis and misdiagnosis. The blood pressure of more than half of the patients increased at the onset of the disease, and some blood pressure asymmetry may be observed in peripheries secondary to the members malperfusion. About half of the patients have the symptoms of skin whitening, increased respiratory rate, and massive sweating.

Severe shock and death may occur when aortic dissection ruptures and results in pericardial or pleural effusion, creating cardiac tamponade or hemorrhagic shock. Due to collateral arteries dissection, malperfusion syndrome can occur during aortic dissection. The myocardial infarction may be another reason for the death. Acute myocardial infarction can occur when the endovascular rupture of the proximal dissection covers the ostium of the coronary sinus, or the dissection is extended to the coronary artery. Since it usually affects the right coronary sinus, it is more common to have inferior wall myocardial infarction. Some degree of dizziness, syncope, or even stroke may be detected if supra-aortic trunks are involved. The dissection of the descending thoracic aorta may create medullary ischemia with paraplegia. When it is associated with abdominal arteries, the patient may have abdominal pain with visceral ischemia like mesenteric, which could be fatal. Involvement of the renal artery may present with hematuria, oliguria, and renal impairment. If the hepatic artery is involved, jaundice and elevation of serum transaminase can also occur when the AD ruptures. Lower extremity pain, skin cooling, and other lower extremity ischemia symptoms can appear if the abdominal aorta or iliac artery are involved.

Aortic valve insufficiency is caused by dissection of the aortic root, particularly sinotubular junction, which can provocate prolapsus of the commissure of the aortic valve to create aortic valve insufficiency. Another etiology is the prolapsus of the intimal flap in the aortic valve during the diastole, or avulsion of the annulus due to dissection flap. This situation may provoke cardiogenic shock.

- **Treatment**

Type A aortic dissection is a very dangerous disease with rapid progression and a high mortality rate. Therefore, the treatment of aortic dissection is very important. Medication should bring blood pressure to a reasonable range before treatment, whether surgery or interventional therapy is selected. In the over-acute phase, the target of hypotension is 100-120mm Hg[188–190]. Relieve pain and pay attention to rest. Antihypertensive medications (β blockers, Ca blockers) are used to reduce blood pressure, and analgesics can be used for severe pain. The gold standard is aortic resection and replacement by prosthesis of the ascending aorta in Type A aortic dissection. If the horizontal aorta is involved, the aortic arch should be totally or partially replaced. If the aortic root is involved or dilated, the aortic valve can be replaced, depend on the aortic valve disease. The descending thoracic aorta dissection is treated preferentially by a conservative way using the hypotension medications. Endovascular surgery should be performed if the medical treatment is not efficient[47].

In the chronic phase, the main treatment goal is to prevent the recurrence of dissection and rupture and perform surgery at a selective time. Whether Type A or Type B aortic dissection, the existing dissection and long-term postoperative complications are important issues.

Chapter 2 - Biaxial tensile test

In recent years, more and more research on the biomechanical properties of the aorta has been published in purpose to explore the characteristics behavior of the aortic wall. The main experimental methods are the uniaxial tensile test, biaxial tensile test, and inflation tests. Each of these techniques has advantages and shortcomings. In this thesis, the biaxial tensile test is the main experiment method used to obtain the ex-vivo biomechanical properties.

2.1 State of the art

The aorta is located in a complex human environment. A study dating back to the late 19th century demonstrated that blood flow and pressure changes contribute to lumen radius and wall thickness changes[191]. Precisely, Roy demonstrated that aortic elasticity exhibits nonlinear behavior, with higher dilation in physiological stress and lower dilation under high pressure[191]. Its biomechanical behavior is sensitive to the environment, temperature, and loading rate. It makes researchers put forward a complex problem on accurately describing the aortic wall's biomechanical properties. In the experimental and biomechanical analysis of aortic materials, it is necessary to know the performance of the aorta in advance and choose proper experiment conditions according to the known structure. In general, the aortic wall can be regarded as a typical soft tissue and multilayer composite material with the following mechanical properties:

1) **Heterogeneity**. Aortic wall composition and structure can be different due to physiological changes because of growth and remodeling in the presence of complex mechanical and physiological influences[15].
2) **Anisotropy**. The mechanical response of the aortic wall varies along the direction of the material. It is caused by the circumferential cyclic loading of the cardiovascular system. Generally speaking, the circumferential force stimulation of the healthy aorta leads to the increase of the distribution of elastic fibers and collagen fibers along the circumferential direction and leads to the circumferential tissue stiffness higher than the longitudinal tissue stiffness.

3) **Nonlinearity**[192]. The stress-strain curves of blood vessels in tension are usually nonlinear. This is caused by the collagen fibers gradually being pulled apart during loading.
4) **Incompressibility**[193]. The early experimental results of Thomas et al. showed that the maximum volumetric compression strain of the aorta was 0.0165%, and the mean volumetric modulus was $4.44\times10^{6}g/cm^{2}$. It shows that the volume of the aorta is conserved when stretched. Therefore, in the case of only principal strain and no shear strain, the longitudinal, circumferential, and radial tension coefficients (stretch ratio) of the aorta satisfy that the product of the three phases is 1.
5) **Hyperelasticity**[194]. In the fatigue test, the loading and unloading curves of aortic tissue are not fitted. Meanwhile, these curves have prominent hysteresis rings, which show viscoelastic characteristics.
6) **Residual Stress.** It refers to the more evenly distributed stress in blood vessels under normal conditions[195], which is related to proteoglycans in the aortic wall[196].

Based on these characteristics, currently, there are several biomechanical experimental methods associated with the aortic wall, including three principal types: uniaxial tensile test, biaxial tensile test, and inflation test.

2.1.1 Uniaxial tensile test

At present, most of the aortic biomechanics experiments are based on the theory of Fung et al. [195]. They helped advance the ability to quantify arterial wall stress and the associated stiffness, which are crucial for evaluating the wall's mechanics. Their uniaxial tensile studies on soft tissues demonstrated an intimate relationship between material stiffness and stress. More importantly, they firstly described that stress increases almost exponentially with stretch.

Uniaxial tensile tests can measure the tension and the stress of material in a single direction. Uniaxial machines can be divided into horizontal uniaxial stretching or vertical uniaxial stretching (Fig. 2-1). Also, the stretching method can be divided into unilaterally fixed stretching or simultaneous bilateral stretching.

The uniaxial tensile test is widely used in aortic wall biomechanics on not only animals but also humans. The earliest records date back to Mohan and Melvin's abdominal aortic biomechanics experiment in 1982[197]. In the decades followed, more and more studies on the aorta were published. These include aortic biomechanics studies in rats, horses, pigs, and other animals[198–202]. Among these, more studies are on the aorta of pigs.

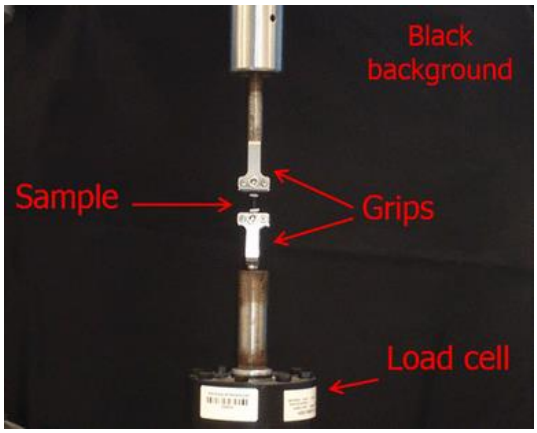

Figure 2-1. Uniaxial tensile test machine (vertical uniaxial stretching). (From de Gelidi et al., 2016 [203])

To review the uniaxial tensile experiments, Table 2-1 documents the published studies according to the anatomy location, the status of the sample, the pathological classification of the sample, the number of samples, the aortic quadrants obtained, and the direction of the uniaxial stretch. The state of the samples before the experiment (fresh or thawed) and the storage time of the samples have been specially marked. The samples were divided into ascending thoracic aorta (ATA) and descending thoracic aorta (DTA) according to the anatomical position of the aortas. In biomechanical experiments, the state of the sample is critical. The samples are classified into healthy samples and aortic aneurysm samples. Aortic aneurysm samples are divided into aneurysms with Marfan syndrome, aortic aneurysm samples with tricuspid aortic valve (AsAA-TAV), and aortic aneurysm samples with bicuspid aortic valve (AsAA-BAV). The number of cases in these studies is indicated in the table. Aortic quadrant refers to aortic sample partitioning. Due to the definition of partitioning varies among different works of literature, this section will be annotated according to the anatomy standards (Fig. 2-2). The experiment of the aortic wall can be defined into circumferential and longitudinal directions corresponding to the direction of blood flow in the aorta.

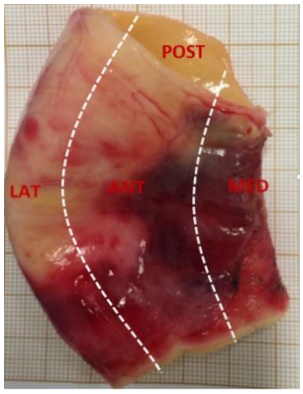

Figure 2-2. Regional division of ascending aortic aneurysm. LAT = lateral; ANT = anterior; MED = medial; POST = posterior

Year	Authors	Anatomy location	Tissue statue	Pathologies	Population	Aortic quadrant	Direction
1982	Mohan and Melvin[197]	DTA	1-7 days in fridge	Healthy	31	ND	LON/CIR
1996	Raghavan et al. [204]	ATA	within 24 h in fridge	Healthy	7	ND	LON
				Aneurysmal	45	ND	LON/CIR
2003	Vorp et al.[11]	ATA	within 48 h in fridge	Healthy	10	ND	LON/CIR
				Aneurysmal	26	ND	LON/CIR
2006	Di Martino et al.[9]	ATA	within 48 h in fridge	AsAA - unruputed	16	ND	CIR
				AsAA - ruputed	9		
2002	Okamoto et al.[205]	DTA	1-4 days in fridge	AsAA - Marfan Syndrome	6	ND	CIR
				AsAA-BAV	33	ND	CIR
				AsAA-TAV	15	ND	CIR
2009	Iliopoulos et al.[12]	ATA	within 24 h in fridge	Aneurysmal	12	Medial, anterior, lateral, and posterior	ND

Year	Authors	Anatomy location	Tissue statue	Pathologies	Population	Aortic quadrant	Direction
2010	Duprey et al.[13]	ATA	within 48 h in fridge	AsAA-BAV	6	Medial/Lateral	LON/CIR
				AsAA-TAV	6	Medial/Lateral	LON/CIR
2012	García et al.[206]	ATA	within 24 h in fridge	Healthy	23	ND	LON/CIR
				AsAA-TAV	14		
2013	Khanafer et al. [207]	ATA	within 48 h in fridge	Aneurysmal	3	ND	ND
2014	Forsell et al.[208]	ATA	ND	AsAA-TAV	11	ND	ND
				AsAA-BAV	13		
2018	Ferrara et al.[209]	ATA	12 - 48 h in fridge	Aneurysmal	68	Medial + Lateral	LON/CIR
2019	Sherifova et al.[210]	DTA	-24°C （8 - 154 days）unfreeze	Healthy	12	ND	LON/CIR
				Aneurysmal	9		
2021	Amabili et al.[211]	DTA	within 48 h in fridge	Healthy	13	ND	LON/CIR

Table 2-1. Literature review of the uniaxial tensile test on the human aorta. DTA = descending thoracic aorta; ATA = ascending thoracic aorta; AsAA-TAV = ascending aortic aneurysm associated with tricuspid aortic valve; AsAA-BAV = Ascending Aortic Aneurysm Associated with Bicuspid Aortic Valve; ND = not defined; LON= longitudinal; CIR = circumferential.

Vorp et al.[11] conducted uniaxial tensile tests on the human ascending aortic aneurysm and healthy ascending aortic tissue in both longitudinal and circumferential directions and found that the aneurysm tissue showed low stress in both longitudinal and circumferential directions. Using similar research methods, Iliopoulos et al.[12] showed that AsAA is the heterogeneity, with the lateral region longitudinally being the weakest and least stiff. Ferrara et al. found that the AsAA tissue shows a stiffer value in the circumferential direction than the longitudinal direction, greater curvature than smaller curvature[212]. However, the research of 21 aortic walls (12 healthy control samples and 9 aneurysmal samples) showed that the failure stress of longitudinal is higher than circumferential direction[213]. Meanwhile, a relative advantage in strength and stiffness was also seen in the medial quadrant (Fig. 2-2) compared to the lateral one for a circumferential orientation. In contrast, the longitudinal one shows the opposite.

In general, the uniaxial tensile method has the following advantages:

- Only a small sample width or length (1 cm) size is required.
- Samples can be loaded to an extensive strain range (elongation greater than 1.6).
- The implement is simple.

However, there exist certain inconveniences:

- A single sample can only show one orientation of biomechanical characteristics. However, as shown previously, the aortic tissue can be anisotropic.
- The experiment is mostly holding the aorta through grips, so the failure rate in the experiment is relatively high. It can be due to excess or insufficient clamping force, which leads to sampling sliding.
- The current uniaxial tensile test is to obtain samples by punching a bone-like cutter (Fig. 2-3). During the shearing of thick aortic samples, the impact on the cutter may cause pre-damage to the samples, which can lead to a larger area of the upper surface and a smaller area of the bottom surface. Sheared samples and trapezoidal lateral sections, affecting the experimental results.
- In most uniaxial experiments, the number of samples of each aorta is not the same, which will lead to different weights of different aortic walls in the final results and affect the authenticity[209].

Figure 2-3. Bone-shaped punch cutter for uniaxial tensile test. (From Lim and Hoag, 2013 [214])

2.1.2 Biaxial tensile test

The typical structure of the biaxial tensile testing machine is with four drivers, which can be independently controlled for load or displacement of each driver to realize the test of two loading directions. However, due to the influence of sample structure or clamping method, currently, most of the biaxial tensile deformation of the aortic sample tested is generally less than 50%. The main controversy in biaxial tensile experiments on the aorta is how the samples are fixed. In traditional biaxial tensile tests, the material is usually cut into a cross shape and gripped through grips (Fig. 2-4). However, the large sample area required for the cross shape is not common in aortic experiments. In existing biaxial tensile tests, the samples are usually fixed with hooks.

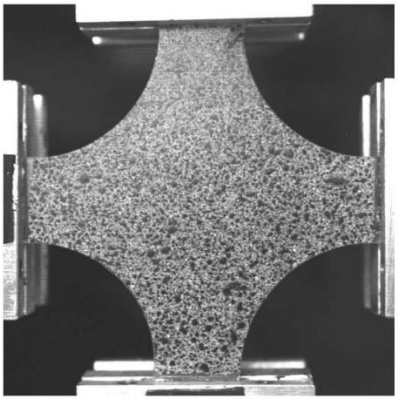

Figure 2-4. Cross-shaped sample fixing in the traditional biaxial tensile test. (From Seibert et al., 2014[215]*)*

Similar to the uniaxial experiment, the main aortic study material is the thoracic aorta on animals[216–218]. More and more biaxial tensile experiments have been reported in human aorta biomechanical properties research in recent years (Table 2-2).

In the manner of biaxial tensile tests, we try to have a review of the published research comparison. Table 2-2 documents the studies according to the anatomy location, the status of the sample, the pathological classification of the sample, the number of samples, the aortic quadrants obtained, and the holding method. The holding method refers to the way the specimens are connected to biaxial tensile arms. It is recorded as grips or hooks. Apart from the holding method, other catalogs have been mentioned in the uniaxial tensile test literature review.

Year	Author	Anatomy location	Tissue statue	Pathologies	Population	Aortic quadrant	Holding Method
2006	Vande Geest et al.[219]	ATA	within 48 h in fridge	Healthy	8	ND	ND
				Aneurysmal	26		
2009	Choudhury et al.[220]	ATA	within 24 h in fridge	Healthy	5	Medial, anterior, lateral, and posterior	Surgical hooks
				AsAA-TAV	5		
				AsAA-BAV	6		
2012	Haskett et al. [221]	ATA	within 36 h in fridge	ND (obtained from autopsy)	31	ND	Barbless hooks
		Aortic arch					
		Descending aorta					
		Suprarenal aorta					
		Abdominal aorta					
2012	Azadani et al. [222]	ATA	within 24 h in fridge	Healthy	19	ND	Fishhooks
				Aneurysmal	18		
2012	Azadani et al.[223]	ATA	within 24 h in fridge	Aneurysmal	14	Anterior and posterior	Fishhooks
		Aortic sinuses					

Year	Author	Anatomy location	Tissue statue	Pathologies	Population	Aortic quadrant	Holding Method
2013	Pham et al.[224]	ATA	unfreeze	AsAA	20	ND	ND
				AsAA-BAV	20		
				AsAA-BAA	15		
2019	Deplano et al.[225]	ATA	within 50 h in fridge	Healthy	5	ND	Barbless hooks
				Dissected	3		
2019	Di Giuseppe et al.[15]	ATA	-80 °C unfreeze	AsAA-TAV	26	Medial, anterior, lateral, and posterior	Fishhooks
				AsAA-BAV	10		

Table 2-2. Literature review of the biaxial tensile test on the human aorta. ATA = ascending thoracic aorta; PA = pulmonary artery; AsAA-BAA = ascending aortic aneurysm associated with bovine aortic arch; AsAA-BAV = ascending aortic aneurysm associated with bicuspid aortic valve; ND = not defined; LON= longitudinal; CIR = circumferential.

Vande Geest et al.[219] found out that the circumferential stiffness of the aneurysmal aorta increased compared with the healthy aorta. Choudhury et al.[220] has found that lateral quadrants of the aorta showed a higher stiffness. Meanwhile, the average stiffness of the aorta associated with TAV tissues was lower[220]. Among all the studies, the study of Azadani et al. was based on the human ascending aortic aneurysms and aortic root samples[222,223]. According to them, the ascending aorta exhibits nonlinear responses and isotropy to biaxial stress loads in both circumferential and longitudinal directions. The ascending aorta aneurysm is significantly stiffer than the normal aorta.

Biaxial tensile tests in common aortic sample applications have the advantages of:

- Small sample size (1.5 cm × 1.5 cm or 2.0 cm × 2.0 cm)
- Access to measuring circumferential and longitudinal data on the same specimen.

However, some disadvantages cannot be avoided:

- A common way to fix a sample is to load with grips. As discussed in the uniaxial test section, there is a certain level of sample loading failure during the manipulation of the grips. Since the samples in the biaxial tensile tests should be fixed in two directions (four grips), the risk of failure is more elevated (Fig. 2-5).

Figure 2-5. Grips loading in the biaxial tensile test.

- Most of the hooks used, according to the literature, are fishhooks with barbs (Fig. 2-6). In the sample installation, the barb can provocate a bigger hole than those without barbs. Meanwhile, it is possible to damage the sample during the loading process.

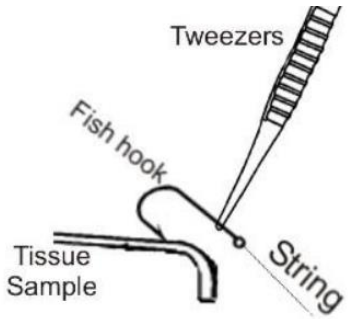

Figure 2-6. Fishhook loading process.

2.1.3 Inflation test

The budge inflation tests are based on the theory of biaxial tensile tests. The surrounding area is fixed in an inflatable device to form a sealed or fixed surface. Fluid can be injected at a controlled rate to expand the tissue until it ruptures. The pressure can be measured during the experiment (Fig. 2-7).

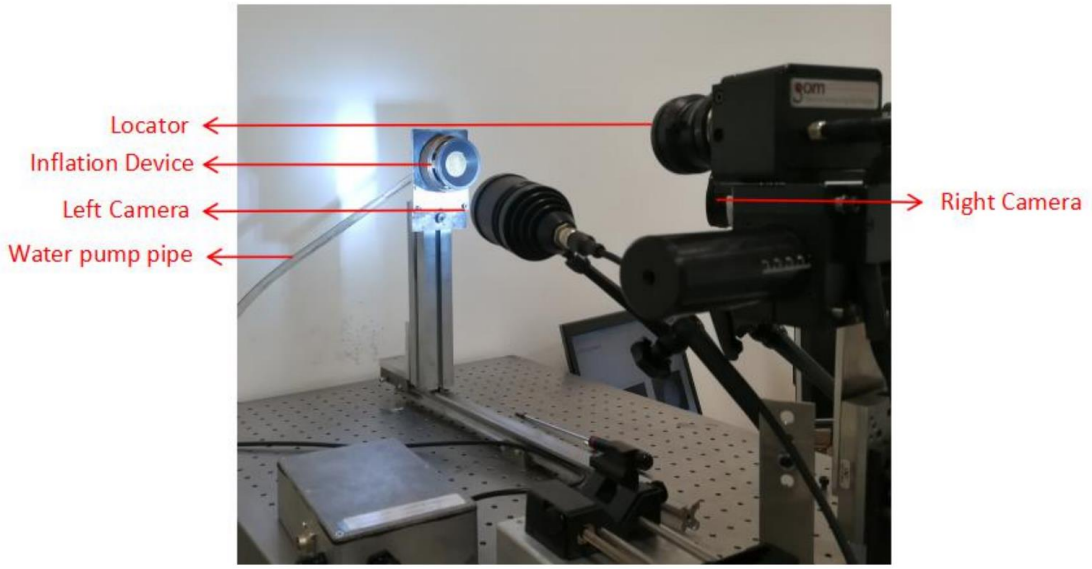

Figure 2-7. Inflation test machine.

The study of Kim et al. showed the circumferential mechanical properties of descending aorta[226]. They found that the stiffness of the dorsal aortic wall is greater than that of the ventral aortic wall[227]. There is another study of the distension experiment on the human aorta published by Duprey et al.[14]. They conclude that aortic rupture can be strongly associated with the physiological modulus of tissues' elasticity. According to them, the patient's age, the ascending thoracic aorta's diameter, and the valve's actual phenotype are irrelevant. Another inflation test on biomechanical properties differentiates the media and adventitia layer of healthy aortas and aneurysms. They showed that the media layer has less stiffness than the adventitia and the aortic wall is less stiff in the healthy aortic wall than in the aneurysmal aortic wall[226].

The inflation test is one of the best experimental methods that can simulate the way of aortic rupture. It has the advantage of measuring circumferential and longitudinal directions as the biaxial tensile test. Moreover, with a proper calculation method, the measurement can be multiaxial.

However, inflation tests also have limitations: a large aortic sample size (4 cm × 4 cm, or more) is required[226]. Due to the anatomy of the aorta, it is impractical to obtain a 4 cm length of the aortic wall in all quadrants, especially the medial quadrant up to 4cm. Therefore, inflation tests are often unable to test various areas (greater curvature and

smaller curvature) of the aorta. Unfortunately, existing aortic studies[220] have shown that the medial quadrant has less stiffness value, which can be the key to the biomechanical properties study of the aorta.

In general, the patients with an aortic aneurysm are around or more than 65-year-old or even older[228]. The local area of the aortic wall can be defective as a reason of calcification, which makes it complicated to provide the large surface of the experiment request. In the final results, it is possible to obtain the output of the calcified region instead of the original aortic wall. It can lead to the results being incomparable.

2.1.4 Discussion

As discussed previously, uniaxial, biaxial, and inflation tests have been wildly used in exploring the biomechanical properties of the aorta.

In the mentioned publications above[9–14,197,204–209,211–213,219–228], the main research discussions of biomechanical experiments are as follows: 1. Is the aortic wall anisotropic or isotropic? 2. Does the aortic wall present regional heterogeneity? 3. What are the factors that affect the biomechanical properties of aortic aneurysms?

- **Directional effect**

The results of most biomechanical experiments showed that the aortic wall presents anisotropy and nonlinearity[12,209,212,213,219,222,224]. However, it is still controversial whether the aortic stiffness is higher in the circumferential or the longitudinal direction. A higher aortic wall stiffness was found in the circumferential direction than in the longitudinal one, in most publications[11,12,209,224]. On the contrary, some studies demonstrated that the aortic walls in both ascending aorta and aortic sinuses are isotropic[223,229]. This theory was also supported by Choudhury et al.[220] with their research on 16 ascending aortic samples. Sherifova et al. proposed that a higher circumferential aortic stiffness can be found in the healthy control aorta, while the aneurysmal aorta showed isotropy behavior[210]. According to a study of 31 autopsies, the aorta shows more anisotropic after the age of sixty[221]. Meanwhile, the distal aorta acts more anisotropic than the proximal aorta[221].

- **Regional effect**

In the regional point of view, the quadrant with greater curvature (lateral quadrant in Fig. 2-2) is stiffer than the in small curvature (medial quadrant, Fig. 2-2)[13,207,220]. Theoretically, under simultaneous pressure, the lateral quadrant can persist a higher elongation than the medial quadrant[13]. According to Choudhury et al., the circumferential direction shows a higher regional heterogeneity, especially in the healthy control group. On the contrary, Iliopoulos et al. found that the ascending aortic tissue had uniform strength and stiffness in the circumferential direction[12]. They showed that the regional heterogeneity was observed only in the longitudinal direction.

To be specific, the anterior quadrant has less stiffness than all other quadrands[12]. Rather than that, some other studies have shown that there is no regional difference observed in the aortic wall stiffness[11,222].

- **Impact of clinical factors of ascending aortic aneurysms**

According to our knowledge, only a few articles discussed the influence of clinical risk factors on aortic aneurysms from the biomechanical point of view. The limitation is usually the sample size[208,220,224]. Most of them compared the stiffness differences of two types of aortic valves (TAV and BAV). Studies indicate that aortic aneurysms associated with BAV are stiffer than the aortic wall associated with TAV[10,13,208,220,224]. The total sample size of these experimental studies was relatively small (from 11 to 35). However, a larger sample size with 68 aortic walls published by Ferrara et al. did not find any difference in the aortic wall stiffness depending on the two valve types[209]. There were also experiments mentioned about the aging impact on aortic biomechanical properties[14,205,207,207,209,224]. Most experiments indicate that aortic strain decrease with age[205,209,224]. Moreover, Haskett et al. found out that with aging, the aortic walls were stiffened[221]. However, there are other studies that have shown no aortic stiffness change with aging[207,209]. Few studies have explored clinical risk factors. Only Pham et al. and Ferrara et al. described patients with hypertension and normal blood pressure[209,224]. Ferrara et al. proved that aortic aneurysms in hypertensive patients had lower stress and strain[209]. Pham et al. suggested that patients with hypertension had a higher longitudinal stiffness than those with normal blood pressure[224]. In comparisons between healthy controls and aortic aneurysms, experiments have shown that the stiffer value can be found in the aneurysmal aorta and aortic dissection than in the healthy aorta[219,222,225]. But it might differ from the quadrants and the directions[220].

To conclude, there is strong debate about the anisotropy or isotropy of the aortic wall in the biomechanical studies of the aorta reported so far. Furthermore, controversial opinions were shown related to the aortic wall regional heterogeneity. In addition, to our knowledge, there is no comparative study on clinical risk factors of ascending aortic aneurysms such as aortic insufficiency, aortic stenosis, coronary artery disease, and aortic diameter.

Before designing the experiment, we need to specify that the experimental method of our work should take into account regional and directional effects at the same time. And it is necessary to collect and consider series of different clinical factors.

On the one hand, the uniaxial tensile test cannot describe the bi-dimensional behavior of the aorta, as it can only be applied in one direction per specimen. According to our literature review, the aorta is more likely to present anisotropy behavior. Therefore, even uniaxial tests provide necessary information about the aorta's mechanical performance according to the literature, they are not sufficient to describe the overall performance of the aortic wall. On the other hand, by the limitation of the aortic size,

the inflation test is restricted to a single aortic location instead of a comprehensive location of the entire aorta.

In our experiment, the biaxial tensile test was used to avoid the above limitations. Firstly, to prevent the aortic wall damage from the grip loading, we used surgical hooks instead of fishhooks (with bards) to avoid damage to the samples. In all aortic biomechanical experiments, samples were preserved freshly in a relatively long duration (within 24 h to 48 h)[9,11–13,60,204–206,208,211,219–223]. Secondly, soft tissue degradation can be found from damage parameters after 24 h conservation[230,231]. Our experiment will try to shorten the storage time of the samples (cf. Table 2-3 for the timeline). Due to the limited sample size (largest study with 68 aortic samples[209]), the current reported biomechanical experiments on ascending aortic aneurysms are limited to comparing aortic valve types, age, and gender. As far as our knowledge, there are no existing biomechanical properties with biaxial tensile tests analysis considering different pathologies of aortic aneurysms.

2.2 Calculation equation

From the mechanical point of view, materials, whether crystalline or amorphous, are not completely rigid. The action of external loads on materials or components can cause deformation. When a material deforms, there is a strain on the particles in all directions internally. Strain can be mainly divided into normal strain and shear strain. The longitudinal length change divided by original length is defined as longitudinal normal strain. The physical meaning is deformation per unit length. When deformation exceeds a certain limit with eliminating the external force, the object can be completely restored to its original state. This deformation is called elastic deformation. In continuum mechanics, the strength of the internal forces is called stress. Stress can also be divided into normal stress (perpendicular to the surface) and shear stress (parallel to the surface).

Young's modulus was named in 1807 after the result obtained by a British doctor and physicist, Thomas Young. Young's modulus is an index to measure the degree of difficulty in producing elastic deformation of solid materials. The higher the value is, the greater the material's stiffness will be, and the greater the strain force will be induced by the deformation of the material. In the elastic range, Young's modulus of most materials follows Hooke's law. It describes the relationship between strain and stress. For the elastic materials, applying a load F can produce a length l change. Where the external force perpendicular to the cross-sectional area is the stress σ, and the length variation in its vertical direction is the strain $\mathcal{E}$.

Cauchy stresses and strains are determined by force and length. Strain indicated the ratio of resting specimen length (after preconditioning) l_0 divided by deformed length ${}_{\Delta}l$, where ${}_{\Delta}l$ is the value difference between the resting specimen length and the load-filled specimen practical length l.

$$\varepsilon = \frac{l - l_0}{l_0} \quad (1)$$

Cauchy stress σ refers to the amount of tensile load F recorded during the test per unit loaded cross-sectional area A of the specimen[195]. In the previous section (section 2.1), aortic tissue can be defined as incompressible. Area A is equal to the resting specimen cross-sectional area A_0, where A_0 can be computed from the load-free specimen thickness and length l_0,

Cauchy stress σ can be computed as:

$$\sigma = \frac{F}{A_0} \quad (2)$$

Based on the stress-strain curve (Fig. 2-8. a), Young's modulus at different stress levels can be calculated as the first derivative of stress overstretch:

$$E = \frac{\sigma}{\varepsilon} \quad (3)$$

Since Young's modulus is the first derivative of stress overstretch, which is the tangent of the stress-strain curve, the second curve of Young's modulus and stress can be computed as Fig. 2-8. b. In our biaxial tensile test, we mainly focus on the maximum value of Young's modulus. It indicates the highest value of the aortic wall stiffness before the aortic rupture.

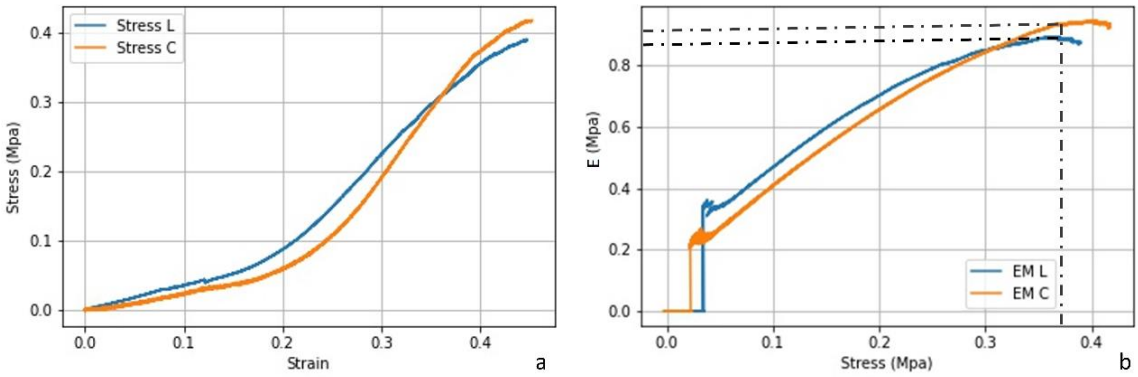

Figure 2-8. Curves computed from biaxial tensile test. a) stress-strain curve, b) Young's modulus-stress curve. Line with dashes refers to the maximum value of Young's modulus of longitudinal and circumferential direction. E = Young's modulus; L = longitudinal; C = circumferential

2.3 Aortic tissue and experimental hooks preparation

All of the human aneurysmal and dissected aortic wall samples involved in this thesis were taken from the Cardio-Vascular and Thoracic Surgery Department of the University Hospital of Dijon, Dijon, France. National ethical committee approval has been obtained (2018-A02010-55). The study has been registered on ClinicalTrials.gov (clinical registration number: NCT03817008). According to French law, no written consent is required for this study. A written summary of the study was provided to all patients according to the ethics committee. Patient consent was obtained verbally, and the investigator physician has signed and countersigned a letter attesting to the patient's consent.

A healthy human was obtained from the autopsy and collected by the Anatomy and Pathology Department of the University Hospital of Dijon, Dijon, France. According to French law, there is no ethical consent required.

The total time between the sample harvested from the surgery (mentioned in section 1.4) and the finalizing of the experiment was no more than eight hours. The main timeline is shown in Table 2-3.

Time	Process
0h	The samples were removed from the patient
+0.5h	The practical aortas were stored and frozen at -80 ℃
+1h	Histological fixations were performed
+3h	In-vitro biaxial tensile tests were carried out
+8h	In-vitro biaxial tensile tests were completed

Table 2-3. The timeline of the aortic samples' preparation

After receiving the samples, each sample was photographed to record the original aortic shape and size. The visible fat outside the outer membrane was carefully removed with surgical used scissors and forceps. Generally, the fat is thicker on the medial edges and lateral quadrants (Fig. 2-9). The thickness of fat in this section can be up to 1.5 - 2 mm, which can have a high impact on the calculation of the stress.

Figure 2-9. The aortic wall without fat removal.

After, the aortic walls were partitioned. A small clip was placed at the distal end of the lateral quadrant of the ascending aorta, which is an indicator of the distal section of the aorta, located between the anterior to the lateral portion of the ascending aorta (Fig. 2-10). The sample was then cut according to four quadrants defined by the location of the heart.

Figure 2-10. The surgical clip on the aorta.

The length of the samples obtained by aortic replacement is from1.8 cm to 3.5 cm for the smaller curvature region (medial) and 3.7 cm - 9.5 cm for the greater curvature region (lateral) (Fig. 2-11. a). The "arrow" mark on the aortic wall refers to the direction of blood flow (Fig. 2-11. b). It is the indication of the longitudinal (LON) and circumferential (CIR). According to the location of the clip, the ascending aorta can be divided into four regions: medial (MED), anterior (ANT), lateral (LAT), and posterior (POST) (Fig. 2-11. c). To minimize the impact on samples during cutting, we did not use a punch cutter similar to the uniaxial tensile test. Instead, a 1.5 cm × 1.5 cm "tattoo" made by the surgical used blue pen is used to identify the sample size. With the help of the surgical used scalpels, the specimen area was separated. If there was adhesion of the aortic specimen border, surgical scissors were used to finalize the cutting process (Fig. 2-11. d). Depending on the size of the aortic wall, in total, 5 to 14 specimens were

sectioned from each aorta. Specifically, the minimum number of the aortic specimens was 5: one specimen each is located in the MED, ANT, and POST quadrants, two specimens in the LAT quadrant. The maximum number of the specimens obtained so far was 14. Two specimens are located in the MED quadrant, 3 specimens in the ANT quadrant, 4 specimens in the POST quadrant, and 5 specimens in the LAT quadrant.

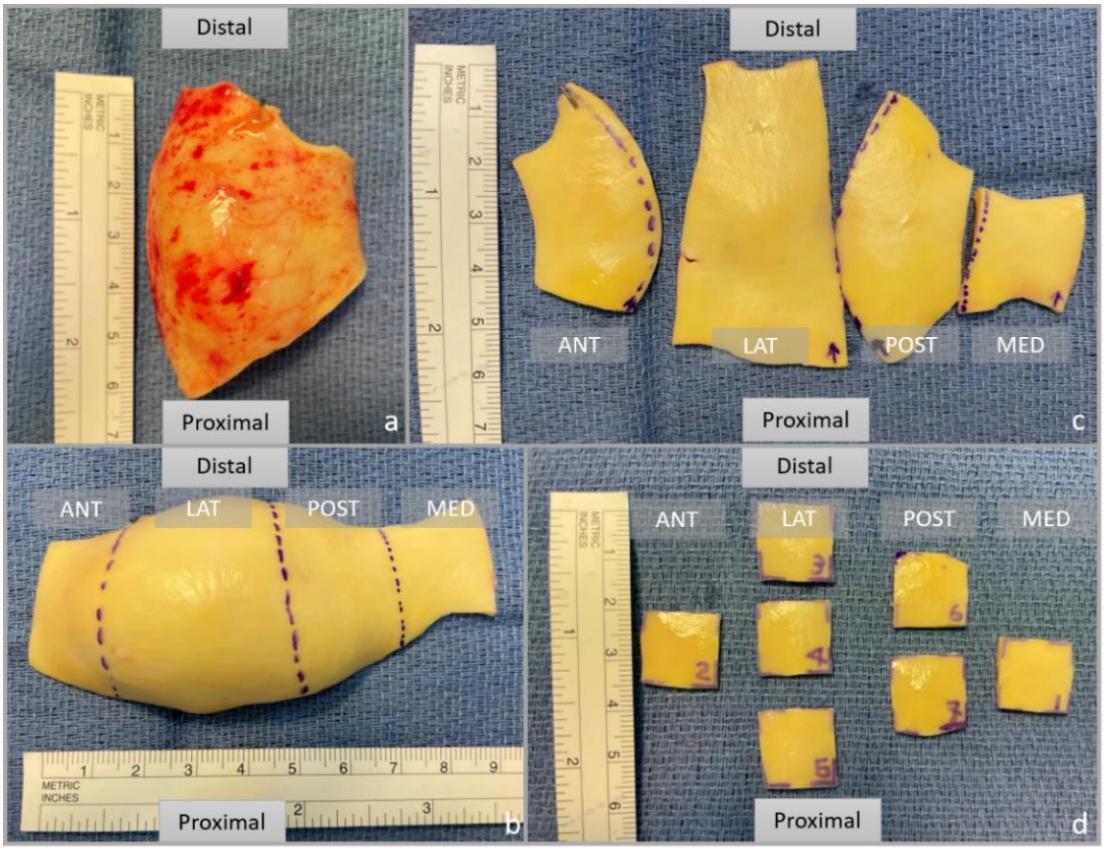

Figure 2-11. Anatomical view of the ascending aortic wall with seven specimens obtained. a) global view of the ascending aorta. b) opened internal aorta according to MED, ANT, LAT, POST, c) separated quadrants, d) specimen view based on quadrants. MED = medial; ANT = anterior; LAT = lateral; POST = posterior.

As described in section 2.1.2, the main shortcomings of the biaxial tensile test are the manipulation of the grips installation and the damage of samples from the fishhooks' barbs. In our experiment, in order to design experiments with less tissue damage and relatively simple specimens installation, we used the surgical used hook, which is a half-circle of 26 mm in diameter (Fig. 2-12. a). Two sutures-holders were fixed in the one-third curvature and two-thirds curvature of the semi-circle hook (marked in red, Fig. 2-12. a), respectively. The curved surgical used hook is shown in Fig. 2-12. b. To ensure that each hook has the same curvature, we used a standard card to calibrate the shape of the hooks (Fig. 2-12. c).

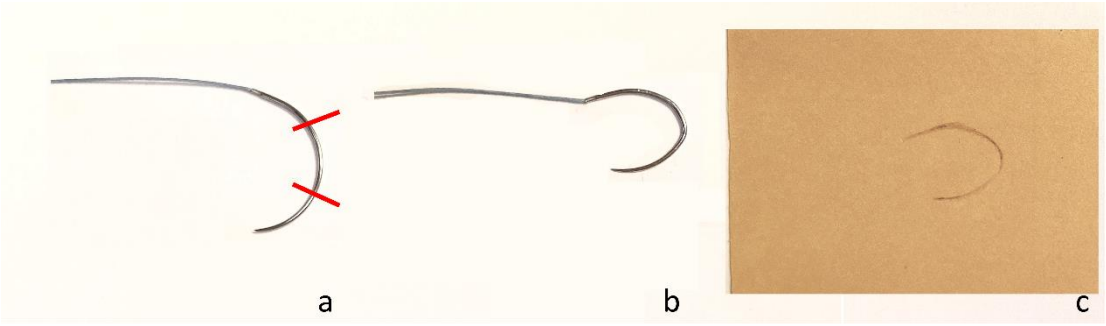

Figure 2-12. The surgical hook preparation. a) original shape of the surgical hook (26 mm diameter) with marks of the suture-holders locations in red, b) curved hook, c) calibration card.

2.4 Aortic wall thickness measurement

The thickness measurement of biomechanical experiments was carried out by an electronic thickness micrometer (Litematic VL-50, Mitutoyo®, Japan, Fig. 2-13). The accuracy of this instrument is 0.01 N. It can minimize the pressure applied to the sample before the experiment.

Figure 2-13. Electronic thickness micrometer (Litematic VL-50, Mitutoyo®)

The thickness of each specimen was measured five times, located in the center and the four corners of the true region of the specimen. Fig. 2-14 indicates the detailed measured thickness location of each specimen.

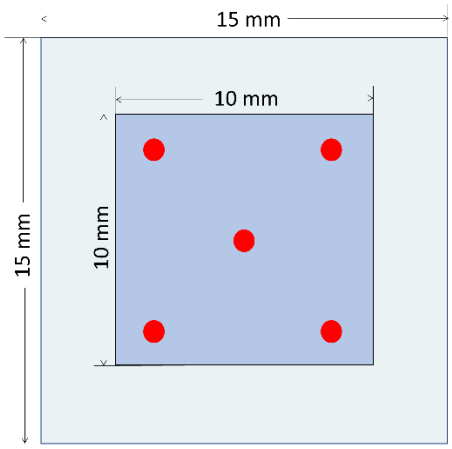

Figure 2-14. Detailed thickness measuring locations (five points in red) in the true zone of specimen in 10 mm square.

An error value of 0.02 mm can be observed during the data recording. It is due to the gravity influence of the measuring arm of the instrument (Fig. 2-15). Therefore, 3 s - 5 s waiting in each measurement record is necessary to avoid value variation.

Figure 2-15. Data displacement on thickness measurement recording.

2.5 Biaxial tensile test setting

The biaxial tensile test machine ((LM1, TA Instruments, ElectroForce® System Group, USA) was used for all of the experiments (Fig. 2-16). The maximum measuring tension of this instrument is 200 N, with a sensitivity of 0.01 N. The tensile arms can be displaced from +6.5 mm to -6.5 mm, with 0.0001 mm of sensitivity.

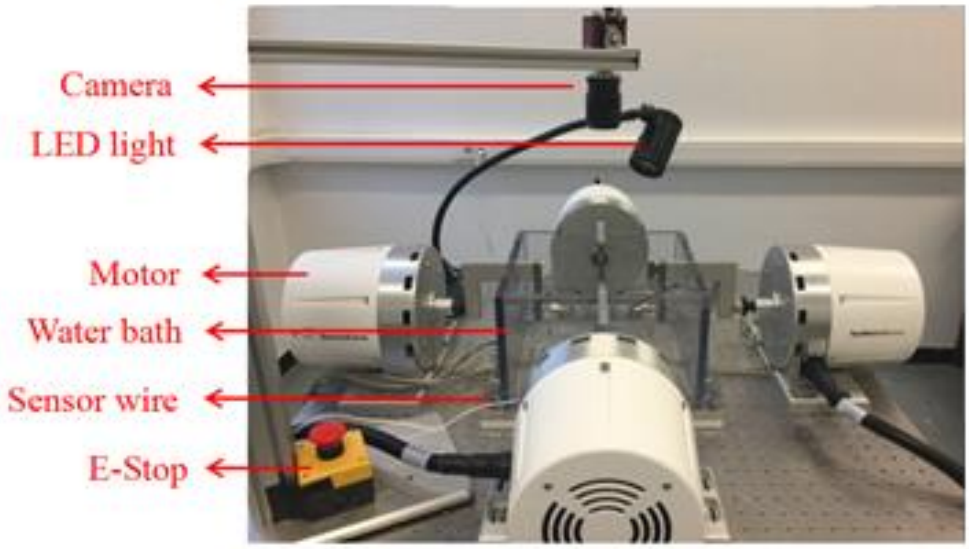

Figure 2-16. Biaxial tensile test machine.

During the experiment, 6.5 L-7 L of the 0.9% concentration of saline water was placed in the water bath to simulate the human body temperature as 37 ± 0.1 ℃.

Sixteen curved surgical hooks with sutures were placed on the specimens (four hooks per side) to be installed on four tensile arms (Fig. 2-17). Most of the surgical hooks were in the shape of a semicircle.

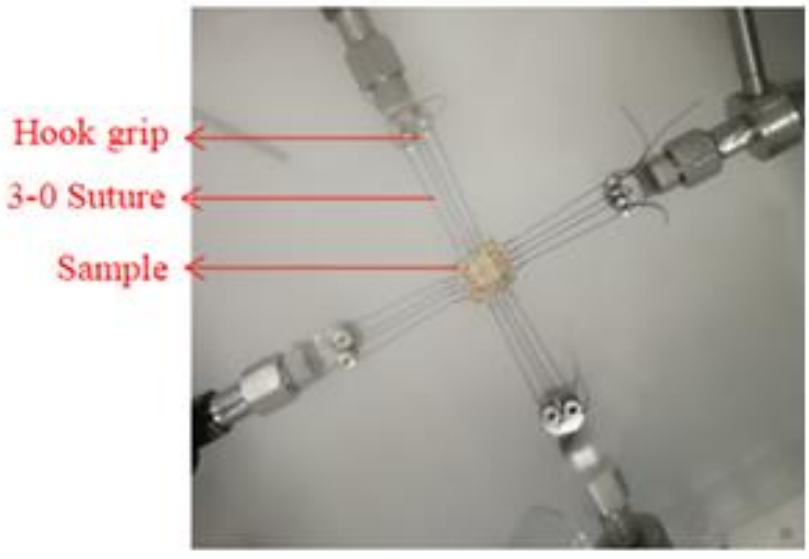

Figure 2-17. Sample displacement during the test.

Among known biomechanical experiments on the aorta, the extent of preconditioning stretching reported is controversial (5% or 10%)[10,11,222]. In order to design the preconditioning values for this experiment, we measured the shrink degree of 20

ascending aortic aneurysm walls. Precisely, the circumference perimeter of the aortic walls was measured once before the entire aortic wall quadrant separation. The second length is measured after the first separation of the aortic quadrant. Two values were recorded respectively to obtain the shrink degree (Table 2-4).

No.	Initial circumferential length (cm)	Post-incision circumferential length (cm)	Shrink degree (%)
1	7.3	6.1	16.44
2	9.8	8.8	10.20
3	9.9	9	9.09
4	11.7	9.6	17.95
5	9.2	8.9	3.26
6	10.2	9.8	3.92
7	14.3	12	16.08
8	9.7	9	7.22
9	13.4	11.1	17.16
10	12.4	10.6	14.52
11	15.2	13.7	9.87
12	12.5	11.9	4.80
13	10.8	9.2	14.81
14	10.6	9.1	14.15
15	11.4	10.9	4.39
16	12.4	11.7	5.65
17	13.1	12.5	4.58
18	12.2	11.4	6.56
19	12.8	12	6.25
20	14.5	13.6	6.21
Mean ± SD	11.67 ± 1.99	10.55 ± 1.88	9.66 ± 5.08

Table 2-4. Shrink degree measurement in 20 ascending aortic aneurysm walls.

The initial circumferential length of the twenty aortic walls tested was 11.67 ± 1.99 mm. The post-insition circumferential length was 10.55 ± 1.88 mm. The shrink degree of the circumferential direction was found between 3.26% to 17.95%, with a mean value of 9.66%. According to this information, the preconditioning can be defined as 10% in

both longitudinal and circumferential directions, with 10 cycles repeated. Moreover, the aortic specimens were stretched at a 10 mm/min rate and load-free setup until rupture.

All operations were manipulated by the WinTest® 8 software (TA Instruments, ElectroForce® System Group, USA, Fig. 2-18). The starting position of the tensile arms was placed -6 mm to ensure that the maximum tensile displacement could be obtained during the experiment. Moreover, the document can be exported as a .csv file with the information of time-based displacements and forces from each tensile arm.

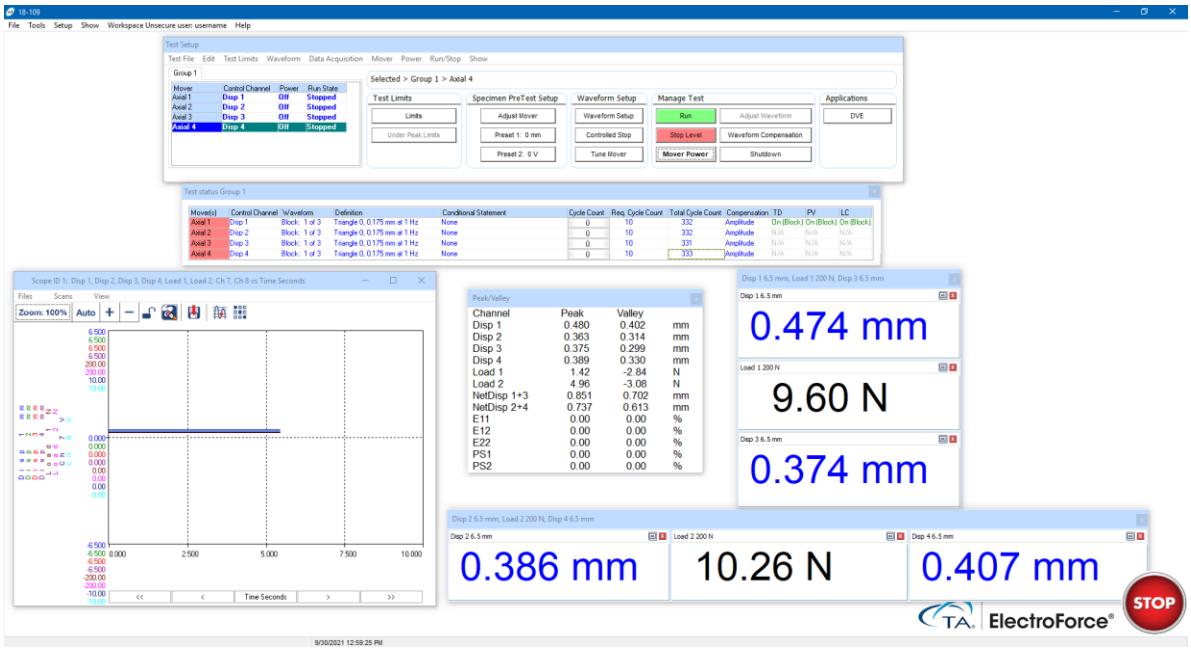

Figure 2-18. WinTest® 8 software platform.

The exported files were computed by Spyder (Anaconda Inc., Austin, TX, USA)[232], which is an open-source distribution of the Python programming languages[233] for scientific computing. The inputs of the computational procedure are the .csv files and the data of the average thickness of the related specimens (marked in the red zones, Fig. 2-19). Based on the information of the specimen installation, the calculation was indicated in two directions (longitudinal and circumferential) of the aortic wall (marked in the green zones, Fig. 2-19). As described in section 2.2, the stress-strain curves and Young's modulus-stress curve were computed (marked in the yellow zone, Fig. 2-19), with the value of maximum stress, maximum strain, and maximum Young's modulus (marked in the blue zone, Fig. 2-19)

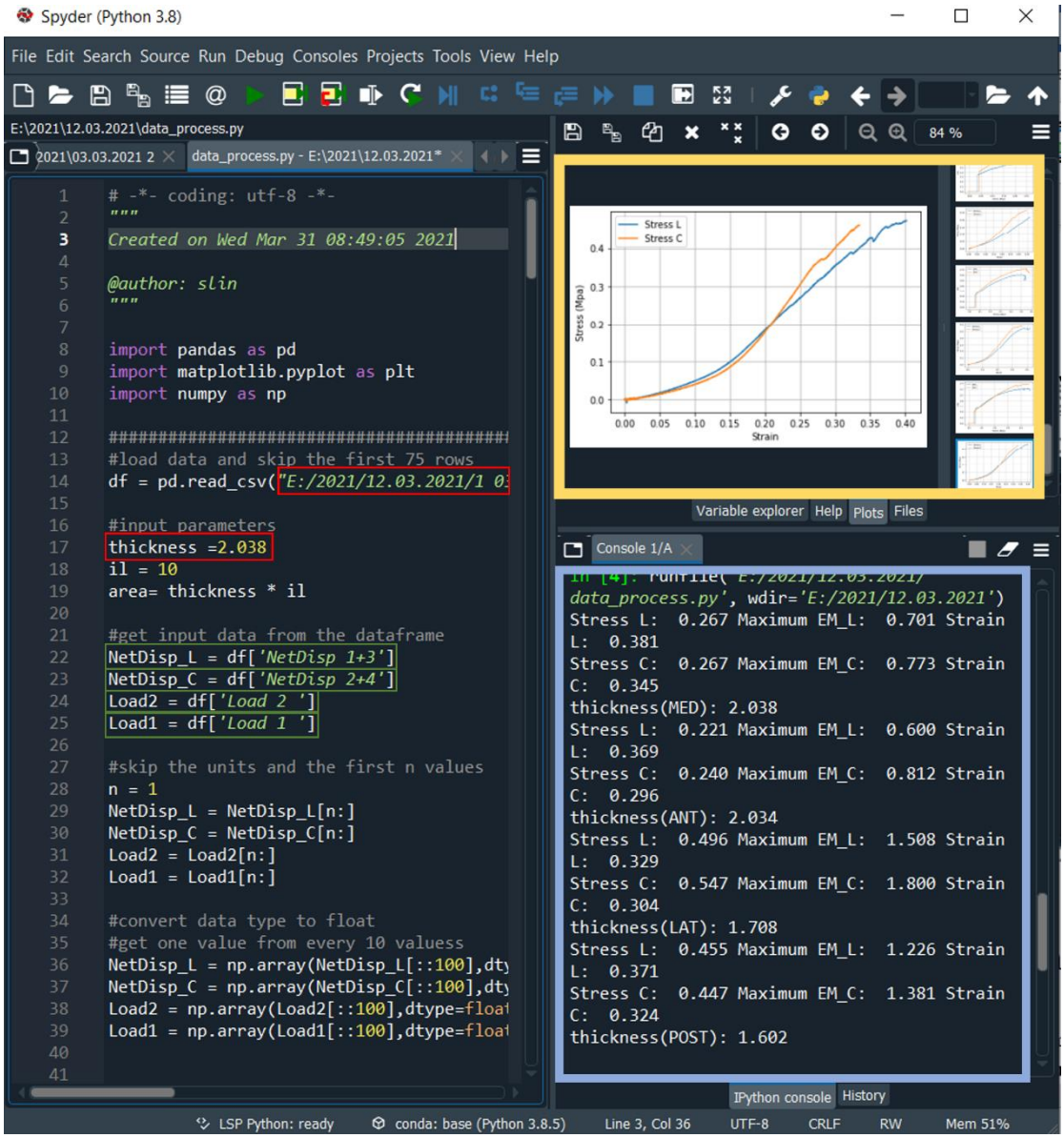

Figure 2-19. The computational data process in Python with the information of the inputs (red zone), directional indication (green zone), output curves (yellow zone), and output values (blue zone).

2.6 Biaxial tensile test on the systematic material

Biaxial tensile tests are widely used in human science. The main application is in the research on biomechanical properties of human soft tissue such as pericardium, heart valves, ligaments, tendons, and skin[234–239]. In recent years, more and more biomaterials and bioprostheses like bioprosthetic aortic valves[239]. In order to make synthetic modeling from the 3D printed aorta in the 4D flow magnetic resonance imaging (MRI), we were looking for a material with similar stiffness to the human aorta. As far as we know, there are no studies on biaxial tensile tests of 3D printed aorta materials.

2.6.1 3D printing technique

3D printing, also known as Additive Manufacturing, is an emerging rapid prototyping technology. Unlike traditional subtraction manufacturing processes, 3D printing is a technique in which materials are deposited or bonded layer by layer to form 3D objects. The 3D printing technique was invented in the United States in the mid-1980s. Charles Hull (founder of 3D systems) and S. Scott Crump (founder of Stratasys®, Rehovot, Israel) are pioneers of 3D printing technology. In the late 1980s and early 1990s, a group of technology companies in the United States, represented by 3D Systems (Washington, USA) and DTM company, successively developed three-dimensional Selective Laser Assimilation (SLA), Selective Laser Sintering (SLS), and Fused Deposition Modeling (FDM) and other mainstream technologies. The most significant difference between 3D printing and traditional manufacturing lies in the process of product formation. In the traditional manufacturing industry, the manufacturing process generally includes modeling, cast or forged, cut, parts assembly, and other processes. 3D printing eliminates the complicated process that avoids the need for a mold. As a result, 3D printing can overcome some designs that are impossible to achieve with traditional manufacturing and create more complex structures[240]. At present, 3D printing equipment has been widely used in aerospace, automotive, consumer electronics, industry, construction, and other fields[241,242]. Functions expand from the earliest teaching and display to industrial mold manufacturing or direct manufacturing.

With the continuous development of 3D printing technology, 3D printing technology in medicine is also well exploited. The technology uses computational 3D imaging software to sort out the 2D tomography data to get 3D reconstruction images regenerated into Standard Tessellation Language (STL) documents. Then they can be printed out as 3D models in the way of layer and stack to construct a three-dimensional form. The production process of a 3D printing model generally includes three stages: model acquisition, 3D printing, and post-printing processing. The current printing methods commonly used in the medical field include direct 3D printing, SLS, FDM, stereolithography, biomaterial printing, inkjet printing. 3D printing has been widely used in orthopedics, oral and maxillofacial surgery, vascular surgery, and other medical fields due to its advantages of precision, convenience, and personalization[243–246]. In recent years, more and more 3D printing technologies have been applied to aorta remodeling. However, due to the complexity of the cardiovascular system, there is no comprehensive and mature 3D printing technology applied in this field up to date.

2.6.2 3D printed artery

As described in sections 1.2 and 2.1, the aorta is a hyperelastic material. From the 3D printing point of view, the main focus is finding an elastic printing material. Currently, elastic printing materials are mainly divided into thermoplastic polyurethanes and thermoplastic elastomers (TPE). It mainly refers to the traditional sense of rubber, including unsaturated rubber such as natural rubber, styrene-butadiene rubber, neoprene

rubber, and saturated rubber, such as ethylene-propylene rubber and silicone rubber. It has been successfully used 3D printing technology to print elastic products such as ball boots, bicycle tires, and car tires. TPE has the characteristics of both plastic and rubber. It has the high elasticity of rubber at room temperature and can be molded like plastic at high temperatures. It is suitable for printing with FDM technology and SLS technology. Typical types used in 3D printing are thermoplastic polyurethane (TPU), polyamide (TPA), and polystyrene (TES). TPU is a block copolymer consisting of high polarity polyurethane (PU) or polyurea segment and polyester or polyether segment alternately. Usually, TPU has the characteristics of sufficient elasticity, high stiffness, wear resistance, and oil resistance[247].

3D printing of the aorta is mainly based on the remodeling of aortic images from CT or MRI. The main goal of these studies was to provide a more direct and specific visual view of the aorta for surgical plan exploration and medical education[248]. A common disadvantage of these models is that the printed aortic material is highly rigid, lacking tactility and softness in practical operation (Fig. 2-20).

Figure 2-20. 3D printed aortas with the aortic valve. (From Levin et al., 2020 [249]*)*

According to Ho et al., 3D printing models were done for two patients with aortic arch aneurysms[248]. The anatomical details of the aortic structure and lesion were successfully reproduced, including the size and shape of true and false lumen[248]. Anwar et al. pointed out that there are two primary 3D printed heart models: blood pool and hollow models. The blood pool model was a three-dimensional solid display of the blood pool in the heart cavity and the blood vessel[250]. It was created by dividing the blood pool signal. The model is usually derived from contra-enhanced CT or MRI. This model provided good visualization of the great vessels, the extracardiac vessels, and surrounding structures such as the trachea and esophagus. However, the disadvantage is that the understanding of intracardiac anatomy is limited. The hollow model is a cavity model that uses a grid to represent the myocardium and blood vessel walls around the blood pool signal. It is essential to digitally remove the blood pool signal to display the heart cavity and obtain a model that can show the heart anatomy in detail. Vranicar

et al.[251] conducted a study using 3D printing to evaluate blood vessel abnormalities. They used CT data on heart anatomy in 12 patients with aortic coarctation and vascular rings to create a 3D-printed model. Schmauss et al.[252] simulated the cardiovascular system in adults and children using 3D printing. They used CT or MRI images from eight patients, printed with polyester. Since their interest is to have a detailed visual view of the complex anatomy, no detailed data on material properties were reported. According to Kurenov et al., they had printed ten human pulmonary arteries with the material of Rubber-like resin (TangoPlus, Stratasys Ltd.©, Israel)[253]. They had used the 3D geometry based on CT images, with two commercial software such as Amira 5.5 (FEI Visualization Sciences Group, Burlington, the USA) and Vitrea 3D version 6.5.1 (Vital Images, Inc, Toshiba Medical Systems, Minnetonka, the USA). The tensile stretch of the printed PA was between 0.0055 - 0.0103 MPa. To our knowledge, it is the only publication concerned about the biomechanical properties of the printed material.

Chapter 3 - Biomechanical properties of the ascending aortic aneurysms

The ascending aortic aneurysm (AsAA) is a high-risk cardiovascular disease with an increasing incidence over the years. The impact of the risk factors (age, gender, smoking, diabetes, hypertension, obesity, aortic valve disorder, coronary artery disease, etc.) stays unclear up to date. This chapter compares different clinical risk factors according to biomechanical properties obtained from the biaxial tensile test.

3.1. Introduction

AsAA can lead to an aortic dissection, one of the fatal cardiovascular diseases, with an increased incidence over recent years[254,255]. As it is described in section 1.2, each year, ascending thoracic aortic aneurysms affect approximately 5.6 to 10.4 cases per 100,000 persons[2]. Multiple risk factors exist, including age, gender, race, hypertension, smoking, congenital diseases such as the bicuspid aortic valve (BAV), genetic diseases such as Marfan syndrome or Ehlers-Danlos syndrome[256,257]. Up to the moment, AsAA surgical recommendation is based on a monitored aortic diameter[6], in particular, the aortic expending rate and the maximum diameter (Fig. 1-11). Few observations indicated that AsAA could rupture or dissect regardless of the size of the aorta[258–260]. Early studies[261,262] claimed that the factors affecting aneurysms are positively correlated with atherosclerotic vascular disease (ASVD). Segmental atherosclerosis precedes the growth of an aneurysm, which may be closely related to the gate connection of elastin. In recent years, there has been a tendency to consider that the triggering mechanism of an aneurysm can be more complex, and the factors of risk prediction need to be considered in more aspects, which may not be directly related to atherosclerosis[263]. As is described in chapter 2, the biaxial tensile test is a biomechanical analysis experiment that has been widely used to evaluate the biomechanical characteristics of the AsAA[220,225,264]. Compared with uniaxial tensile tests[213] and bulge inflation tests[14], this method can simultaneously obtain longitudinal

and circumferential stress-strain curves with smaller sample sizes. Multiple experiments[15,220] have shown that the stiffness in different AsAA anatomical areas (i.e., anterior, posterior, medial, and lateral) is not the same. Our study aims to conduct a detailed grouped analysis of the biomechanical parameters of aneurysms and determine the differences in their mechanical properties according to regional heterogeneity of human tissue harvested during the surgery of ascending aortic replacement.

3.2 Materials and methods

Biaxial tensile tests of the AsAA wall were freshly performed after the ascending aortic wall replacement. Based on each patient's medical information, the following subgroups were classified: age, gender, hypertension, obesity, smoking history, aortic insufficiency, aortic stenosis, coronary artery disease, and aortic diameter.

3.2.1 Population of one hundred AsAA

From December 2018 to May 2021, one hundred AsAA patients (63 ± 12 years old) were recruited. The French national ethics committee approved the study (2018-A02010-55). It has been recorded on ClinicalTrials.gov (https://clinicaltrials.gov/, clinical registration number: NCT03817008). According to the ethics committee, all patients have received the written information of the study. Oral consent has been obtained from the patient, and attestation of the patient's oral consent has been signed by the investigator's physician and countersigned by the patient. The French law does not require written consent for this study.

The patients' information was collected prospectively through the patients' surgical protocol and the anesthetist consultation reports. There was attention to gender, age, smoking history, arterial hypertension (HTA), diabetes, dyslipidemia (DYS), body mass index (BMI), coronary artery disease (CAD), aortic insufficiency (AI), aortic stenosis (AS), aortic valve (AV) type, and the diameter of AsAA. The AsAA diameters were obtained by pre-operative MRI or computed CT exam.

Fifteen subgroups were designed based on the general factors, atherosclerotic vascular disease (ASVD) risk factors, coronary artery disease, aortic valve issue, and AsAA diameter. This information is detailed as follow:

- **General factors**

There were two subgroups associated with the general factors: age and gender. The definition of the age was actual patient age at the aortic replacement operation. Only males and females were recorded in the gender subgroup.

- **Atherosclerosis vascular disease risk factors**

There were six subgroups in the ASVD risk factors: HTA, DYS, obesity (according to BMI), diabetes, smoking history, and a subgroup of collection of risk factors.

This classification contained the subgroups of presence versus absence of four ASVD risk factors (HTA, DYS, obesity, diabetes). The impact of smoking was defined into three levels: no smoking history, with smoking history, and active smoking. Meanwhile, an additional subgroup was designed to cumulate five risks of ASVD: patients with no ASVD risk factor were defined as 0. Patients with one, two, three risk factors were defined as 1, 2, 3, respectively. Patients who presented more than three risk factors were defined as 4/5. Biomechanical properties were compared between these five groups (0, 1, 2, 3, 4/5).

- **Coronary artery disease**

The patients with AsAA associated with coronary artery disease were subgrouped. According to the clinical record, four types were defined; "Normal" as no coronary artery disease was reported, and three other types (Type I: atheroma; Type II: coronary artery stenosis; Type III: aneurysmal coronary artery) of disease were also recorded.

- **Aortic valve issue**

Four subgroups were included in this section: AI, AS, AI combined with AS, and AV types.

According to the patients' clinical record, AI was classified into 5 degrees (0, 1, 2, 3, and 4). The subgroup of AS was classified as with or without AS. In our research, each degree of AS and AI was compared in the subgroup, respectively.

In order to have combined information of AI and AS (Table 3-1), the subgroup of aortic valve diseases was created to compare the biomechanical properties of the AsAA, according to the following situation: a) AsAA with low AI grade and without AS (- AI / - AS), b) AsAA with high AI grade but without AS (+ AI / - AS), c) AsAA with low AI grade but with AS (- AI / + AS), d) AsAA with high AI grade and AS (+ AI / + AS). The low AI grade group included AI degrees as 0, 1, 2. The high AI grade group indicated severe AI degrees as 3, 4. Another comparative analysis of the aortic valve disorder was about the absence or the presence of AS.

AI degree	AS	Subgroup
0, 1, 2	No AS	- AI/ - AS
3, 4	No AS	+ AI / - AS
0, 1, 2	With AS	- AI / + AS
3, 4	With AS	+ AI / + AS

Table 3-1. the definition of the combined group of AI and AS. AI = aortic insufficiency, AS = aortic stenosis.

According to the type of AV, a large population of patients (n = 42) had AsAA associated with BAV (AsAA-BAV), leading to another subgroup comparing AsAA's biomechanical properties. Table 3-2 summarizes the different subgroups.

- **The diameter of the AsAA**

Only 2 out of 100 patients were excluded in the subgroup of ascending aortic diameter due to the absence of diameter information during the emergency hospitalization.

	Risk factors	Subgroups	No. patients
General factors	Gender	Male (62 ± 13 yd)	72
		Female (66 ± 12 yd)	28
	Age	Less than 59 yd	32
		More than 60 yd	68
ASVD risk factors	Smoking	Never smoked	56
		With smoking history	27
		Smoking	17
	HTA	-	26
		+	74
	Diabetes	-	91
		+	9
	DYS	-	58
		+	24
	Obesity	-	70
		+	30
	Combined risks of ASCD	0	11
		1	29
		2	25
		3	23
		4/5	12
CAD		Normal	76
		Type I	14
		Type II	9
		Type III	1
AV risks	AI	0	44
		1	13
		2	18
		3	15
		4	10
	AS	-	75
		+	25

	Risk factors	Subgroups	No. patients
AV risks	Combined of AV disorder	- (AI)/ - (AS)	52
		- (AI)/ + (AS)	23
		+ (AI)/ - (AS)	23
		+ (AI) / + (AS)	2
	AV type	TAV	58
		BAV	42
AsAA diameter		< 45 mm	26
		≥ 45 mm, < 50 mm	23
		≥ 50 mm, < 55 mm	36
		≥ 55 mm	13

Table 3-2. Subgroups of the population. "-": no factor reported; "+": with the factor presented. yd = year old; TAV = tricuspid aortic valve, BAV = bicuspid aortic valve, HTA = arterial hypertension; DYS = dyslipidemia; AV= aortic valve, AI = aortic insufficiency, AS = aortic stenosis, CAD = coronary artery disease.

3.2.2 Experimental method

The tissue status was kept fresh under the instruction of the protocols (cf. section 2.3). The aortic walls were cut in square size (15 mm x 15 mm) with marking the circumferential (CIR) and longitudinal (LON) directions with partitioning related to medial (MED), posterior (POST), lateral (LAT), and anterior (ANT) quadrants. The thickness of each specimen was measured 5 times (cf. section 2.4). The biomechanical experiments were carried out by biaxial tensile tests (cf. section 2.5). The calculation equations associated with the biomechanical properties were detailed in section 2.2.

3.2.3 Statistical analyses

Statistical analyses were performed with Stata® Software[265] (version 15, Stata Corporation, College Station, TX, USA).

Quantitative variables were described by their mean and standard deviation (SD). A random-effects generalized least squares regression model was used to pool the estimated effects. The confidence interval of 95% was accepted in the continuously featured subgroups (i.e., age, BMI, and ascending aorta diameter) and double featured subgroups (i.e., gender, HTA, diabetes, dyslipidemia, and aortic valve types, aortic stenosis, and coronary artery disease) by using linear mixed model[266]. Other variables that appeared to be related in the initial analysis with a p-value of less than 0.2 were considered in the multivariate model[267]. Meanwhile, a robust variance estimator was considered for all the variance[268].

Bootstrap was performed to verify the internal validation of regression models for final statistical results[269].

3.3 Results

This section is focused on the wall thickness and the maximum value of Young's modulus for one hundred AsAA walls according to four quadrants (MED, ANT, LAT, POST).

3.3.1 Aortic wall thickness

The aortic wall thickness differed from the aortic quadrants (Table 3-3).

	MED	**ANT**	**LAT**	**POST**	**Mean**
Wall Thickness *Mean ± SD (mm)*	2.114 ± 0.421	1.916 ± 0.424	1.817 ± 0.345	1.875 ± 0.386	1.93±0.411

Table 3-3. Mean wall thickness according to the quadrants. MED = medial; ANT = anterior; LAT = lateral; POST = posterior.

Overall, the AsAA wall can be measured around 2 mm, in which the lateral quadrant was the less thick, while the medial quadrant was the thickest among all the quadrants. The mean thickness can reach a 16% difference based on the quadrants.

According to the subgroup of AV types, the thickness of TAV and BAV is described in Table 3-4.

	TAV *Mean ± Std. Dev. (mm)*	**BAV** *Mean ± Std. Dev. (mm)*
MED	2.255±0.446	1.92±0.293
ANT	2.028±0.454	1.761±0.325
LAT	1.899±0.359	1.703±0.294
POST	1.976±0.387	1.735±0.341
Mean	2.039±0.431	1.78±0.322

Table 3-4. Wall thickness according to valve types. TAV = tricuspid aortic valve; BAV = bicuspid aortic valve; MED = medial; ANT = anterior; LAT = lateral; POST = posterior.

In general, the thickness of the AsAA wall associated with BAV was significantly smaller than associated with TAV ($p < 0.05$). This pattern can be observed in all the quadrants. Specifically, the mean thickness of the aortic wall associated with TAV was more than 2 mm, and the mean thickness of the aortic wall associated with BAV was 1.78 mm. The thickness difference between quadrants was 19% when AsAA was associated with TAV and 13% with BAV.

Linear regression can be observed between the aortic wall mean thickness and the ascending aortic diameter (p = 0.0157). When the diameter increased, the aortic thickness increased with a ratio of 0.0125 (Fig. 3-1)

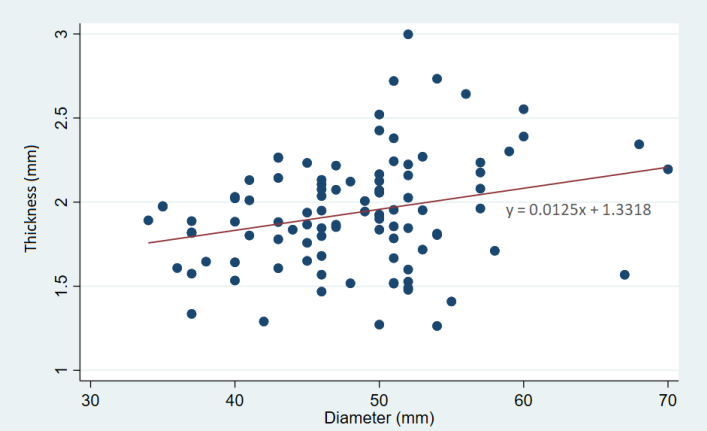

Figure 3-1. The distribution of aortic thickness and AsAA diameter (p = 0.0157).

3.3.2 Biomechanical properties

In general, the lateral quadrant presented a greater value of maximum Young's modulus than the rest of the quadrants (p < 0.05), while the medial quadrant showed a smaller value (p < 0.05). The maximum Young's modulus in the longitudinal direction was significantly higher than that in the circumferential direction (p < 0.001). The detailed information is shown in Table 3-5.

	AsAA	
	Circumferential *Mean ± Std. Dev. (MPa)*	Longitudinal *Mean ± Std. Dev. (MPa)*
MED	0.739 ± 0.316	0.829 ± 0.347
ANT	0.875 ± 0.311	0.955 ± 0.343
LAT	1.212 ± 0.472	1.294 ± 0.448
POST	1.074 ± 0.41	1.245 ± 0.431

Table 3-5. Maximum Young's modulus of CIR and LON directions in different quadrants (MED, ANT, LAT, POST). MED = medial; ANT = anterior; LAT = lateral; POST = posterior.

- **Multivariant calculation**

In the multivariant estimation, the impact factors of the age (p = 0.066), smoking (p = 0.0527), diabetes (p = 0.034), aortic stenosis (p = 0.0175), coronary artery disease (p = 0.0000), and aortic diameters (p =0.02) were significantly influencing the maximum value of Young's modulus. It has been verified by 200 and 1000 Bootstrat mode.

- **Age impact**

According to the age, the maximum value of Young's modulus in the different AsAA regions considering directions of CIR and LON is depicted in Table 3-6. The stiffness of AsAA of patients over 60 years old was statistically significantly higher ($p < 0.05$) from patients less than 59 years old.

		Less than 59 years old *Mean ± Std. Dev. (MPa)*	**More than 60 years old** *Mean ± Std. Dev. (MPa)*
MED	CIR	0.650 ± 0.170	0.781 ± 0.358
	LON	0.744 ± 0.224	0.869 ± 0.387
ANT	CIR	0.772 ± 0.220	0.924 ± 0.335
	LON	0.834 ± 0.224	1.011 ± 0.374
LAT	CIR	1.104 ± 0.376	1.262 ± 0.504
	LON	1.197 ± 0.389	1.337 ± 0.468
POST	CIR	1.031 ± 0.339	1.093 ± 0.439
	LON	1.221 ± 0.396	1.251 ± 0.449

Table 3-6. Age impact (less than 59-year-old and more than 60-year-old). Comparison of maximum Young's modulus according to circumferential and longitudinal directions in different quadrants. CIR = circumferential; LON = longitudinal; MED = medial; ANT = anterior; LAT = lateral; POST = posterior.

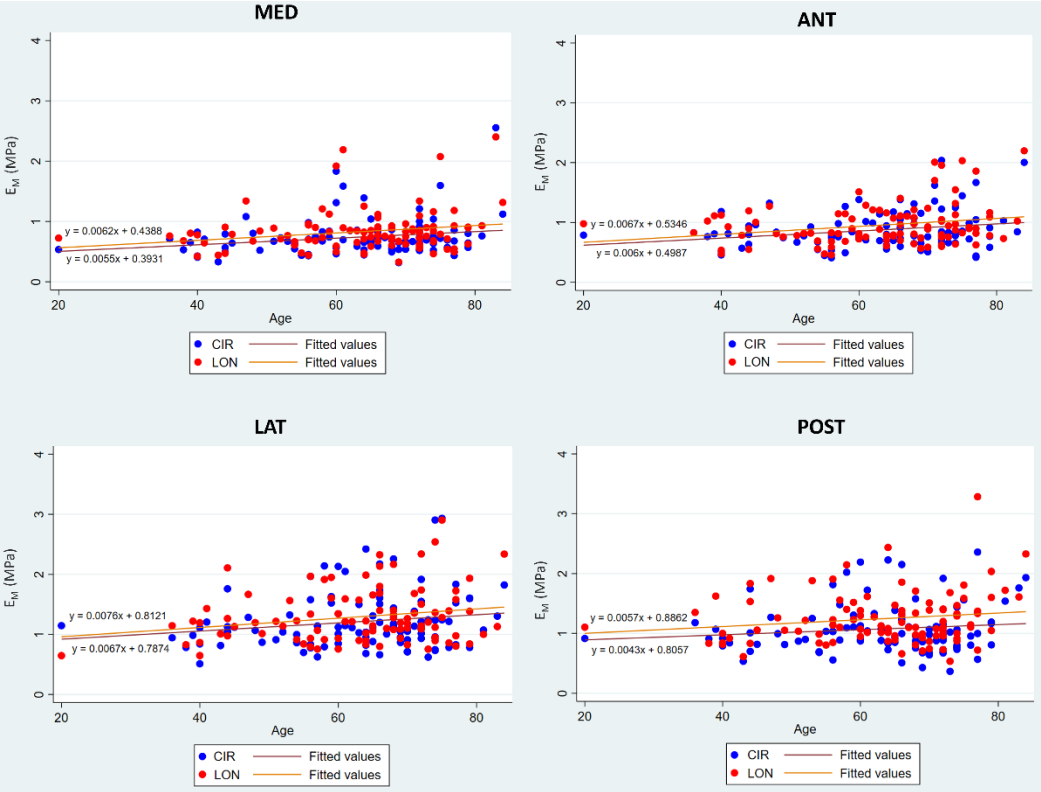

Figure 3-2. Impact of age based on different quadrants ($p = 0.009$). E_M = maximum value of Young's modulus; CIR = circumferential; LON = longitudinal; MED = medial; ANT = anterior; LAT = lateral; POST = posterior.

Even a spread of the data was shown in the graphs in Fig. 3-2. A positive correlation can still be statistically significant in CIR and LON directions in all quadrants. With aging, the maximum value of Young's modulus was increased ($p < 0.01$). Among the four quadrants, the increasing ratio of the maximum Young's modulus at the level of the POST quadrant was the smallest, while the LAT quadrant displays the greatest.

- **AsAA diameter**

The ascending aortic diameter was highly related to the maximum value of Young's modulus. In general, it can be observed a linear relationship (Fig. 3-3). Although there was a sign of dispersion, a positive correlation can be observed in both CIR and LON directions in all quadrants. With the diameter increased, the maximum value of Young's modulus increased ($p < 0.05$). Among four quadrants, the increasing ratio of the MED quadrant was the smallest, while the LAT quadrant provided the greatest.

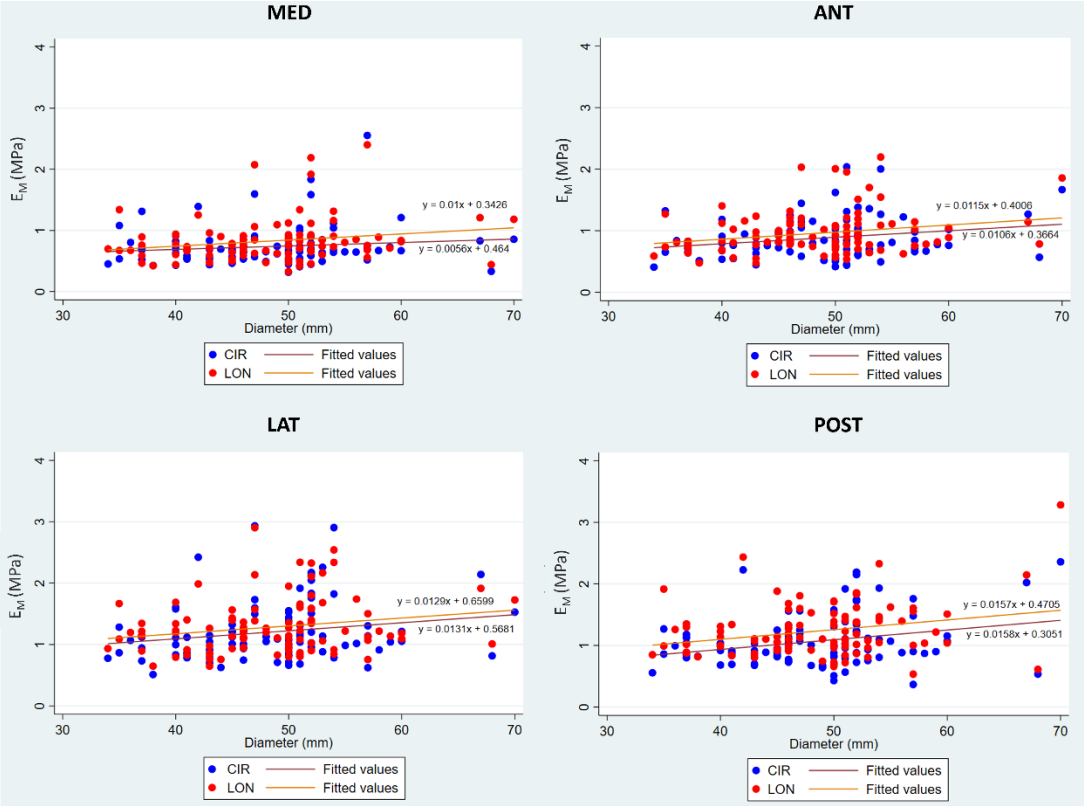

Figure 3-3. Impact of diameter based on different quadrants ($p = 0.009$). E_M = maximum value of Young's modulus; CIR = circumferential; LON = longitudinal; MED = medial; ANT = anterior; LAT = lateral; POST = posterior.

- **Gender**

The gender impact was statistically significant between males and females ($p < 0.05$, Table 3-7, Fig. 3-4). The mean difference can be observed in the MED quadrant. In

the female group, the maximum value of Young's modulus was around 26% - 33% more than in males.

		Male	**Female**
		Mean ± Std. Dev. (MPa)	*Mean ± Std. Dev. (MPa)*
MED	CIR	0.685 ± 0.205	0.911 ± 0.501
	LON	0.775 ± 0.269	0.997 ± 0.493
ANT	CIR	0.857 ± 0.303	0.919 ± 0.327
	LON	0.927 ± 0.336	1.020 ± 0.353
LAT	CIR	1.158 ± 0.378	1.338 ± 0.635
	LON	1.268 ± 0.397	1.349 ± 0.555
POST	CIR	1.031 ± 0.344	1.179 ± 0.528
	LON	1.207 ± 0.376	1.325 ± 0.542

Table 3-7. Gender impact. Comparison of maximum Young's modulus according to circumferential and longitudinal directions in different quadrants (MED, ANT, LAT, POST). CIR = circumferential; LON = longitudinal; MED = medial; ANT = anterior; LAT = lateral; POST = posterior.

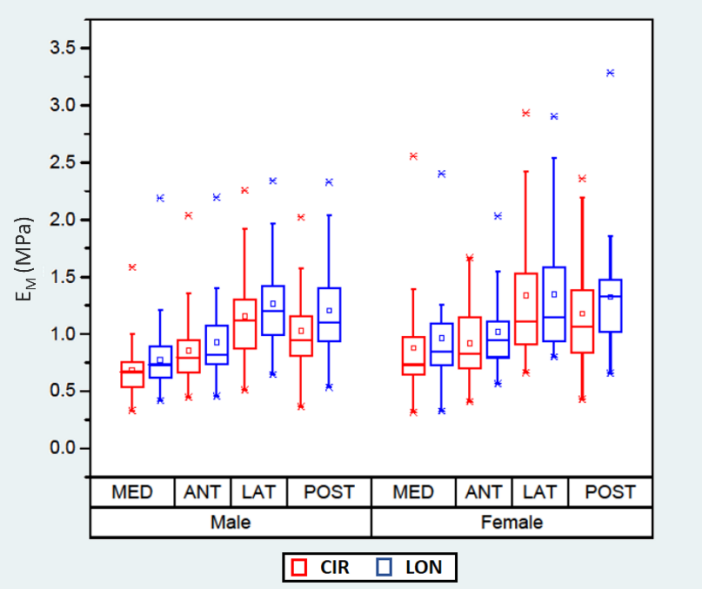

Figure 3-4. Gender impact. Comparison of maximum Young's modulus according to circumferential and longitudinal directions in different quadrants (MED, ANT, LAT, POST). E_M = maximum value of Young's modulus; CIR = circumferential; LON = longitudinal; MED = medial; ANT = anterior; LAT = lateral; POST = posterior.

- **Diabetes**

There was a significant stiffness difference ($p < 0.05$) between the AsAA wall in patients with diabetes and without diabetes (Table 3-8 and Fig. 3-5). The maximum Young's modulus difference was 26% in the LAT quadrant in both directions (CIR

and LON). In the POST quadrant for the patients associated with diabetes, the difference greatly varied in direction: a mean value of 1.4 MPa in the longitudinal direction and 1.122 MPa in the circumferential direction.

		No diabetes *Mean ± Std. Dev. (MPa)*	**Diabetes** *Mean ± Std. Dev. (MPa)*
MED	CIR	0.731 ± 0.317	0.826 ± 0.305
	LON	0.815 ± 0.33	0.968 ± 0.489
ANT	CIR	0.866 ± 0.319	0.958 ± 0.174
	LON	0.942 ± 0.35	1.068 ± 0.223
LAT	CIR	1.183 ± 0.473	1.487 ± 0.344
	LON	1.262 ± 0.442	1.586 ± 0.41
POST	CIR	1.068 ± 0.412	1.122 ± 0.391
	LON	1.225 ± 0.436	1.409 ± 0.35

Table 3-8. Diabetes impact. Comparison of maximum Young's modulus according to circumferential and longitudinal directions in different quadrants (MED, ANT, LAT, POST). CIR = circumferential; LON = longitudinal; MED = medial; ANT = anterior; LAT = lateral; POST = posterior.

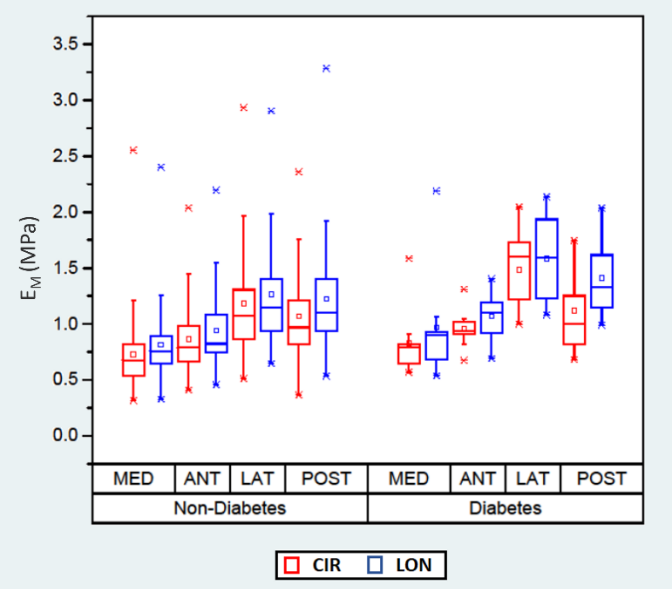

Figure 3-5. Diabetes impact. Comparison of maximum Young's modulus according to circumferential and longitudinal directions in different quadrants (MED, ANT, LAT, POST). E_M = maximum value of Young's modulus; CIR = circumferential; LON = longitudinal; MED = medial; ANT = anterior; LAT = lateral; POST = posterior.

- **Smoking**

The maximum value of Young's modulus was significantly different according to smoking (Table 3-9 and Fig.3-6). In the active smoking group, a lower stiffness (p =

0.0519) can be observed in the level of 0.64 MPa to 1.192 MPa, according to the quadrants and directions. The regional and directional difference between the no smoking history group and the active smoking group was between 7.42% and 19.7%. Moreover, there was no significant difference of the maximum Young's modulus between the AsAA associated with smoking history and no smoking history.

		No smoking history *Mean ± SD (MPa)*	**With smoking history** *Mean ± SD (MPa)*	**Active smoking** *Mean ± SD (MPa)*
MED	CIR	0.742 ± 0.366	0.796 ± 0.252	0.64 ± 0.196
	LON	0.835 ± 0.382	0.894 ± 0.336	0.706 ± 0.187
ANT	CIR	0.86 ± 0.301	0.96 ± 0.346	0.793 ± 0.27
	LON	0.956 ± 0.339	0.994 ± 0.338	0.89 ± 0.373
LAT	CIR	1.249 ± 0.543	1.236 ± 0.353	1.055 ± 0.356
	LON	1.302 ± 0.504	1.341 ± 0.377	1.192 ± 0.351
POST	CIR	1.088 ± 0.427	1.133 ± 0.412	0.938 ± 0.335
	LON	1.245 ± 0.392	1.373 ± 0.523	1.04 ± 0.322

Table 3-9. Smoking impact (no smoking history, with smoking history versus active smoking). Comparison of maximum Young's modulus according to circumferential and longitudinal directions in different quadrants (MED, ANT, LAT, POST). CIR = circumferential; LON = longitudinal; MED = medial; ANT = anterior; LAT = lateral; POST = posterior.

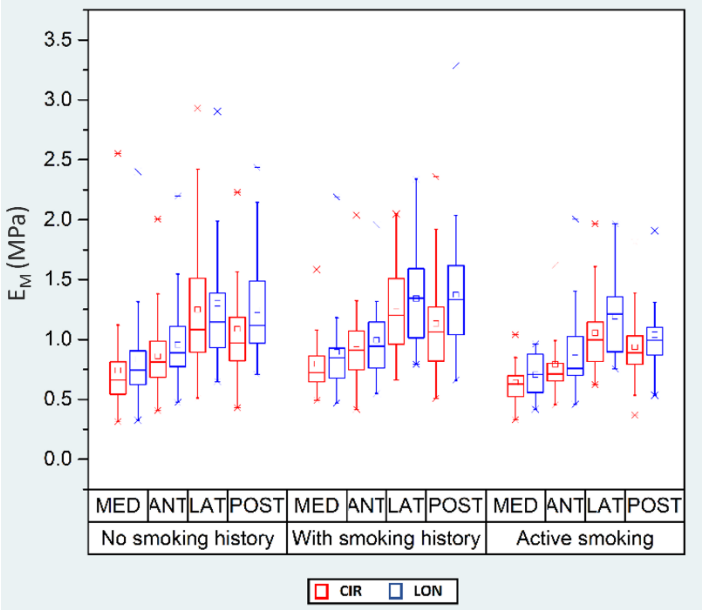

Figure 3-6. Smoking impact (no smoking history, with smoking history versus active smoking). Comparison of maximum Young's modulus according to circumferential and longitudinal directions in different quadrants (MED, ANT, LAT, POST). E_M = maximum value of Young's modulus; CIR = circumferential; LON = longitudinal; MED = medial; ANT = anterior; LAT = lateral; POST = posterior.

- **Aortic insufficiency**

In the subgroup of AI, the degree of aortic insufficiency differed according to the maximum Young's modulus (Fig. 3-7). Globally, a decrease of the maximum value of Young's modulus was found out with the AI degree increasing ($p = 0.1808$). Meanwhile, this pattern was verified between the overall values of each degree ($p < 0.05$).

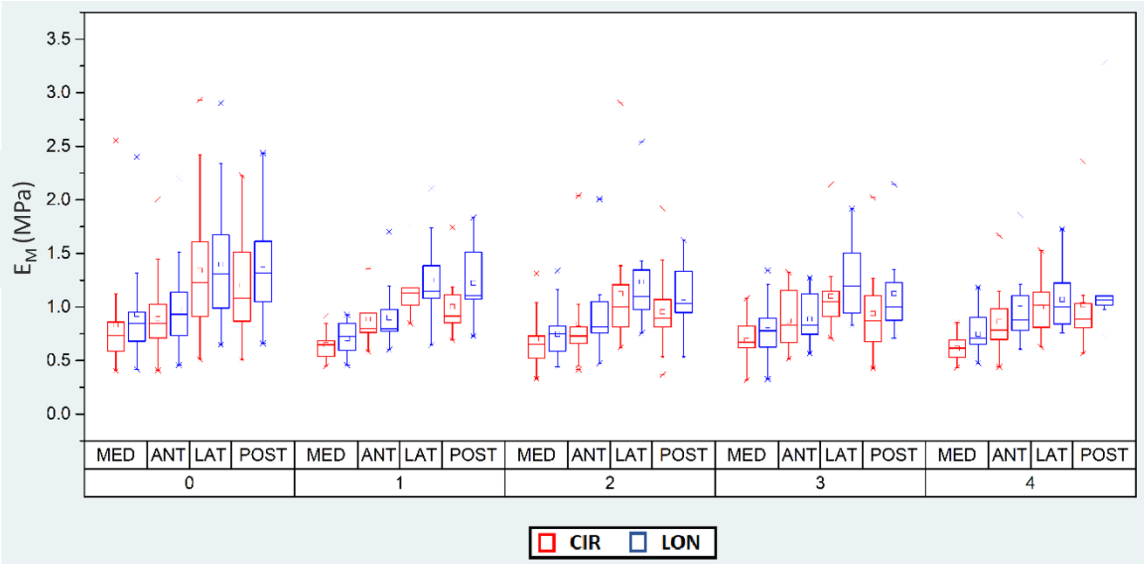

Figure 3-7. Aortic insufficiency (degree from 0, 1, 2, 3, and 4, respectively). Comparison of maximum Young's modulus according to circumferential and longitudinal directions in different quadrants (MED, ANT, LAT, POST). E_M = maximum value of Young's modulus; CIR = circumferential; LON = longitudinal; MED = medial; ANT = anterior; LAT = lateral; POST = posterior.

A higher stiffness of AsAA of patients with low AI grades can be observed as statistically significant ($p < 0.05$) than patients with high AI grades (Table 3-10). A mean difference of the maximum value of Young's modulus can be found between 1.36% to 18.99%, according to the longitudinal direction in the ANT quadrant and circumferential direction in the LAT quadrant, respectively.

		Low aortic insufficiency grades *Mean ± Std. Dev. (MPa)*	**High aortic insufficiency grades** *Mean ± Std. Dev. (MPa)*
MED	CIR	0.767 ± 0.350	0.650 ± 0.159
	LON	0.849 ± 0.373	0.757 ± 0.240
ANT	CIR	0.878 ± 0.320	0.864 ± 0.284
	LON	0.965 ± 0.360	0.922 ± 0.284
LAT	CIR	1.263 ± 0.502	1.058 ± 0.323
	LON	1.334 ± 0.481	1.168 ± 0.306

		Low aortic insufficiency grades	High aortic insufficiency grades
		Mean ± Std. Dev. (MPa)	*Mean ± Std. Dev. (MPa)*
POST	CIR	1.109 ± 0.405	0.970 ± 0.409
	LON	1.266 ± 0.388	1.170 ± 0.538

Table 3-10. Aortic insufficiency (low AI grades (0, 1, 2) versus high AI grades(3, 4). Comparison of maximum Young's modulus according to CIR and LON directions in different quadrants (MED, ANT, LAT, POST). CIR = circumferential; LON = longitudinal; MED = medial; ANT = anterior; LAT = lateral; POST = posterior.

- **Aortic stenosis**

In the group of AS, the difference of maximum value of Young's modulus was statistically highly significant (p = 0.0175) between the patients with AS and those without AS (Fig. 3-8)

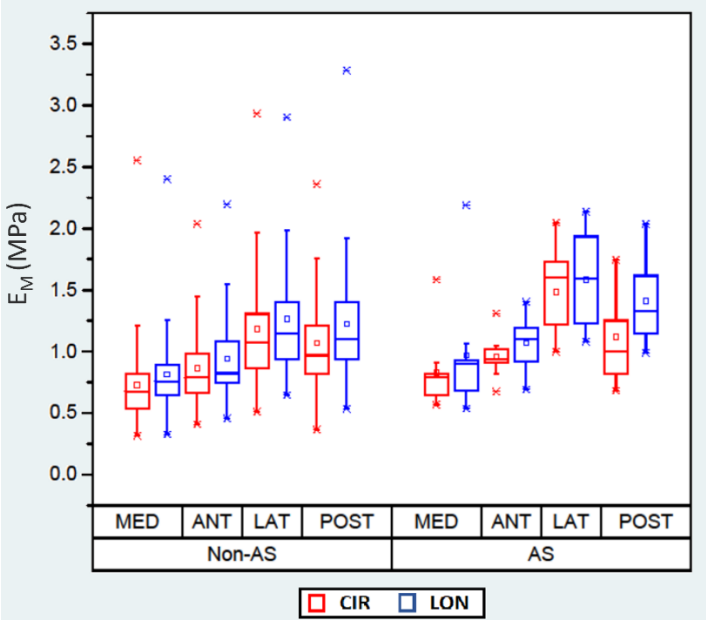

Figure 3-8. Aortic stenosis (no AS, degree 1 and 2 of AS). Comparison of maximum Young's modulus according to circumferential and longitudinal directions in different quadrants (MED, ANT, LAT, POST). E_M = maximum value of Young's modulus; CIR = circumferential; LON = longitudinal; MED = medial; ANT = anterior; LAT = lateral; POST = posterior.

For the AsAAs associated with AS, the aortic walls were stiffer than those with no AS. A difference in the mean value was higher in the LAT and POST quadrants than the other two quadrants. Specifically, a difference of maximum Young's modulus between LAT and POST quadrants of the AsAA with AS can be 16.43% to 20.92%. In contrast, the difference between MED and ANT quadrants of the AsAA with AS can be 3.58 % to 8.93% (Table 3-11).

		No aortic stenosis *Mean ± Std. Dev. (MPa)*	Aortic stenosis *Mean ± Std. Dev. (MPa)*
MED	CIR	0.721 ± 0.331	0.792 ± 0.256
	LON	0.815 ± 0.356	0.873 ± 0.302
ANT	CIR	0.863 ± 0.336	0.908 ± 0.214
	LON	0.944 ± 0.356	0.981 ± 0.297
LAT	CIR	1.137 ± 0.436	1.433 ± 0.505
	LON	1.230 ± 0.409	1.476 ± 0.513
POST	CIR	1.007 ± 0.397	1.274 ± 0.383
	LON	1.169 ± 0.418	1.460 ± 0.400

Table 3-11. Aortic stenosis (presence versus absence). Comparison of maximum Young's modulus according to of circumferential and longitudinal directions in different quadrants (MED, ANT, LAT, POST). CIR = circumferential; LON = longitudinal; MED = medial; ANT = anterior; LAT = lateral; POST = posterior.

- **The combined subgroup of AI and AS**

The maximum Young's modulus in crossing comparison subgroup of the aortic valve dysfunction (no AI nor AS, with AI and without AS, with AS and without AI, and with both AI and AS) was significant (p = 0.089, Table 3-12 and Fig. 3-9). The presence of the AS involved the AsAA wall for higher stiffness. However, when AsAA is associated with AI, the aortic wall was found less stiffness. In combination with both AS and AI, the aortic wall showed a lower stiffness than the AsAA not associated with AS or AI in the following quadrants: MED, ANT, POST. On the contrary, the LAT quadrant shows a different pattern when the AsAA was associated with AS and AI.

		No AS nor AI *Mean ± SD (MPa)*	AS and no AI *Mean ± SD (MPa)*	AI and no AS *Mean ± SD (MPa)*	AI and AS *Mean ± SD (MPa)*
MED	CIR	0.752 ± 0.383	0.801 ± 0.265	0.653 ± 0.165	0.691 ± 0.07
	LON	0.836 ± 0.402	0.878 ± 0.314	0.765 ± 0.248	0.809 ± 0.03
ANT	CIR	0.865 ± 0.356	0.909 ± 0.223	0.863 ± 0.301	0.902 ± 0.083
	LON	0.956 ± 0.383	0.984 ± 0.31	0.925 ± 0.301	0.95 ± 0.075
LAT	CIR	1.185 ± 0.478	1.438 ± 0.522	1.034 ± 0.321	1.375 ± 0.361
	LON	1.267 ± 0.446	1.485 ± 0.53	1.157 ± 0.311	1.368 ± 0.335
POST	CIR	1.024 ± 0.387	1.302 ± 0.385	0.972 ± 0.434	0.963 ± 0.204
	LON	1.168 ± 0.339	1.487 ± 0.405	1.185 ± 0.569	1.143 ± 0.124

Table 3-12. Crossed comparison of the absence of both AI and AS, presence of AS but the absence of AI, presence of AI but the absence of AS, and present of both AI and AS. Comparison of maximum Young's modulus according to CIR and LON directions in different quadrants (MED, ANT, LAT, POST). AI = aortic insufficiency; AS = aortic stenosis; CIR = circumferential; LON = longitudinal; MED = medial; ANT = anterior; LAT = lateral; POST = posterior.

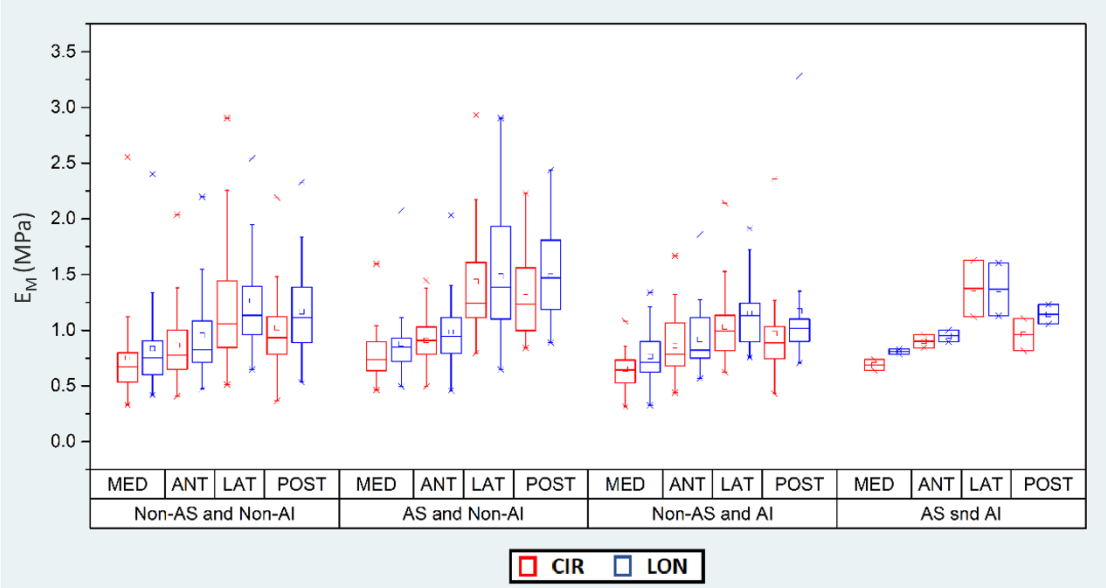

Figure 3-9. Crossed comparison of the absence of both AI and AS, presence of AS but the absence of AI, presence of AI but the absence of AS, and present of both AI and AS Comparison maximum Young's modulus according to CIR and LON directions in different quadrants (MED, ANT, LAT, POST). E_M = maximum value of Young's modulus; CIR = circumferential; LON = longitudinal; MED = medial; ANT = anterior; LAT = lateral; POST = posterior.

- **Coronary artery disease**

In the coronary artery disease (CAD) factors subgroup, the maximum value of Young's modulus in the different AsAA wall regions is depicted in Table 3-13. The CIR direction in the LAT quadrant of patients without CAD was significantly stiffer than those with CAD AsAA ($p < 0.05$). On the other hand, the overall result of all quadrants and both directions in the subgroup of patients' AsAA with CAD and without CAD was significant ($p < 0.001$).

		No coronary artery disease *Mean ± Std. Dev. (MPa)*	**Coronary artery disease** *Mean ± Std. Dev. (MPa)*
MED	CIR	0.738 ± 0.339	0.752 ± 0.228
	LON	0.837 ± 0.379	0.793 ± 0.207
ANT	CIR	0.851 ± 0.283	0.950 ± 0.379
	LON	0.946 ± 0.314	0.978 ± 0.425
LAT	CIR	1.265 ± 0.499	1.035 ± 0.310
	LON	1.313 ± 0.463	1.220 ± 0.393
POST	CIR	1.095 ± 0.407	1.002 ± 0.413
	LON	1.259 ± 0.384	1.184 ± 0.560

Table 3-13. Coronary artery disease (presence versus absence). Comparison of maximum Young's modulus according to CIR and LON directions in different quadrants (MED, ANT, LAT, POST). CIR = circumferential; LON = longitudinal; MED = medial; ANT = anterior; LAT = lateral; POST = posterior.

- **Aortic valve types**

Surprisingly, it was found out that there is no statistical difference in the stiffness between the AsAA associated with TAV or BAV (Table 3-14).

		TAV *Mean ± Std. Dev. (MPa)*	**BAV** *Mean ± Std. Dev. (MPa)*
MED	CIR	0.760 ± 0.382	0.713 ± 0.190
	LON	0.868 ± 0.416	0.779 ± 0.203
ANT	CIR	0.895 ± 0.356	0.847 ± 0.236
	LON	0.970 ± 0.407	0.931 ± 0.227
LAT	CIR	1.212 ± 0.521	1.208 ± 0.396
	LON	1.283 ± 0.475	1.302 ± 0.411
POST	CIR	1.034 ± 0.441	1.125 ± 0.358
	LON	1.227 ± 0.468	1.260 ± 0.378

Table 3-14. AV types (TAV and BAV). Comparison of maximum Young's modulus according to circumferential and longitudinal directions in different quadrants (MED, ANT, LAT, POST). TAV = tricuspid aortic valve; BAV = bicuspid aortic valve; CIR = circumferential; LON = longitudinal; MED = medial; ANT = anterior; LAT = lateral; POST = posterior.

- **Hypertension, dyslipidemia, and obesity**

The results of the maximum value of Young's modulus in the different AsAA wall regions according to the risk factors of dyslipidemia, obesity, and HTA are shown in Table 3-15, Table 3-16, Table 3-17, respectively. There was no statistical difference in any of these three subgroups of the ASVD risk factors.

		No Dyslipidemia *Mean ± Std. Dev. (MPa)*	**Dyslipidemia** *Mean ± Std. Dev. (MPa)*
MED	CIR	0.742 ± 0.350	0.741 ± 0.264
	LON	0.845 ± 0.380	0.819 ± 0.298
ANT	CIR	0.879 ± 0.342	0.869 ± 0.261
	LON	0.958 ± 0.379	0.947 ± 0.286
LAT	CIR	1.187 ± 0.464	1.243 ± 0.482
	LON	1.259 ± 0.459	1.336 ± 0.430
POST	CIR	1.075 ± 0.428	1.071 ± 0.384
	LON	1.226± 0.471	1.262 ± 0.371

Table 3-15. Dyslipidemia (with dyslipidemia presented versus absent) Comparison of maximum Young's modulus according to CIR and LON directions in different quadrants (MED, ANT, LAT, POST). CIR = circumferential; LON = longitudinal; MED = medial; ANT = anterior; LAT = lateral; POST = posterior.

		No obesity *Mean ± Std. Dev. (MPa)*	**Obesity** *Mean ± Std. Dev. (MPa)*
MED	CIR	0.728 ± 0.267	0.764 ± 0.412
	LON	0.821 ± 0.295	0.847 ± 0.446
ANT	CIR	0.898 ± 0.323	0.818 ± 0.273
	LON	0.955 ± 0.461	0.949 ± 0.327
LAT	CIR	1.221 ± 0.451	1.185 ± 0.496
	LON	1.291 ± 0.421	1.292 ± 0.445
POST	CIR	1.088 ± 0.421	1.038 ± 0.382
	LON	1.256 ± 0.460	1.205 ± 0.354

Table 3-16. Obesity (with obesity presented versus absent). Comparison of maximum Young's modulus according to CIR and LON directions in different quadrants (MED, ANT, LAT, POST). CIR = circumferential; LON = longitudinal; MED = medial; ANT = anterior; LAT = lateral; POST = posterior.

		No HTA *Mean ± Std. Dev. (MPa)*	**HTA** *Mean ± Std. Dev. (MPa)*
MED	CIR	0.692 ± 0.040	0.754 ± 0.346
	LON	0.794 ± 0.042	0.843 ± 0.383
ANT	CIR	0.831 ± 0.038	0.890 ± 0.341
	LON	0.883 ± 0.038	0.979 ± 0.379
LAT	CIR	1.170 ± 0.084	1.225 ± 0.484
	LON	1.220 ± 0.072	1.317 ± 0.470
POST	CIR	1.127 ± 0.072	1.053 ± 0.421
	LON	1.303 ± 0.086	1.219 ± 0.425

Table 3-17. Hypertension (with HTA presented versus absent). Comparison of maximum Young's modulus according to CIR and LON directions in different quadrants (MED, ANT, LAT, POST). HTA = Hypertension; CIR = circumferential; LON = longitudinal; MED = medial; ANT = anterior; LAT = lateral; POST = posterior

- **The cumulated subgroup of five ASVD factors**

The results concerning the cumulated subgroup of five risk factors that influence ASVD are presented in Table 3-18. According to the statistics, there was no stiffness difference of AsAA wall between patients with numbered risk factors and no ASVD risk presence.

		0 *Mean ± Std. Dev. (MPa)*	1 *Mean ± Std. Dev. (MPa)*	2 *Mean ± Std. Dev. (MPa)*	3 *Mean ± Std. Dev. (MPa)*	4/5 *Mean ± Std. Dev. (MPa)*
MED	CIR	0.635 ± 0.118	0.773 ± 0.345	0.737 ± 0.414	0.753 ± 0.206	0.733 ± 0.329
	LON	0.756 ± 0.200	0.877 ± 0.384	0.814 ± 0.402	0.811 ± 0.191	0.844 ± 0.468
ANT	CIR	0.839 ± 0.205	0.910 ± 0.352	0.840 ± 0.357	0.857 ± 0.242	0.928 ± 0.328
	LON	0.893 ± 0.189	1.001 ± 0.425	0.921 ± 0.340	0.905 ± 0.253	1.061 ± 0.392
LAT	CIR	1.103 ± 0.414	1.298 ± 0.555	1.158 ± 0.393	1.187 ± 0.520	1.257 ± 0.363
	LON	1.112 ± 0.370	1.374 ± 0.506	1.212 ± 0.384	1.315 ± 0.515	1.389 ± 0.309
POST	CIR	1.051 ± 0.329	1.093 ± 0.450	1.159 ± 0.475	1.009 ± 0.364	0.991 ± 0.319
	LON	1.196 ± 0.370	1.233 ± 0.476	1.362 ± 0.524	1.165 ± 0.297	1.198 ± 0.380

Table 3-18. Cumulated atherosclerotic vascular disease factors. Compare maximum Young's modulus according to CIR and LON directions in different quadrants (MED, ANT, LAT, POST). CIR = circumferential; LON = longitudinal; MED = medial; ANT = anterior; LAT = lateral; POST = posterior

3.4 Discussion

The mechanical properties and morphological characteristics of aortic tissue are important for maintaining cardiovascular health, while dysfunction is related to cardiovascular diseases' occurrence and development.

Our study found that age, gender, aortic valve disorder (aortic insufficiency and aortic stenosis), coronary aortic disease, and the diameter of ascending aortic wall statistically impact aortic stiffness. Among these factors, age, the diameter of ascending aorta, smoking, aortic valve disorder, and coronary aortic disease, and the diameter are highlighted in multivariant estimation. We have surprisingly found that valve types do not affect the AsAA stiffness.

In our observation, the AsAA wall average thickness was 1.93 mm. There was a spread variety according to the aortic quadrants. Studies showed that, in general, the aortic thickness is between 1.52 mm to 2.67 mm[270–272]. The thickness varies from different thickness measurement methods: histological slides, MRI, and ex-vivo fresh tissue. An earlier study in 1980 reported that the thickness difference between in vivo and in vitro measurements was within 20%[273]. Furthermore, based on our knowledge, the quadrantal thickness difference can be 18%.

From the biomechanical point of view, the lateral quadrant was the stiffest among all four quadrants, while the lowest aortic stiffness was found in the MED quadrant. There is a common discussion in the literature about whether the ascending aortic wall is anisotropic or isotropic. This information is crucial because isotropy or anisotropy determines the experimental method's choice. According to Deplano et al., it may be related to the age of the patient[225]. In younger patients and very elderly patients, the

aortic behavior was reported as isotropic[223,229]. The aortic wall behaved more anisotropically in wide age groups and patients around 60-year-old[221,274,275]. However, the specific circumferential direction or longitudinal direction that showed more substantial stress is controversial. Our study on 100 aortic samples ranged in age from 20 to 84 years, where more than half of the population was between 56 to 72 years. We found out that the aneurysmal aortic walls behaved anisotropically. Meanwhile, the longitudinal direction was significantly stiffer than the circumferential direction. Similar result has been found in the biaxial tensile test[276,277]. These observations justified the choice of the biaxial tensile test instead of the uniaxial one.

With aging, the increase of the aortic stiffness has been ascribed to numerous factors, including a decrease of elastin[278,279] as well as an increase of medial thickness, collagen density, and collagen content[196,279,280]. Other studies showed that natural aging might bring more stiffness in all arterial tissues [281,282]. In our observations, the stiffness of the aorta increased with age and showed a linear relationship. The growth trend varied significantly from region to region and direction to direction.

According to Qui et al., in the female population, less collagen and an increase of elastin can be observed[283]. Moreover, a recent histological aortic study on the autopsy of the population older than 80 years showed that females have stiffer aortic walls than male[284]. Based on our results, aortic stiffness was generally higher in women than in men. However, gender was not a significant factor in the multivariant statistical comparison of co-effects. The female (66 ± 12 years) in our sample were significantly ($p < 0.05$) older than the male (62 ± 13 years). Therefore, gender and age cannot be ruled out in the combined effect of the biomechanical mechanism affecting the aorta.

Pathologically, the increase in aortic diameter was due to elastin fragmentation and loss[285]. The loss of the elastin gene might cause aortic aneurysms[286]. Moreover, some studies have shown that the increase of aortic diameter was closely related to energy loss[287]. The aortic diameter was also associated with other factors such as age, sex, body size, etc[288]. It indicates that the abnormal aortic diameter was linked with multiple factors. In our study, the diameter of ascending aortic aneurysm was positively correlated with aortic stiffness. The scope of the regression line in the medial aorta was lower than in other areas.

Smoking is a significant risk factor for abdominal aortic aneurysms. According to Aune et al., active smokers and former smokers had 5 times and 2 times increased risk compared to never smokers, respectively[289]. In addition, there was a strong dose-response relationship between the increased number of cigarettes per day and increased pack per year, and increased risk of abdominal aortic aneurysm. Our study found some changes in aortic stiffness in active smokers compared to those who had smoked and those who had never smoked. This decrease varied in different quadrants, between 10% and 20%. Due to missing information on the detailed history of smoking, we could not indicate that the smoking history affects the aorta.

The Boodhwani classification[290] indicated that aortic stenosis is directly correlated with aortic diameter. The sinotubular junction is the boundary between zones 0 and 1 and is the fixation of aortic valve conjunctions[291]. Anatomically, the sinus duct junction stretches the aortic valve during dilatation, narrowing the aortic valve by reducing the aortic valve coaptation (type Ib). It might explain our results: higher levels of aortic stenosis are associated with dilated aortas, as we have shown that the aortic wall stiffness was higher in the AsAAs associated with aortic stenosis than those without aortic stenosis. Meanwhile, other studies have shown that under the action of AS, the high-speed blood flow will be more concentrated, thus reducing the generation of surrounding vortices[292]. Campobasso et al. showed that rigid AsAA might have the most significant variation in wall stress distribution. Sharp changes in peripheral vascular resistance may significantly increase the risk of rupture[293]. These hypotheses consolidated our results since we showed that AS has the most significant influence on the aortic stiffness in the lateral and posterior regions under the influence of blood flow. Twenty-five patients with AsAA had AS, and 2 of them had AS and AI simultaneously. According to the results of the biaxial tests, we found out that the aortic wall was more sensitive to become stiffer if it is associated with AS. The most fragile part was the medial wall. According to Wilton and Jahangiri[294], aortic dilatation resulted from aortic stenosis because of the acceleration of the blood flow, increasing shear stress of the aortic wall making post stenotic aortic dilatation.

According to the latest US guidelines on the bicuspid aortic valve surgery[295], AI was not a factor to be considered, while AS was an important one. In our experimental observations, aortic insufficiency was associated with aortic stiffness, and aortic stiffness decreased with the increasing insufficiency levels. This was the opposite of the biomechanism of action of AS. It may suggest that it is essential to follow the level of AsAA dilatation during the patients' regular follow-up of aortic stenosis. Indeed, AsAA may have a higher risk for patients before the severity of AS.

According to Ito et al., multiple studies showed that CAD could increase the risk of AsAA, to be more specific, from 31% to 70%[262]. In our study, we demonstrated that the aortic stiffness decreases when the aorta is associated with CAD.

Surprisingly, we did not find any aortic wall stiffness difference in the AsAA associated with TAV and BAV. Previous studies have shown that significant stress was found in the BAV sample than in the TAV sample[296–298]. However, in a study of 68 patients with the uniaxial tensile test, there is no significant difference in the aortic wall stiffness between AsAA-TAV and AsAA-BAV[209]. As we analyzed previously, the biomechanical properties of the aorta are determined by a variety of pathological and physiological factors. A detailed comparison of the information between patients with TAV and BAV is shown in Table 3-19.

		TAV	BAV	p-value
Age (years)	Mean	67	58	<0.001
	Median	69	60	
Male (%)		76	81	0.735
Active smoking (%)		18	14	<0.05
Diabetes (%)		10	3	0.212
Obesity (%)		22	21	0.793
DYS (%)		33	28	0.506
HTA (%)		53	48	0.158
Diameter (mm)		48.93 ± 7.71	47.38 ± 6.02	0.086
High AI grade (%)		28	16	0.440
AS (%)		12	31	0.210
CAD (%)		31	10	<0.001

Table 3-19. Clinical characteristics of patients whose aneurysmal aortic wall associated with TAV or BAV. TAV = tricuspid aortic valve; BAV = bicuspid aortic valve; HTA = arterial hypertension; DYS = dyslipidemia; AI = aortic insufficiency; AS = aortic stenosis; CAD = coronary artery disease.

TAV patients were significantly older than BAV patients in our population, with a mean age difference of nine years. Moreover, we showed that age was positively correlated with aortic stiffness. According to Hosoda et al., the physiological morphology of the aorta varies significantly around the age of 60. The patients with TAV in our population are mostly more than 60 years old, while the age of BAV patients is majorly less than 60 years old. Therefore, we can conclude that valve morphology has a much smaller effect on aortic wall stiffness than the age factor in our sample size.

Limitations remain in this study. Firstly, there are no control samples from healthy ascending aorta included. This limited us from the comprehensive evaluation of the impact of clinical risk factors between healthy aorta and AsAA from the biomechanical point of view. As discussed in section 1.2, connective tissue disorder and familial risk are the important factors for AsAA. Unfortunately, our study did not take into account these factors. Moreover, studies have shown that smoking is associated with aortic aneurysms, depending on smoking cessation intensity and duration of smoking cessation[289,299].

Another limitation is that although we found that some of the risk factors can provocate significant changes in the biomechanical properties of the AsAA wall, our results were not supported by histology. Histological assessment of elastin and collagen content may provide more information. It can explain the influence of the risk factors on tissue microstructure and related biomechanical properties.

In conclusion, the main finding was that atherosclerosis risk factors do not play key roles in the biomechanical properties of the human aorta. In contrast, age, gender, aortic diameter, aortic stenosis, and aortic insufficiency do. To be more specific, the stiffness of ascending aortic aneurysm was positively correlated with the patient's age and the diameter of the ascending aorta. Meanwhile, the stiffness of the aorta decreased with the degree of aortic insufficiency, while aortic stenosis resulted in increasing aortic stiffness. Surprisingly, we did not find a relationship between aortic valve types (tricuspid aortic valve and bicuspid aortic valve) and ascending aortic aneurysm.

Chapter 4 - Biomechanical properties linked with the ascending aortic aneurysms associated with quadricuspid aortic valve

Among all patients recruited in the University Hospital of Dijon, three patients with ascending aortic aneurysm (AsAA) were selected for biomechanical and histological studies: one with quadricuspid aortic valve (QAV), one with tricuspid aortic valve (TAV), and one with bicuspid aortic valve (BAV). In this study, we focused on the behavior of the aorta associated with QAV, considering the in-vitro biomechanical characteristics and the histological study.

4.1 Introduction

The standard aortic valve has three leaflets. The aortic valve has two leaflets in 1.3% of the population, known as the bicuspid valve (BAV)[300]. As described in chapter 1, AsAA is a life-threatening pathology causing a permanent dilatation associated with a high risk of aortic dissection, which may result in the patient's death. The surgical guidelines of AsAA are not the same based on different valve types (TAV and BAV). There are currently no surgical guidelines for AsAA with quadricuspid aortic valve (AsAA-QAV). The aortic valve has four leaflets in less than 0.0004% of the population, called quadricuspid aortic valve (QAV)[153]. An ascending aneurysm is associated with the bicuspid valve in 30% of cases. Nevertheless, it is rare to observe an AsAA associated with a quadricuspid valve. Only a few case reports have been published on the surgical treatment[301,302]. According to our knowledge, there is no academic research on AsAA-QAV. In this chapter, we would like to study the biomechanical behavior of AsAA-QAV based on the biaxial tensile test as well as histological information.

4.2 Patients and method

Three AsAA patients with QAV, TAV, BAV, respectively, were selected in this research. The biaxial tensile tests were performed. And the maximum value of Young's modulus was the mean evaluation of this study.

4.2.1 Population

A sixty-three-year-old female with hypertension had an aneurysm at the level of the ascending thoracic aorta (the maximum diameter of 52 mm, measured by MRI) and dilatation at the level of the sinotubular junction (38 mm for the maximum diameter of AsAA) associated with QAV. In order to design a comparison study, one fifty-eight-year-old male patient with BAV (53 mm for the maximum diameter of AsAA) and another forty-four-year-old male patient with a tricuspid aortic valve (53 mm for the maximum diameter of AsAA) were chosen based on similar clinical characteristics.

Indeed, the pathologic profile of all three patients was roughly the same:

- the maximum aortic diameter was 52 mm/53 mm.
- only one ASDV risk index
- no aortic valve disorders

4.2.2 Biaxial tensile test preparation

The samples of the aortic wall were obtained from the aortic replacements' surgeries. The in-vitro experimental study started within 30 minutes after the aortic replacement. The aortic wall samples were preserved in phosphate-buffered (PBS) saline during the operation room transfer to the laboratory for biaxial tensile experiment. The aortic walls were cut in square size (15 mm x 15 mm, n = 14) by medial (MED), posterior (POST), lateral (LAT), and anterior (ANT) quadrants, with marking the circumferential (CIR) and longitudinal (LON) directions on each specimen (cf. section 2.3). Besides, considering the 5 points, an average thickness was measured with the help of an electronic micrometer (cf. section 2.4). The biomechanical experiments were carried out by a biaxial tensile test machine (cf. section 2.5). Each specimen was placed in 10 times of 10% preconditioning to deform the contraction caused by the sectioned aorta. A further stretch at a rate of 10 mm/min was set till rupture. Five points have been marked on each specimen to track the in-plane movement by a digital camera (Prosilica GE, Allied Vision Technologies, Germany).

As shown in section 2.2, based on the information of real-time load and displacement obtained by the biaxial tensile and the calculated average thickness, the maximum value of Young's modulus was computed for both CIR and LON directions (defined as E_C and E_L).

4.2.3 Histological process

All the AsAA walls were sampled in the lateral quadrant for histological analysis. The segments were fixed in 10% neutral formalin buffer during 48 - 72h and transferred in 70% ethanol. The fixed aortic tissue was then placed in an embedding box for wax immersion. Each piece of tissue was cut into 5µm cross-sections and stained with Masson trichrome and Verhoeff staining. It is combined staining, especially for aortic tissue. The collagen fibers of the aortic wall appear blue under Masson Trichome. Elastic fibers show black color under Verhof staining. The collagen and elastin are quantified by Qupath software[303] (https://qupath.readthedocs.io/en/stable/).

4.3 Results

The results were analyzed in two ways:

- Biomechanics properties, which mainly focused on the thickness and the maximum value of Young's modulus
- Histology, which primarily focused on the quantification of collagen and elastin fibers.

4.3.1 Biomechanical properties

As described in Chapter 3, the observation of the maximum Young's modulus value in the LAT quadrant was the highest among all regions, while the value of the MED quadrant was the lowest. Therefore, stress-Young's modulus curve of MED and LAT quadrants were chosen for comparison (Fig. 4-1).

In the MED quadrant, the maximum Young's modulus of CIR direction was greater than the LON direction in all three aortic wall samples. The maximum Young's modulus in the CIR direction of AsAA-TAV was higher than the one in both LON and CIR directions of AsAA-BAV and AsAA-QAV.

The CIR direction was higher than the one in the LON direction in the LAT quadrant only in the AsAA-TAV sample. Furthermore, the AsAA-TAV showed a higher value of maximum Young's modulus than AsAA-BAV and AsAA-QAV in both directions. However, in both AsAA-BAV and AsAA-QAV samples, the LON direction had a greater maximum Young's modulus than the CIR direction.

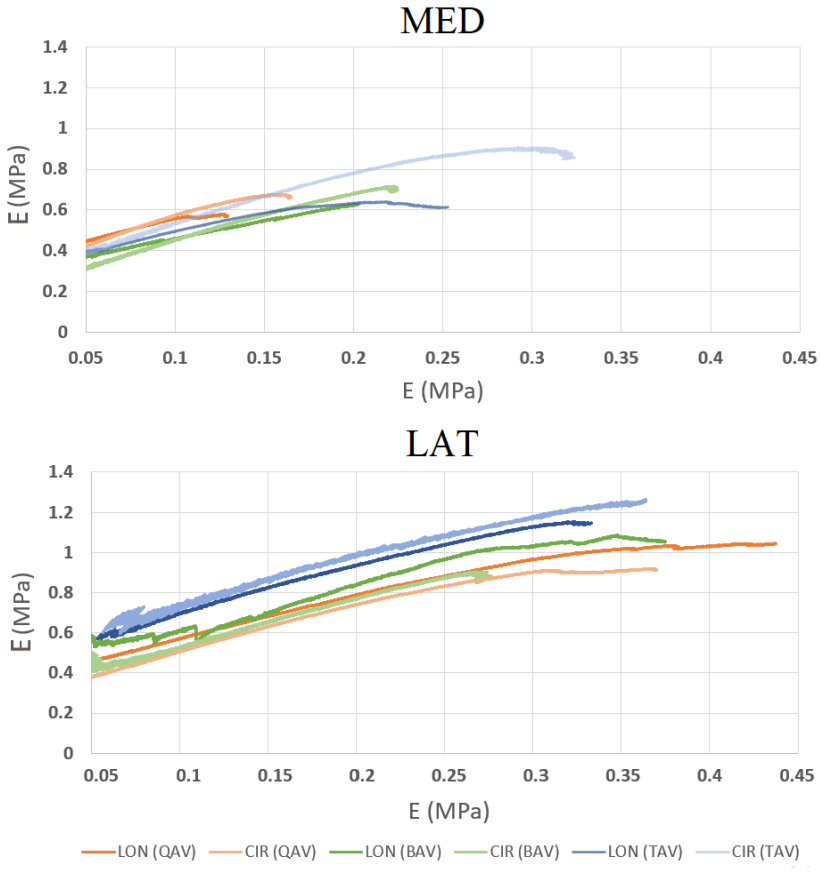

Figure 4-1. Young's modulus-stress curves on the ascending aortic aneurysms associated with QAV, BAV, and TAV. TAV = tricuspid aortic valve; BAV = bicuspid aortic valve; QAV= quadricuspid aortic valve ; CIR = circumferential; LON = longitudinal; MED = medial; ANT = anterior; LAT = lateral; POST = posterior.

In the ANT quadrant, AsAA-TAV showed a greater value of the maximum Young's modulus than for AsAA-QAV and AsAA-BAV. However, in the POST quadrant, a smaller value of the maximum Young's modulus was found in AsAA-TAV than for AsAA-QAV and AsAA-BAV.

From the aortic wall thickness point of view, the AsAA-QAV was thicker than the two other cases (Table 4-1).

			AsAA-QAV	**AsAA-TAV**	**AsAA-BAV**
MED	Maximum Young's modulus (MPa)	LON	0.579	0.630	0.661
		CIR	0.676	0.891	0.717
	Thickness (mm)		2.41	2.256	1.714
ANT	Maximum Young's modulus (MPa)	LON	0.698	0.775	0.667
		CIR	0.889	0.941	0.932
	Thickness (mm)		2.06	1.64	1.498

			AsAA-QAV	AsAA-TAV	AsAA-BAV
LAT	Maximum Young's modulus (MPa)	LON	1.034	1.145	1.087
		CIR	0.911	1.250	0.905
	Thickness (mm)		2.212	1.78	1.306
POST	Maximum Young's modulus (MPa)	LON	0.913	0.667	1.083
		CIR	1.509	0.814	1.384
	Thickness (mm)		2.064	1.574	1.586

Table 4-1. The maximum Young's modulus on circumferential and longitudinal directions and the thickness in different quadrants. AsAA-TAV = ascending aortic aneurysm associated with tricuspid aortic valve; AsAA-BAV = ascending aortic aneurysm associated with bicuspid aortic valve; AsAA-QAV = ascending aortic aneurysm associated with quadricuspid aortic valve; CIR = circumferential; LON = longitudinal; MED = medial; ANT = anterior; LAT = lateral; POST = posterior.

4.3.2 Histological analysis

As can be seen in Fig. 4-2, the collagen and fiber bundled in the aorta form a cross-network. The adventitia and intima of the aortic wall in all three samples had legible boundaries. The intima and media of the aorta of ASAA-QAV and ASAA-BAV were relatively distinguishable. In contrast, the intima and media of ASAA-TAV were not clearly demarcated.

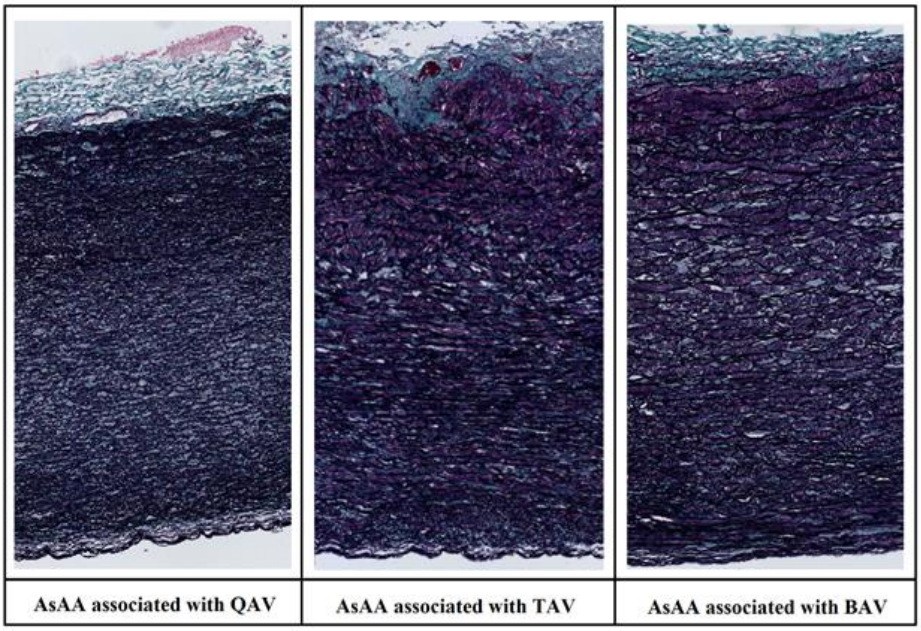

Figure 4-2. Histological images with Masson Trichrome and Verhoef staining in cross-sections of each AsAA associated with different valve types. Black color: fiber; blue color: collagen. From bottom to top of the image: the tunica intima, media, and adventitia. AsAA = ascending aortic aneurysms; QAV = quadricuspid aortic valve; TAV = tricuspid aortic valve; BAV = bicuspid aortic valve.

In terms of histology, AsAA-QAV provided a less quantity of collagen (Fig. 4-2). Indeed, the content of collagen was higher in AsAA-TAV than in AsAA-BAV and AsAA-QAV. Moreover, the elastin content of AsAA- QAV showed a similarity with AsAA-BAV and a higher value than for AsAA-TAV (Table 4-2).

AsAA Type	Collagen (%)	Elastin (%)
AsAA-QAV	19.95	27.37
AsAA-TAV	26.28	21.59
AsAA-BAV	23.09	28.37

Table 4-2. The content of the collagen and elastin in the AsAA-QAV, AsAA-TAV, AsAA-BAV. AsAA-TAV = ascending aortic aneurysm associated with tricuspid aortic valve; AsAA-BAV = ascending aortic aneurysm associated with bicuspid aortic valve; AsAA-QAV = ascending aortic aneurysm associated with the quadricuspid aortic valve.

4.4 Discussion

As described in Chapter 3, there was no significant stiffness difference in the aortic wall thickness between AsAA-TAV and AsAA-BAV. In this chapter, we tried to find patients with a similar clinical condition. Overall, AsAA-QAV matched the range of thickness (1.909 ± 0.389 mm) and maximum Young's modulus (1.033 ± 0.434 MPa) in our previous 100 patients.

The most striking finding in our population was that based on maximum Young's modulus and histology, the biomechanical properties of MED and LAT quadrants on AsAA-QAV were similar to AsAA-BAV compared with AsAA-TAV. Regarding maximum stress, the elastic modulus showed similar behavior for the three patients: the lateral quadrant of the aorta showed a higher stiffness (1.062± 0.138 MPa), roughly the double value of the medial quadrant (0.687 ± 0.103 MPa). The CIR direction of the aorta was stiffer than the LON direction, except for the LAT quadrant of both AsAA-BAV and AsAA-QAV.

According to Bersi et al. [304], the local stiffness had a positive relationship with elastin and a negative relationship with collagen. The aorta with TAV had a higher level of collagen content, lower level of elastin[305]. According to Hosoda et al.[278], the range of collagen and elastin in the human aorta was 19% to 30% and 17% to 40%, respectively. The amount of elastin decreased in the AsAA[306]. In our study, the collagen content in the AsAA-BAV and AsAA-QAV had a lower percentage than in the AsAA-TAV. In contrast, the elastin content in the AsAA-TAV was higher than the other two types of the aorta.

Globally, the characteristics of AsAA-QAV can be found as follow: 1) the maximum value of Young's modulus was 0.901 ± 0.289 MPa, 2) the wall thickness was 2.187 ± 0.165 mm, 3) histologically, 19.95% of the collagen and 27.37% of elastin were found in the aortic wall.

There were many potential shortcomings in this study. Due to the rarity of the quadricuspid aortic valve, it was difficult to include more cases of AsAA-QAV. As discussed in Chapter 3, there was no correlation between AsAA-TAV and AsAA-BAV on the maximum value of Young's modulus. That was the main reason that we could not perform a larger control sample base. Histologically, since we only sampled in the LAT quadrant, there was no information on the collagen and elastin difference in the entire aortic quadrants.

In conclusion, the thickness of the aortic wall was higher when it was associated with a quadricuspid aortic valve than two other aortic valve types (TAV and BAV). The stiffness, as well as the content of collagen and elastin of the aorta associated with the quadricuspid aortic valve, was close to that of the bicuspid aortic valve.

Chapter 5 - Biomechanical properties associated with the acute type A aortic dissection

Aortic dissection is an intimomedial rupture with the separation of different layers of the aortic wall. According to the Stanford classification, there are two types of aortic dissection: Type A for the dissections involving the ascending aorta and type B for the dissections that do not involve the ascending aorta[177]. Type A dissection evolution is generally the death because of aortic rupture or malperfusion syndrome due to the progression of the dissection. Our study aims to discover the biomechanical characteristics of the adventitia and media layers (attached with the intima layer) in the dissected aorta (Type A) and perform a comparative study between these two layers.

As described in section 1.4, aortic dissection (AD) is a severe cardiovascular disease with pathological aortic changes resulting from aortic intima rupture. The blood in the endovascular lumen enters the medial layer of the aorta through the intima tear, forming a dissection hematoma, which expands along the longitudinal of the aorta. AD can lead to an aortic rupture in a short period, resulting in the death of the patients. The extension of the false cavity leads to stenosis or even occlusion of the aortic lumen. The ischemic situation of the essential organs supplied by the true cavity, such as the intestinal tract, kidney, lower limbs, etc., can cause serious complications. According to the data published by the International Aortic Dissection Registry, the in-hospital mortality rate of acute aortic dissection is as high as 57%[4]. The statistics did not include the patients who died in the transfer or failed to see doctors in time. The in-hospital mortality rate of Type A aortic dissection (Stanford classification) is 22%, and that of type B aortic dissection is 13%[307]. Nevertheless, the diagnosis and treatment of cardiovascular diseases have made significant progress. However, AD is still one of the most fatal aortic diseases.

5.1 Introduction

In addition to familial history and genetic factors[308–311], biomechanical factors are also closely related to the occurrence and development of aortic dissection. Current clinical studies have found that 72.1% to 76.6% of patients with acute aortic dissection are elicited with hypertension histotry[4,5]. The aortic blood flow rate and the pressure on the aortic wall in hypertensive patients are higher than healthy people[312,313]. Blood flow in the aortic lumen will produce a series of stresses on the aortic wall. The first is the wall pressure perpendicular to the aortic wall, and the second is the wall shear stress parallel to the aortic wall due to the blood viscosity. Along with the blood flow to the high-speed shaft in the aorta through the membrane, not only will cause the AD to the remote development, the continuous flow can also tear the false AD lumen or form part of the thrombus. These have been proved to be laminated chronic aortic aneurysm sample expansion and severe complications such as dissection rupture[314–318].

At present, there are very few studies with biomechanical tensile tests on dissected aortic samples. The study of Deplano et al.[225] included the healthy aortas and dissected aortas using the biaxial tensile test method. According to them, the stretch of the intimomedial layer is higher, and the ascending aorta becomes stiff due to aortic dissection. Another study was reported by Manopoulos et al.[319]. They used the uniaxial method to observe the aortic regional difference on separated layers. The maximum stress and peak elastic modulus (Young's modulus) of longitudinal specimens are lower than those in the circumference direction. Meanwhile, these values were maximum at LAT and minimum at MED[319]. In our study, the focus is the comparison of the dissected intimomedial layer and adventitia layer. In addition, we would like to seek the cause of the dilatation difference of the dissected aorta.

5.2 Population and method

5.2.1 Population

In this study, eleven aortic dissection samples were collected from aortic harvesting. All patients were admitted for emergency treatment with acute type A (Standford Classification) aortic dissection. There were eight males and three females with an average age of 63 (63 ± 15). Based on the degree of dissection, we divided the aortic samples into two main types: fully dissected (AD-FD) and partially dissected (AD-PD). Fig. 5-1. shows the geometry of AD-FD, in which adventitia and media layers were fully separated. The media and intima layers of the aortic wall were connected as an inner layer. Fig. 5-1. b shows the geometry of the dissected aortic wall where a partial aortic wall was still attached. The attached part was usually at the level of the aorta's medial quadrant, sometimes also along with the anterior and posterior quadrants.

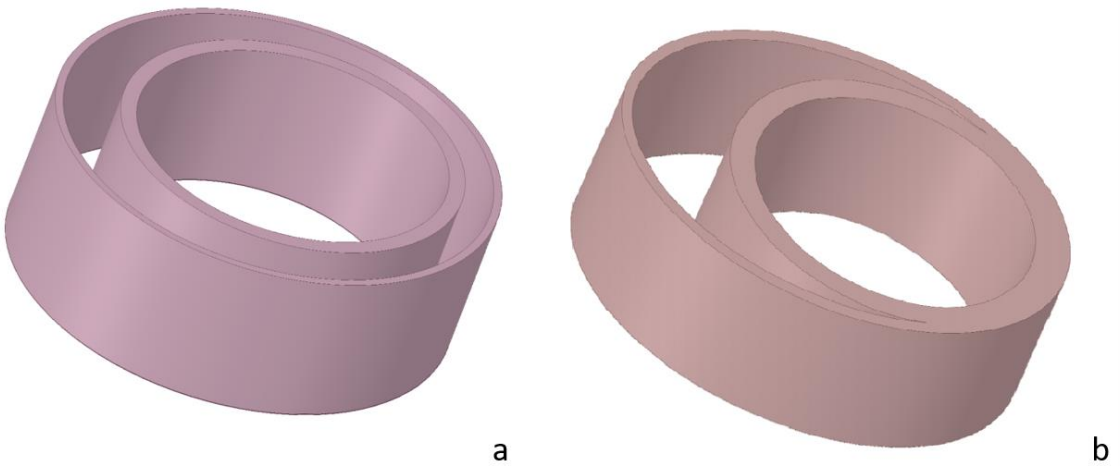

Figure 5-1. Geometries of two types of aortic dissection. a) Fully dissected (AD-FD), b) partially dissected (AD-PD).

5.2.2 Tissue preparation

Four of the aortas belonged to the AD-FD type among the eleven aortic samples, and the rest were AD-PD types. The detailed information of the configuration of the 11 aortic walls can be found in Table 5-1.

Sample No.	Sample Type	MED	ANT	LAT	POST
1	AD-PD	-	S	S	S
2	AD-PD	-	-	S	-
3	AD-FD	S	S	S	S
4	AD-PD	-	S	S	S
5	AD-PD	-	S	S	S
6	AD-FD	S	S	S	S
7	AD-FD	S	S	S	S
8	AD-PD	-	-	S	-
9	AD-FD	S	S	S	S
10	AD-PD	-	S	S	S
11	AD-PD	-	-	S	S

Table 5-1. The information of the dissected quadrans for each aortic dissection. "-" refers to not separated. S = separated; MED = medial; ANT = anterior; LAT = lateral; POST = posterior.

From the eleven harvested aortic walls, 12 undissected specimens and 64 dissected specimens (layer A, n = 32; layer MI, n = 32) were tested. The undissected specimens were obtained from three aortic quadrants: MED (n = 7), ANT (n = 3), and POST (n = 2). The dissected specimens were located in all quadrants: MED (n = 10), ANT (n = 16), LAT (n = 22), and POST (n = 18).

For the AD-FD samples, the aortic wall can be separated into two aortic specimens (Fig. 5-2): adventitia (A) and media-intima (MI). Four different quadrants (MED, ANT, LAT, POST) were tested for both layers.

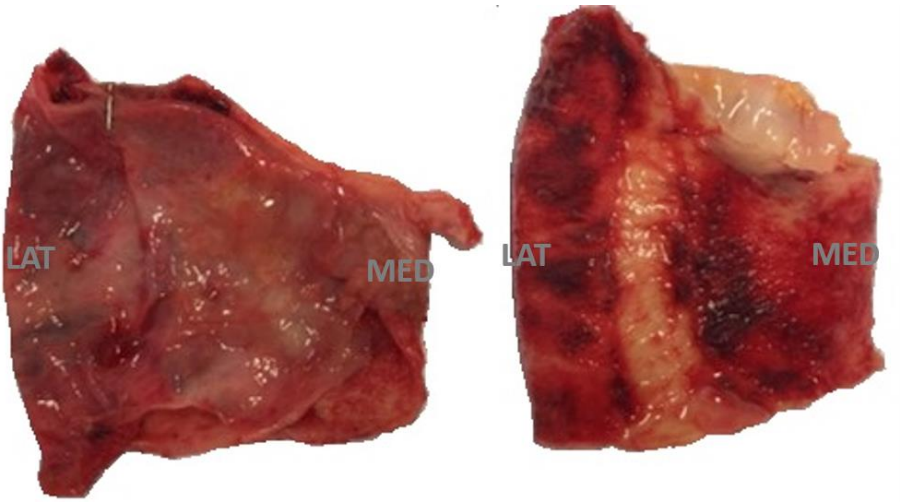

Figure 5-2. Fully dissected aortic sample. Left: adventitia layer; Right: inner layer with both intima and media: layers connected. MED = medial; LAT = lateral.

Based on the dissection degree, the separated layers were tested for both A and MI layers for the AD-PD samples, and the non-separated layers were tested with the complete (C) layer. Fig. 5-3 shows an AD-PD aortic dissection on ANT, LAT, POST quadrants, but not the MED quadrants.

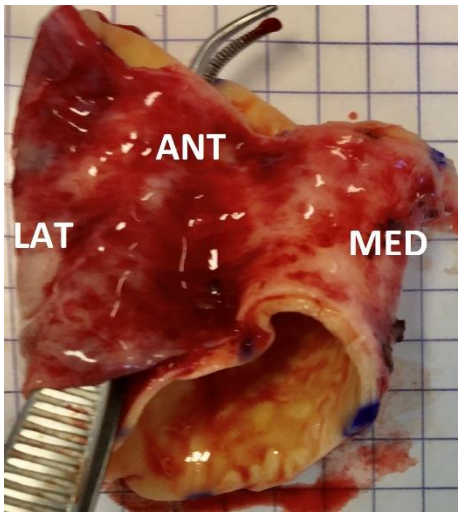

Figure 5-3. Partially dissected aortic sample with only medial quadrant not dissected. MED = medial; ANT = anterior; LAT = lateral.

5.2.3 Experimental method and statistical evaluation

From each quadrant, the sample size of 15 mm x 15 mm was resected. The pre-experimental thickness was measured. The biaxial tensile test was performed on each aortic specimen. More detailed information can be found in sections 2.3, 2.4, and 2.5

As described in section 2.2, thickness, maximum stress (σ_{max}), maximum strain (ε_{max}), and maximum value of Young's modulus (E_{max}) was calculated for each sample.

Concerning the statistical analysis, the extracted data were transferred to Stata software version 16 (Stata Corp, College Station, Texas, USA). Heterogeneity between two layers was assessed using student t-test statistics. The maximum Young's modulus comparison in grouped AD types was based on Kruskal-Wallis equality-of-populations rank test.

5.3 Results

This section is focused on the wall thickness and the maximum value of Young's modulus for eleven dissected aortic walls in three types of layers (layer C, MI, and A) and four quadrants (MED, ANT, LAT, POST).

5.3.1 Aortic wall thickness

Table 5-2 describes the thickness measured for each specimen in the eleven aortic walls. Since the aortic walls were dissected in the lateral quadrant of the aorta, there was no information recorded for the completed layer in LAT.

	Layer	**Thickness** *Mean ± Std. Dev. (mm)*
MED	C	2.525 ± 0.684
	MI	1.799 ± 0.217
	A	0.38 ± 0.077
ANT	C	1.946 ± 0.195
	MI	1.783 ± 0.307
	A	0.398 ± 0.142
LAT	C	-
	MI	1.431 ± 0.267
	A	0.564 ± 0.3
POST	C	2.115 ± 0.222
	MI	1.608 ± 0.305
	A	0.503 ± 0.427

Table 5-2. The thickness of the three types of layers. C = complete layer; A = adventitia layer; MI = media-intima layer; MED = medial; ANT = anterior; LAT = lateral; POST = posterior.

The thickness of the complete aortic layer was significantly higher than layer A, or layer MI ($p < 0.05$). However, if the thickness value of layer A was combined with layer M according to quadrant, the result was not significantly different from the complete aortic layer. On the other hand, layer MI was significantly thicker than the layer A ($p < 0.05$).

5.3.2 Biomechanical properties

The mean value of the maximum Young's modulus in both longitudinal and circumferential directions for layers A and MI is shown in Table 5-3.

Layer	**Longitudinal** *Mean ± Std. Dev. (MPa)*	**Circumferential** *Mean ± Std. Dev. (MPa)*
MI	0.538 ± 0.342	0.588 ± 0.326
A	3.685 ± 1.593	4.631 ± 2.575

Table 5-3. Mean value of Young's modulus in the layer A and the layer MI. A = adventitia layer; MI = media-intima layer.

The mean value of the maximum Young's modulus of the layer MI and layer A was 0.563 MPa and 4.158 Mpa, respectively. It showed that the maximum Young's modulus in layer A was significantly greater than layer MI ($p < 0.05$). There was no significant difference between the longitudinal and circumferential directions.

The mean value of the maximum strain of the layer MI and layer A was 0.236 and 0.317, respectively (Table 5-4). Meanwhile, the mean value of the layer MI and layer A were 0.124 MPa and 1.174 MPa, respectively (Table 5-4). Both the maximum strain and the maximum stress showed a significantly higher value in layer A than layer MI ($p < 0.05$). However, there was no significant difference between the directions.

	Layer	**Longitudinal** *Mean ± Std. Dev.*	**Circumferential** *Mean ± Std. Dev.*
Maximum strain	MI	0.23 ± 0.069	0.243 ± 0.071
	A	0.337 ± 0.128	0.298 ± 0.142
Maximum stress (MPa)	MI	0.116 ± 0.06	0.131 ± 0.054
	A	1.142 ± 0.435	1.207 ± 0.573

Table 5-4. Mean value of the maximum strain and maximum stress in the layer A and the layer MI. A = adventitia layer; MI = media-intima layer.

In both AD-FD and AD-PD groups, the LAT quadrant was dissected. According to the definition of Type A AD, the intima layer was ruptured in the ascending part. We compared the maximum Young's modulus of the layer MI of the LAT quadrant of AD-FD and AD-PD (Table 5-5).

AD-PD		AD-FD	
Longitudinal	**Circumferential**	**Longitudinal**	**Circumferential**
Mean ± Std. Dev. (MPa)	*Mean ± Std. Dev. (MPa)*	*Mean ± Std. Dev. (MPa)*	*Mean ± Std. Dev. (MPa)*
0.829 ± 0.53	0.724 ± 0.458	0.395 ± 0.114	0.443 ± 0.113

Table 5-5. Mean value of Young's modulus of the layer MI of the LAT quadrant of AD-FD and AD-PD. AD-PD = partially dissected type A aortic dissection; AD-FD = fully dissected type A aortic dissection

Even if a higher mean value of the maximum Young's modulus of partially dissected aortic dissection in the layer MI of lateral quadrant can be observed, there was no statistical difference in the stiffness between the two types of AD samples in the layer MI of LAT quadrants.

As we described the biomechanical properties of ascending aortic aneurysms in Chapter 3, we would like to compare the regional difference of maximum Young's modulus between undissected quadrants of aortic dissection and aortic aneurysms (Table 5-6).

	AsAA		AD-PD	
	Longitudinal	**Circumferential**	**Longitudinal**	**Circumferential**
	Mean ± SD (MPa)	*Mean ± SD (MPa)*	*Mean ± SD (MPa)*	*Mean ± SD (MPa)*
MED	0.739 ± 0.316	0.829 ± 0.347	0.711 ± 0.207	0.785 ± 0.261
ANT	0.875 ± 0.311	0.955 ± 0.343	1.047 ± 0.491	0.977 ± 0.438
LAT	1.212 ± 0.472	1.294 ± 0.448	-	
POST	1.074 ± 0.41	1.245 ± 0.431	1.027 ± 0.363	1.02 ± 0.424

Table 5-6. Regional maximum Young's modulus between aortic dissection and aortic aneurysms. AsAA = ascending aortic aneurysms; AD = aortic dissection; MED = medial; ANT = anterior; LAT = lateral; POST = posterior.

Due to the highly unbalanced sample size between AsAA (n = 100, in four quadrants) and AD-PD (MED (n = 7), ANT (n = 3), and POST (n = 2), no statistical test can be performed between AsAA and AD. However, it can be observed that the MED quadrant had less value than other quadrants in both AsAA and AD walls.

5.4 Discussion

Previous studies showed that aortic dissection often occurs in the medial layer of the aortic wall[165] and presents longitudinal rupture[172]. We attempted to investigate the triggering mechanism of AD. The following questions were asked: What are the relative properties of the dissected aortic layers? Why do some aortic dissections rupture completely and others only partially? Does AD have the same biomechanical properties as AsAA?

- **Aortic wall thickness**

There was a significant difference in the thickness of the layer MI and the layer A of the ruptured aorta in this study. According to our observation, the media layer was connected mainly to the intima layer than adventitia. Meanwhile, the separation of the aortic layer does not change the major thickness of the aortic wall. The thickness difference between the two layers varies from 2.55 to 4.73 times, depending on the quadrant. Compared to Fanari et al.[320], they measured the layer MI and full layer by transesophageal echocardiography. The difference between layer MI and layer A was 1.72 times. Comparing with the study of Manopoulos et al.[319], the in-vitro differential thickness measurements were similar to our results. This variation may be due to the in-vitro and in vivo methods. A study had shown that the media layer measured by laser scanning micrometer on fresh aortic tissue was the thickest, followed by the adventitia and intima layers[321] (Fig. 5-4). In our measurements, the thickness of the outer membrane was similar to theirs, which indicated that the outer layer of a ruptured aorta had less adhesion to the medial layer.

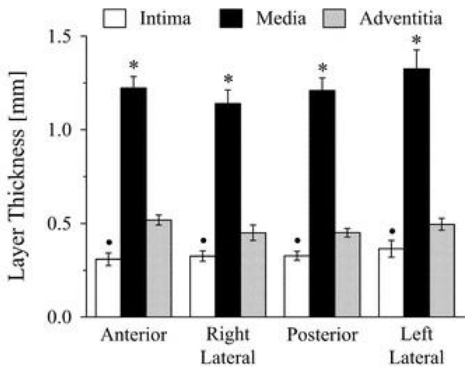

Figure 5-4. The thickness of intima, media, and outer membranes in different regions. (From Sokolis et al., 2012 [321])

- **Biomechanical properties**

Based on our study, we can confirm the layer heterogeneity of the aortic wall with stratified aortic dissection samples. Our results showed that the maximum Young's modulus, maximum strain, and maximum stress of layer A were significantly greater than that of layer MI (Table 5-4). Similar results have been found by Manopoulos et al. in their uniaxial study of 12 aortic dissection samples[319].

Aortic dissection is known to worsen in two ways: the aortic rupture or the layer MI rupture a second time with blood re-entering. In our experiment, we hope to find an explanation based on 64 dissected aortic specimens. We were surprised to find that the stiffness difference between layer MI and layer A can be from 1.77 to 22.21 times. Therefore, we can suggest the following hypothesis: when the stiffness difference between the layer MI and A is small, the high intensity of blood flow can directly break through the adventitia, leading to the rupture of the entire aorta. On the contrary, when the stiffness difference between the layer MI and A is high, the strength of the blood

flow is not enough to break through the adventitia but again tears the media and intima, leading to blood backflow into the aorta.

In our populations, the aortic dissection was separated into two groups in order to explain the cause of the fully dissected aortic wall. Compared with layer A, layer MI was a weaker part since it had the lowest stiffness between the two layers. Thus, another hypothesis was proposed: layer MI in the lateral quadrant can be related to the enlargement of the aortic dissection. In the study, layer MI does not significantly affect the degree of aortic dissection. These results suggest that more factors were affecting aortic dissection, such as blood pressure. The local blood flow pressure was reduced after provocating the "balloon" space in the aortic dissection, which slows down the expansion of dissection.

Pasta et al. argue that thoracic aneurysms were more likely to undergo aortic dissection. They found a significantly lower resistance to aortic dissection than those without aneurysms[322]. They suggested that patients with thoracic aneurysms were more likely to have aortic dissection. Based on our observations, the stiffness distribution of aortic dissection was similar to that of aortic aneurysm, and both showed strong anisotropy. It was the same as most studies on arteries and aortas[14,323,324] but differed from Pasta et al.[322]. This divergence may be related to the differences in sample size and experimental methods.

In this study, the number of aortic dissection samples was limited. According to Manopoulos et al., the longitudinal direction was stiffer than the circumferential direction in both aortic layers (layer MI and layer A)[319]. However, we cannot find this pattern in our population. This difference might be caused by the variety of types of aortic dissection (AD-PD and AD-FD). Furthermore, we divided the sample into two layers: layer A and layer MI, representing the adventitia and intimomedial layers, respectively. In practice, however, we found that part of the medial layer (0.193 ± 0.065 mm) and adventitia layers were attached in one of the AD samples. Since it was a rare situation and this medial layer quantity were few (compared with the part connected with intima), we did not consider the effect of medial layer tissue connected to the adventitia. With the limited population, the age and sex impact of the aortic dissection was explored. Meanwhile, our results were not supported by histology, which can provide detailed information on the elastin and collagen.

To conclude, it was found out that the intimomedial layer had higher thickness but was less stiff than the adventitia. There was no statistical difference in the stiffness between the partially dissected aorta and the complete dissected aorta. In the aortic dissection samples, undissected quadrants showed similar biomechanical behaviors as the aortic wall of ascending aortic aneurysms.

Chapter 6 - 3D printed aorta

This chapter is focused on our study of the biomechanical properties of three 3D printed materials which can simulate the aortic tissue. This research firstly aimed to find 3D printable materials that are more similar to the human aorta. The second aim was to model a healthy human aorta from CT images, using appropriate materials through 3D printing. The ultimate goal is to connect the 3D-printed aortic sample with a pump to simulate the real-time aortic movement in order to perform systematic modeling of the aortic movement in 4D flow MRI.

6.1 Introduction

As described in Section 2.6, 3D printing technology has been widely used in various fields. The technology uses computational 3D imaging software to sort out the 2D tomography data in order to produce 3D reconstruction images. This information can be regenerated into STL files. In recent years, 3D printing technology started to be used in medical fields, such as plastic surgery, orthopedics, dentistry, etc[325–330]. The major processes are remodeling the personalized geometry from CT, or MRI images then print as the prosthesis. However, 3D printing technology is rarely used in the cardiovascular domain. Existing applications are based on cardiovascular education or preoperative simulation[331–334]. The research mainly focuses on the shape of the aorta or artery, instead of the biomechanical properties. That is the reason why the majority of the printed aorta and artery are with hard material. As far as we know, very few studies have explored the use of soft materials in printing arteries or aortas[253,335–337]. There is a common soft material used in these studies: rubber-like material (TangoFLX930™, Stratasys Ltd.©, Israel). However, the simulation subjects are the pulmonary artery, mitral valve, and cerebral vessel. The reported stiffness value in these studies is lower than what we have reported in chapter 3 for the 100 AsAA wall. Therefore, the published information cannot be a reference to our study. This chapter will describe three kinds of elastic materials that have been tested in 3D printing: NinjaFlex® (Fenner Inc., Manheim, USA), Filastic™ (Filastic Inc., Jardim Paulistano, Brazil), and a mixed material of RGD450 and TangoPlus (Stratasys Ltd.©, Israel).

6.2 Material

A non-dilated aorta associated with tricuspid aortic valve from the autopsy of a 64-year-old male was recruited for our study. An open-source 3D medical modeling software, ITK-Snap[338], was used to segment the aortic wall's geometry mask. Then the mask was smoothed by another open-source software, Blender[339]. Detailed information about the process can be found in appendix B.

Different thermoplastic polyurethane and rubber-like materials were tested to search for 3D-printable materials that are more similar to the human aorta.

6.2.1 Thermoplastic polyurethane

For the first phase, we cooperated with Dijon 3D company (Dijon 3D, Dijon, France) on the NinjaFlex material. This material was printed at a temperature of 225-235 ℃. Heating plates were not required during printing. The printing speed was 15-35 milliseconds per meter. The diameter of the original material was 1.75 mm, with 85 shore hardness (SH). MakerBot (MakerBot Industries, USA) 3D printer with loading Thingiverse driver block (MakerBot Industries, USA) dedicated to NinjaFlex printing. The machine was kept at a strict level during the printing process. To minimize the printing error (within 0.02 inches), the 3D printing machine was adjusted by a standard scale.

Different thicknesses of NinjaFlex material were obtained for the experimental use, ranging from 0.175 mm to 1.9 mm with a square of 15 mm × 15 mm (Table 6-1). Fig. 6-1 shows examples of printed NinjaFlex materials.

NinjaFlex thickness (mm)							
0.175	**0.2**	0.225	0.25	0.275	**0.3**	0.325	0.35
0.375	**0.4**	0.425	0.45	0.475	**0.5**	0.525	0.55
0.575	**0.6**	0.625	0.65	0.675	**0.7**	0.725	0.75
0.775	**0.8**	0.825	0.85	0.875	**0.9**	0.925	0.95
0.975	**1**	1.025	1.05	1.075	**1.1**	1.125	1.15
1.175	**1.2**	1.225	1.25	1.275	**1.3**	1.325	1.35
1.375	**1.4**	1.425	1.45	1.475	**1.5**	1.525	1.55
1.575	**1.6**	1.625	1.65	1.675	**1.7**	1.725	1.75
1.775	**1.8**	1.825	1.85	1.875	**1.9**	1.925	1.95

Table 6-1. Printed NinjaFlex material with different thicknesses (material tested marked as bold text).

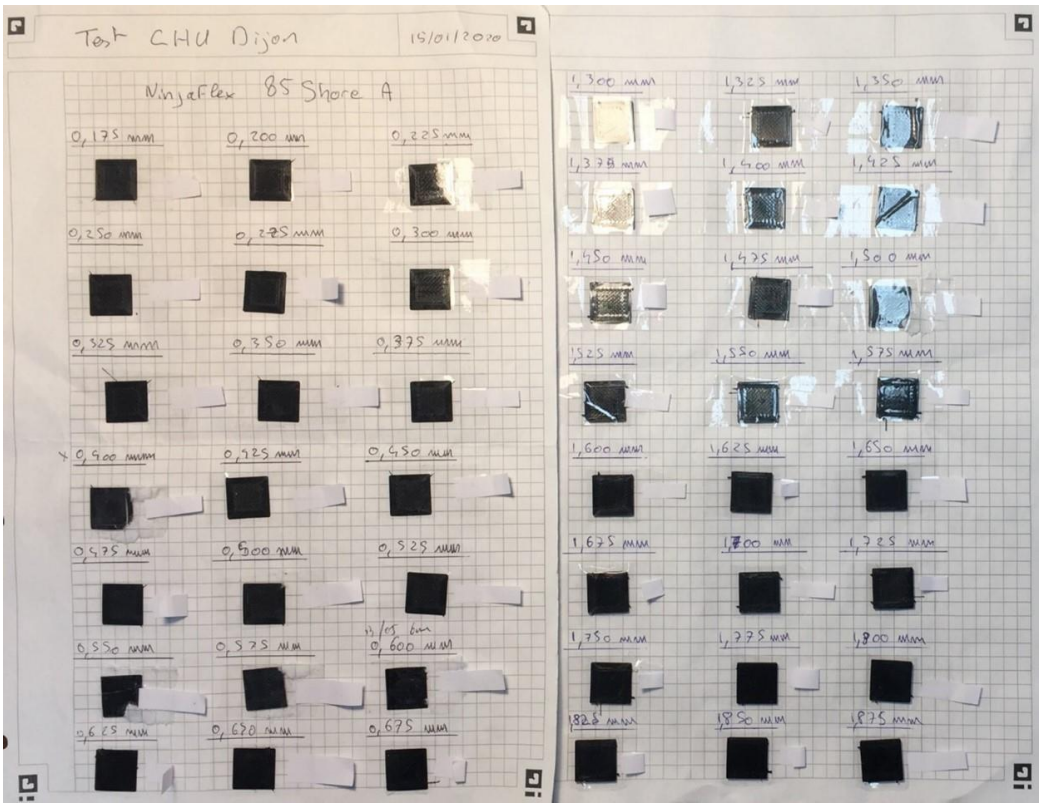

Figure 6-1. Example printed NinjaFlex material.

The uniaxial test was used to study the maximum value of Young's modulus due to the small size of the samples.

In the second stage, the experiments were based on Filastic™ (85SH) soft filament material. Filastic™ materials were printed at the nozzle temperature between 220 and 240 ℃. The heating plate was necessary for printing, and the heating stability should be between 100 and 110 ℃. During the printing procedure, the distance between gear and printing tube was controlled less than 5 mm. The thickness interval of the material could only be controlled within 0.05 mm, because of the material's particularity. The thicknesses of printed Filastic™ are shown in Table 6-2. Fig. 6-2 shows the different printed Filastic™ in the size of 2 cm square.

Uniaxial tests are used in the biomechanical properties' comparison.

Filastic thickness (mm)								
0.1	0.5	0.55	0.6	0.65	0.7	0.75	0.8	0.85

Table 6-2. Printed Filastic material with different thicknesses.

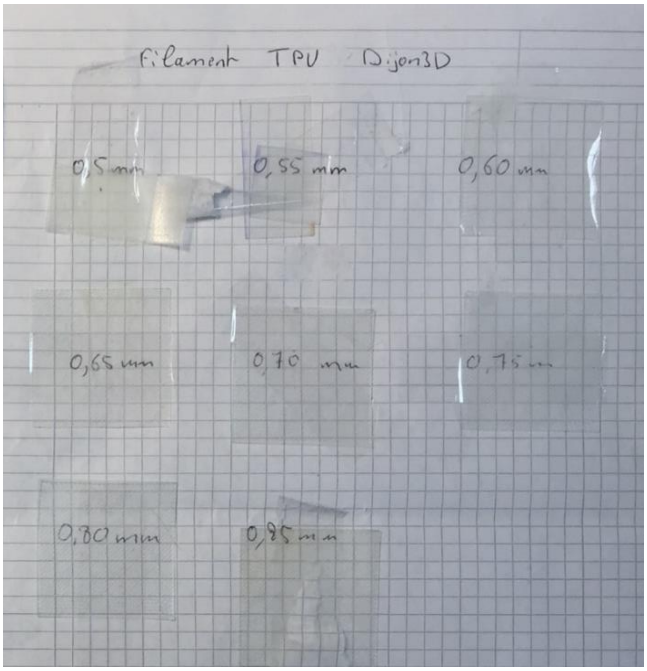

Figure 6-2. Printed Filastic material with different thicknesses.

6.2.2 Rubber-like material (RGD450+TangoPlus)

For the rubber-like material, we cooperated with the ENNOIA company (ENNOIA, Besançon, France). RGD450+TangoPlus is an advanced rubber-like material that can be printed with a smooth surface. It is a mixed material of RGD450 and TangoPlus (Stratasys Ltd.©, Israel) and printed by Connex3^{TM} Object500 3D printer (Stratasys Ltd.©, Israel).

Materials of different shore stiffness were tested in the experiment (Table 6-3). Fig. 6-3 and Fig. 6-4 show RGD450+TangoPlus in 60SH and 70SH and RGD450+TangoPlus in different thicknesses of 50SH and 40SH, respectively.

Biaxial tests were performed to study the maximum Young's modulus value.

RGD450+TangoPlus thickness (mm)				
70SH			2	
60SH			2	
50SH	2	2.5	3	3.5
40SH	2.5	3	3.5	4

Table 6-3. RGD450+TangoPlus material printed with different SH (shore stiffness) and different thicknesses.

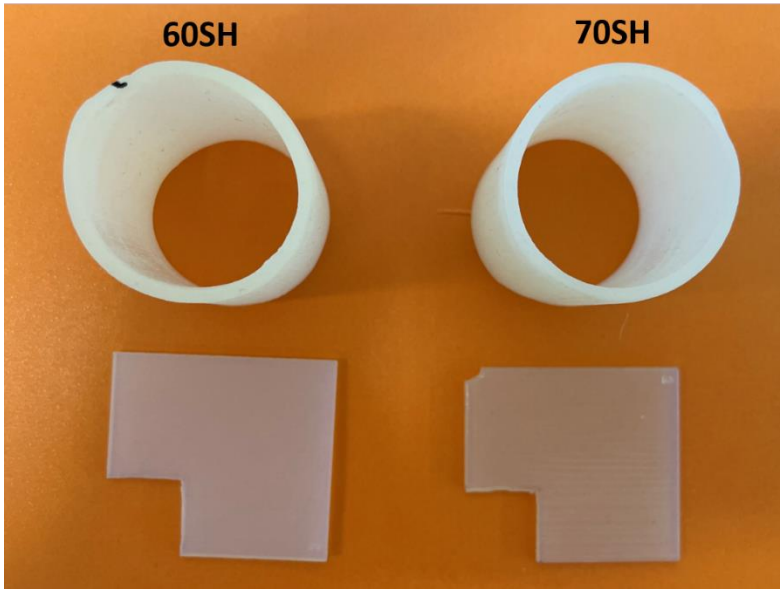

Figure 6-3. Printed RGD450+TangoPlus material of 60SH and 70SH in 2 mm thickness. SH = shore stiffness.

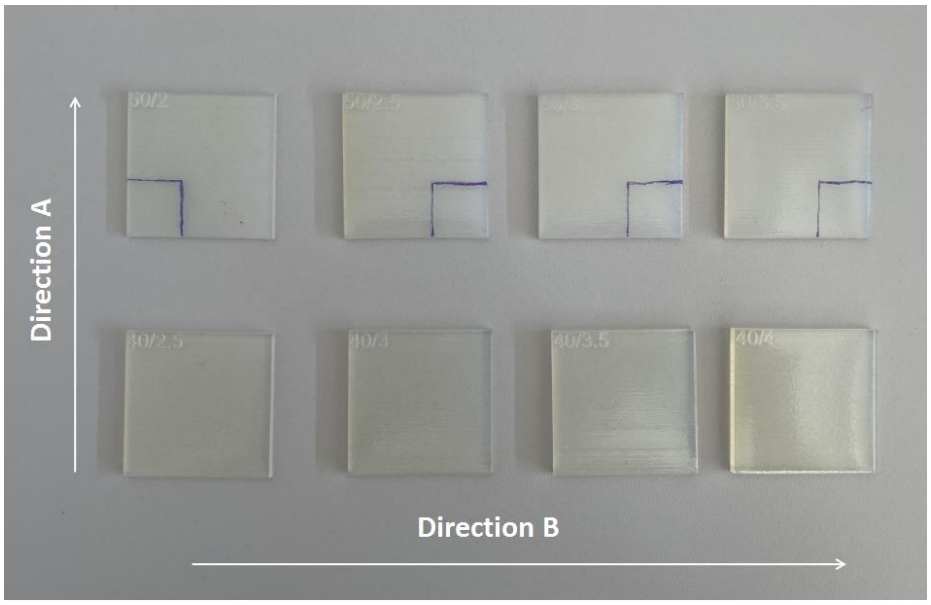

Figure 6-4. Different thicknesses of printed RGD450+TangoPlus material of 40 SH and 50 SH (from left to right: 2.5 mm, 3 mm, 3.5 mm, and 4 mm in thickness).

6.3 Result

The printed material was studied according to two parameters: thickness and maximum value of Young's modulus. In our observation, there was a difference between the expected printed thickness and the experimental measuring thickness. Meanwhile, the maximum Young's modulus was compared between materials.

6.3.1 Thermoplastic polyurethane

Only a part of the material was selected for uniaxial tests to have global information of biomechanical properties due to a large amount of the NinjaFlex material obtained. The specimens tested are shown as the bold texts in Table 6-1.

There was a certain error between the thickness measured in the experiment and the thickness set before printing (Table 6-4). The maximum value of the difference (10.11%) can be observed in the specimen of 1.7 mm thickness of NinjaFlex. Meanwhile, NinjaFlex in 0.6 mm in thickness had less difference (0.33%) between the exported printing thickness and the experimental measuring thickness.

Thickness of NinjaFlex (mm)			
Expected printing thickness	**Experimental measuring thickness**	**Expected printing thickness**	**Experimental measuring thickness**
0.2	0.209	0.3	0.313
0.4	0.423	0.5	0.510
0.6	0.598	0.7	0.694
0.8	0.783	0.9	0.885
1	0.967	1.1	1.052
1.2	1.113	1.3	1.228
1.4	1.329	1.5	1.398
1.6	1.487	1.7	1.528
1.8	1.674	1.9	1.751

Table 6-4. The NinjaFlex thickness difference between expected printed and experimental measuring thickness.

During the experiment, the samples were found printed in different orientations in boundary areas, especially the samples with thickness under 0.8 mm (Fig. 6-5). Specifically, there was an obvious gap between the boundary edge width of 0.2 mm and the central region in all these samples. As can be seen from the figure, the edge of the sample was printed inclinedly (between the thick red line and thin red line), while the sample center was printed vertically (inside the thin red line). It was found out that the rupture of NinjaFlex materials in 0.2 - 0.7 mm occurs at the junction of the two mentioned regions. It was difficult to determine whether the maximum Young's modulus can refer to the biomechanical properties of the material rather than the discontinuous printing in the joints.

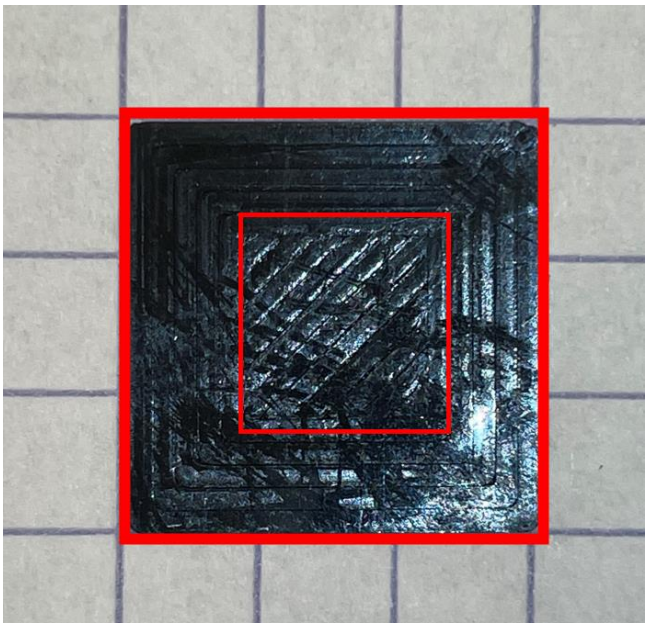

Figure 6-5. Enlarged NinjaFlex sample (the thick red line is the sample boundary, and the thin red line is the gap created during printing.)

The maximum stress and maximum Young's modulus of the tested specimens are shown in Table 6-5.

Biomechanical properties of NinjaFlex		
Printing thickness (mm)	**Maximum stress (MPa)**	**Maximum Young's modulus (MPa)**
0.8	1.384	11.898
0.9	1.331	8.532
1	1.375	9.75
1.1	1.132	8.175
1.2	0.926	8.877
1.3	1.539	9.865
1.4	2.486	9.452
1.5	2.713	10.929
1.6	2.798	11.236
1.7	2.826	10.506
1.8	2.946	10.264

Table 6-5. The maximum stress and maximum Young's modulus of the samples tested in the uniaxial tensile test for NinjaFlex material.

With the thickness increase, the maximum stress showed a rough increasing trend. However, the stiffness did not display a steady increasing trend. The maximum Young's modulus ranges remain from 8.242 to 11.898 MPa.

Filastic materials of different thicknesses have been tested. The thickness error between the expected printing and experimental measurement was ± 0.140 mm (Table 6-6). Table 6-7 shows the biomechanical properties of different Filastic materials.

Thickness of Filastic (mm)			
Expected printed thickness	**Experimental measuring thickness**	**Expected printed thickness**	**Experimental measuring thickness**
0.1	0.078	0.5	0.324
0.55	0.368	0.6	0.445
0.65	0.498	0.7	0.567
0.75	0.615	0.8	0.642
0.85	0.706		

Table 6-6. The comparison between expected printed and experimental measuring thickness of Filastic.

Biomechanical properties of Filastic		
Printed thickness	**Maximum stress (MPa)**	**Maximum Young's modulus (MPa)**
0.1	3.27	15.003
0.5	2.386	12.65
0.55	2.37	13.967
0.6	2.108	21.058
0.65	2.635	23.159
0.7	2.38	18.264
0.75	2.297	12.625
0.8	2.611	25.369
0.85	2.527	8.905

Table 6-7. The maximum stress and maximum Young's modulus for Filastic materials.

For the Filastic material, the maximum stress and maximum Young's modulus did not increase with thickness. It displayed a highly heterogeneous behavior. When the thickness was 0.65 mm, the maximum stress and maximum Young's modulus reached the highest values simultaneously, 2.635 MPa and 23.159 MPa, respectively.

6.3.2 Rubber-like material (RGD450+TangoPlus)

Ten samples of the RGD450+TangoPlus were tested with the biaxial tensile technique. The expected printed thickness of RGD450+TangoPlus material in 70SH and 60SH was similar (± 0.029 mm) as measured during the experiment. However, the 50SH and 40SH material showed larger errors as ± 0.45 mm. The detailed measurements of the thickness are presented in Table 6-8.

Thickness of RGD450+TangoPlus (mm)				
Shore degree	**Expected printed thickness**	**Experimental measuring thickness**	**Expected printed thickness**	**Experimental measuring thickness**
70SH	2	1.971		
60SH	2	1.983		
50SH	2	2.374	2.5	2.806
	3	3.369	3.5	3.907
40SH	2.5	2.781	3	3.443
	3.5	4.185	4	4.491

Table 6-8. The comparison of the thickness between expected printed and the experimental measuring thickness on RGD450+TangoPlus.

Table 6-9 displays the maximum stress and maximum Young's modulus in both directions (A and B).

RGD450+TangoPlus					
Shore degree	**Printed thickness**	**Maximum stress (MPa)**		**Maximum elastic modulus (MPa)**	
		Direction A	**Direction B**	**Direction A**	**Direction B**
70SH	2	0.921	0.816	3.711	3.817
60SH	2	0.477	0.570	2.909	2.641
50SH	2	0.305	0.262	1.041	1.055
	2.5	0.222	0.203	1.253	1.110
	3	0.209	0.156	1.130	1.087
	3.5	0.221	0.221	1.058	1.064
40SH	2.5	0.183	0.152	1.048	0.990
	3	0.155	0.143	0.816	0.947
	3.5	0.174	0.171	0.745	0.699
	4	0.196	0.182	0.739	0.760

Table 6-9. The maximum stress and maximum Young's modulus of the samples tested in the biaxial tensile test for RGD450+TangoPlus.

As RGD450+TangoPlus was printed in different stiffness, it was proved that 70SH was the stiffest, while 40SH was less stiff. Theoretically, materials in the same shore stiffness should have the same value of the maximum Young's modulus regardless of the thickness. However, a variety of the stiffness was observed from 0.699 to 1.048 MPa and 1.041 to 1.253 MPa, in 40SH and 50SH, respectively. Meanwhile, there was no difference in the maximum Young's modulus of directions A and B ($p = 0.9512$).

6.4 Discussion

In order to look forward to a material that is as close as possible to the healthy human aorta, three different materials have been tested.

- **Difference between the expected printing and experimental measuring thickness**

In general, it was found that there was a certain level difference in the thickness between the expected and the experimental measurement. Filastic had the smallest thickness error (maximum of 10.12%) among the three different materials, while NinjaFlex had the largest value (maximum of 33.09%). The thickness error of RGD450+TangoPlus samples had a wide range between 0.85% to 19.57%.

- **Comparison with healthy aortic wall**

Our research aimed to find a suitable 3D-printable material to simulate a healthy aorta in humans. To compare, we obtained a healthy human aorta from an autopsy. The stress-strain curve and stress-Young's modulus curve were computed (Fig. 6-6).

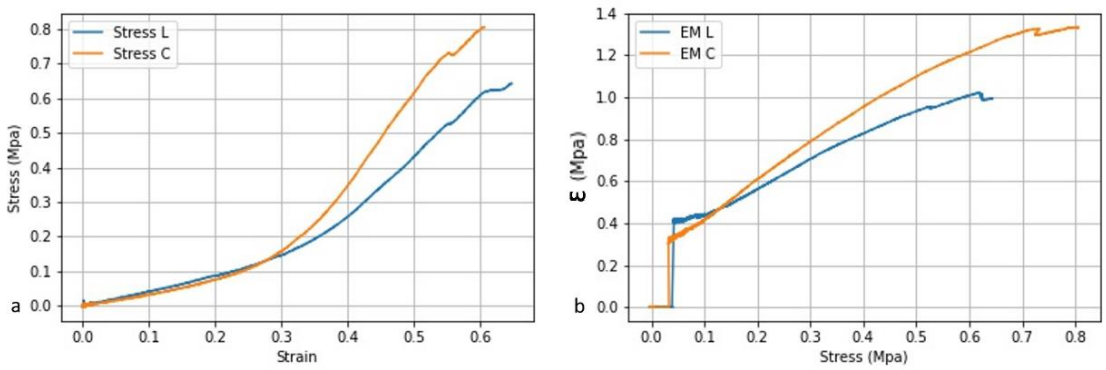

Figure 6-6. Graphs of biomechanical properties of the healthy aortic wall. a) strain-stress curve of the healthy aorta. b) stress-Young's modulus curve of the healthy aorta. L = longitudinal; C = circumferential

A series study on NinjaFlex 3D printed material was performed. Samples less than 0.8 mm of thickness in which the rupture occurred in the gap were eliminated. The piece with less stiffness in the experiment was with 0.8 mm thickness. Fig. 6-7 shows graphs of biomechanical properties of the specimen with a thickness of 0.8 mm.

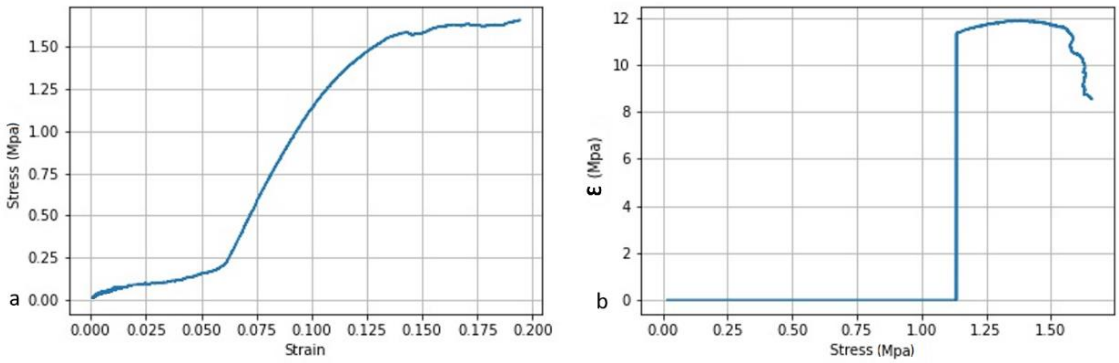

Figure 6-7. Graphs of biomechanical properties of the specimen of NinjaFlex (0.8 mm). a) strain-stress curve; b) stress-Young's modulus curve.

Compared with the healthy aortic wall, a higher stiffness can be observed in the printed NinjaFlex material.

Filastic printed materials of different thicknesses have been tested. According to Table 6-8, the less stiffness sample of Filastic was with the thickness of 0.5 mm. Fig. 6-8 shows graphs of biomechanical properties of the specimen with a 0.5 mm thickness.

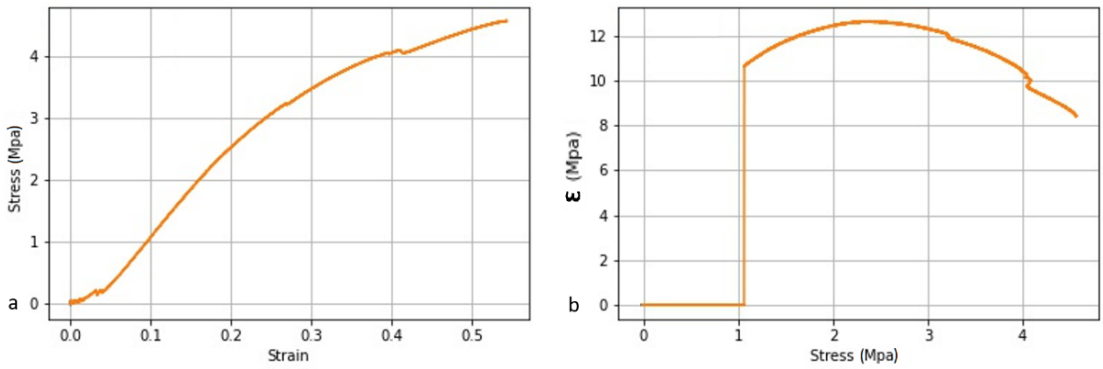

Figure 6-8. Graphs of biomechanical properties of Filastic (0.5 mm). a) strain-stress curve; b) stress-Young's modulus curve.

Higher stiffness was found in NinjaFlex materials than Filastic. Furthermore, both of them have shown a higher stiffness than the healthy human aorta from the biomechanical point of view.

According to Table 6-9, 2 mm of 50SH RGD450+TangoPlus material had a similar value for the maximum Young's modulus than the healthy human aorta. However, it had less value for the maximum stress than the healthy aorta (Fig. 6-9).

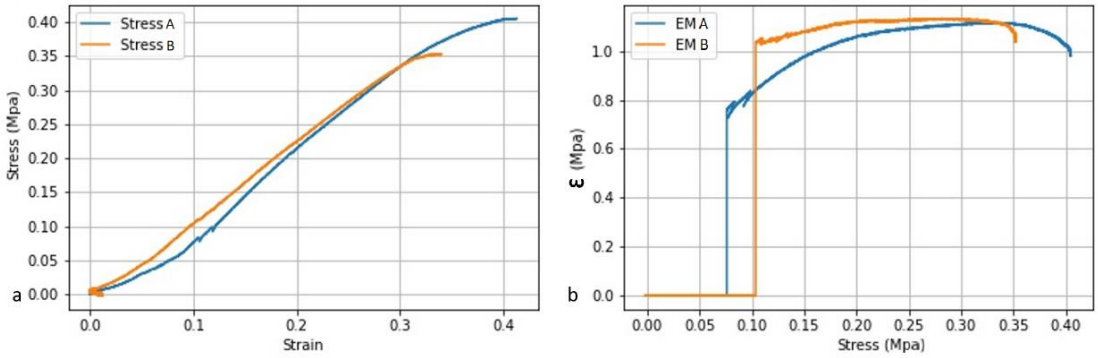

Figure 6-9. Graphs of biomechanical properties of RGD450+TangoPlus (2 mm, 50 SH). a) strain-stress curve; b) stress-Young's modulus curve.

RGD450+TangoPlus had by far the closest biomechanical properties available for 3D printing to the healthy aortic wall.

- **3D printed aorta**

As shown in appendix B, we worked with the Dijon 3D Company (Dijon, France) to print the personalized modeled 3D aorta. A printing defect occurred during the printing process (Fig. 6-10): the medial region of the aortic arch had missing printing material, and irregular burrs appeared on the inner wall of the print. It was due to the high stiffness of the material and the printing equipment quality.

Figure 6-10. Printed personalized aorta. a) the zoomed view of the printed aortic arch. b) the zoomed view of the inner printed aorta

In upcoming works, the focus will be on RGD450+TangoPlus by using the Connex3^{TM} Object500 3D printer, which can ensure the integrity and smoothness of the printing model.

To our knowledge, there is no existing reference of a 3D-printed human aorta. In our study, we focused on comparing the existing healthy human aortic wall in our database. For now, RGD450+TangoPlus in 50SH is the most suitable 3D printable material to represent a healthy human aorta.

Conclusion and perspectives

This thesis aimed at discovering the biomechanical properties of the ascending aortic aneurysms, the aortic dissections, and the 3D printable aortic-like material. We obtained over one hundred healthy and pathological aortas from the University Hospital of Dijon, Dijon, France. The biaxial tensile tests are performed as a biomechanical method of evaluation.

First of all, the results of biomechanical properties of ascending aortic aneurysm and aortic dissection confirmed that the human aortic wall is heterogeneous and anisotropic.

The clinical risk factors of the ascending aortic aneurysms stay unclear up to the moment. Induction factors for AsAA, including the aortic valve types and atherosclerosis risk assessment, have been controversial. Our study found a strong correlation (linear regression) between the aortic wall's thickness and the ascending aorta's diameter. Precisely, the thickness of the aortic wall increased with the diameter of the aorta. Similarly, the stiffness of ascending aortic aneurysm was positively linearly correlated with the patient's age and the diameter of the aorta. In addition, the stiffness of ascending aortic aneurysms was affected by gender, smoking, and aortic valve disorders. The stiffness of the aortic wall decreased with the degree of aortic insufficiency, while aortic stenosis resulted in increasing aortic wall stiffness. Surprisingly, we did not find a relationship between the aortic valve types (tricuspid aortic valve and bicuspid aortic valve) and the ascending aortic aneurysm. The aortic wall stiffness of AsAA associated with different types of aortic valves in our subgroups was more likely related to the age of patients than the aortic valve types. Besides smoking and diabetes, other atherosclerotic risks factors (hypertension, obesity, smoking history) did not affect the biomechanical properties of ascending aortic aneurysms.

Meanwhile, the study of a rare case of AsAA associated with the quadricuspid aortic valve displayed that the thickness of the aortic wall was higher when it was associated with a quadricuspid aortic valve than two other aortic valve types (TAV and BAV). The

stiffness and the content of collagen and elastin of the aorta associated with the quadricuspid aortic valve were close to that of the bicuspid aortic valve.

From the biomechanical experiments of aortic dissection, we could confirm that the intimomedial layer of the aorta was significantly thicker than the adventitia layer. Aortic dissection did not change the overall thickness of the aortic wall comparing with that of AsAA. At the same time, the aortic wall stiffness of adventitia was greater than that of the intimomedial layer. Furthermore, the stiffness difference between the two layers had a large variation (from 1.77 times to 22.21 times). It may explain a common question: why some of the aortic dissections can lead to complete rupture of the aorta, while others induce a second-time intimomedial penetration. On the other hand, we compared the biomechanical properties of aortic dissection samples with the ascending aortic aneurysm samples. It showed that there was no significant difference in aortic wall stiffness between the two pathologies.

The existing 3D printing technologies of the aorta are mainly used in preoperative simulation and teaching as a way of geometric model demonstration. By comparing three different 3D-printed rubber-like materials, we tried to find one material with similar biomechanical properties to a healthy human aorta. Ultimately, we have found that the mixed material of RGD450 and TangoPlus was possible to achieve a similar stiffness as the healthy human aorta. Precisely, the 50 SH RGD450 + TangoPlus (Stratasys Ltd.©, Israel) had nearly the same thickness and stiffness as the human aorta.

The major limitation of this thesis is that the majority of results on biomechanical properties are not supported histologically. Even though all of the aortic samples mentioned previously were histologically sampled and stained, according to the quadrants, quantitative research on collagen and elastin is not performed yet. In the coming year, this part will be completed.

According to the effect of aortic valve types on ascending aortic aneurysms, we did not consider the different types of the bicuspid aortic valve. We will subdivide the bicuspid aortic valve types subgroups and select patients of the same age range for comparison in future work. At the same time, we will consider more biomechanical parameters for evaluation, such as physiological Young's modulus, failure strain, and failure stress.

In terms of 3D printed materials, we do not perform a personalized patient geometry. In the upcoming work, we will test the feasibility of RGD450 + TangoPlus materials in the 3D printing process and accomplish the systematic modeling of the aortic movement from the 4D MRI.

Appendix A - List of Publications

Journal

Siyu Lin, Marie Catherine Morgant, Diana M. Marín-Castrillón, Chloe Bernard, Arnaud Boucher, Benoit Presles, Alain Lalande, Olivier Bouchot. What are the biomechanical properties of an aortic aneurysm associated with quadricuspid aortic valve? *Journals of the American College of Cardiology Case Report*, 2021 (under review)

Siyu Lin, Marie Catherine Morgant, Ludwig Serge Aho Glélé, Diana M. Marín-Castrillón, Arnaud Boucher, Benoit Presles, Olivier Bouchot, Alain Lalande. Local effects of clinicopathological risk factors on local in-vitro biomechanical properties of human ascending aortic aneurysms *Cardiovascular Research*, 2021 (submission under process)

Siyu Lin, Alain Lalande, Meiling Yue, Diana M. Marín-Castrillón, Arnaud Boucher, Benoit Presles, Marie Catherine Morgant, Olivier Bouchot. Identification of regional and layer differences in local biomechanical properties of the aortic dissections. *Journal of Biomechanics*, 2021 (submission under process)

Siyu Lin, Chloe Bernard, Diana M. Marín-Castrillón, Marie Catherine Morgant, Arnaud Boucher, Benoit Presles, Alain Lalande, Olivier Bouchot. 3D printable material of personalized healthy human aorta. (under preparation)

Marie-Catherine Morgant, **Siyu Lin**, Diana Marin-Castrillon, Chloé Bernard, Aline Laubriet, Alexandre Cochet, Alain Lalande, Olivier Bouchot. Comparison of two techniques (in vivo and ex-vivo) for evaluating the elastic properties of the ascending aorta: Prospective cohort study. *PLoS One.* 2021 Sep 13;16(9):e0256278. doi: 10.1371/journal.pone.0256278. PMID: 34516570; PMCID: PMC8437267.

Marie-Catherine Morgant, Johel Miteran, **Siyu Lin**, Aline Laubriet, Alexandre Cochet, Alain Lalande, Olivier Bouchot.Impact of ascending aorta replacement by graft on

elastic properties of descending thoracic aorta evaluated by cardiac magnetic resonance imaging. *Magnetic Resonance Materials in Physics, Biology and Medicine 2020;33(5):641-647*. doi:10.1007/s10334-020-00829-5

Conference Abstracts / Short Papers

Siyu Lin, Marie Catherine Morgant, Alexandre Cochet, Alain Lalande, Olivier Bouchot**.** Local ex-vivo evaluation of the biomechanical properties of the ascending aortic aneurysms. *Archives of Cardiovascular Diseases Supplements.* 2020;12(1):145. doi:10.1016/j.acvdsp.2019.09.316

Siyu Lin, Marie Catherine Morgant, Alexandre Cochet, Alain Lalande, Olivier Bouchot. Biomechanical study on ascending aortic aneurysms associated with quadricuspid aortic valve. *Archives of Cardiovascular Diseases Supplements.* 2020;12(2-4):212. doi:10.1016/j.acvdsp.2020.03.033

Siyu Lin, Marie Catherine Morgant, Alexandre Cochet, Alain Lalande, Olivier Bouchot. Local ex-vivo evaluation of the biomechanical properties of the ascending aortic aneurysms. *Computer Methods in Biomechanics and Biomedical Engineering.* 2019;22(sup1):S413-S414. doi:10.1080/10255842.2020.1714964

Challenges

Bourse de voyage, 44ème congrès de la société de biomécanique, 2019

Appendix B - Aortic wall segmentation

A healthy aorta associated with tricuspid aortic valve from a 64-year-old male was recruited in our study. CT image is obtained for further use. It is necessary to verify the image quality and the exact image to be used in MicroDicom. (Fig. A-1)

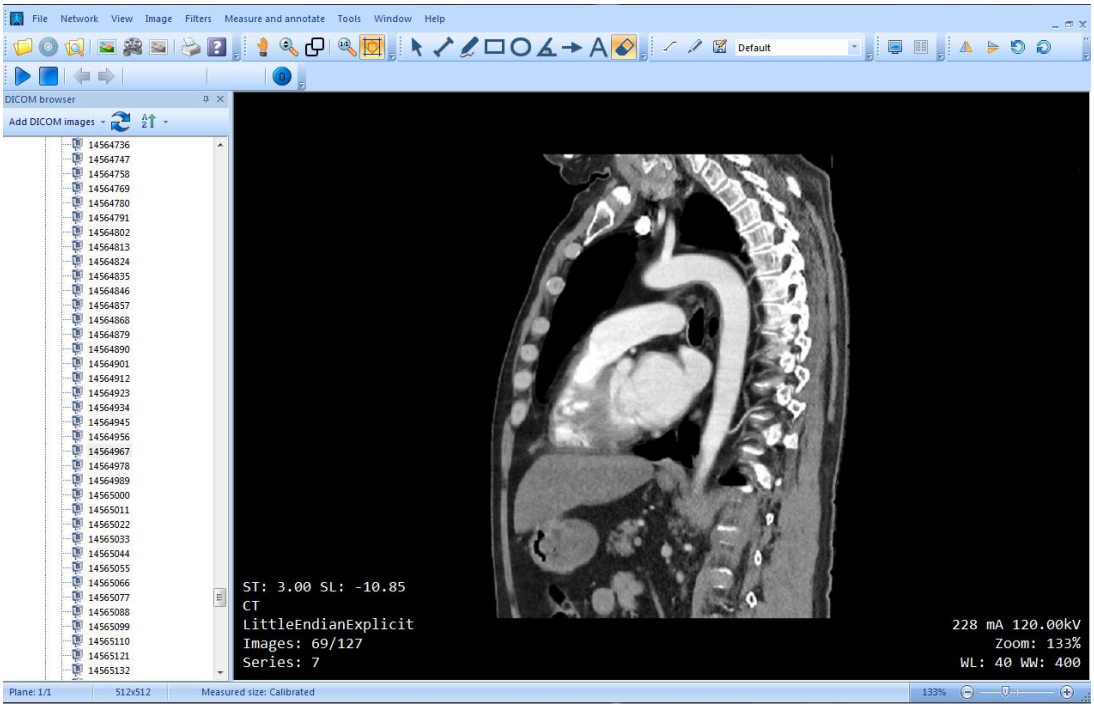

Figure A-1. CT images verified in MicroDicom software.

ITK-Snap is an open-source 3D medical modeling software (http://www.itksnap.org/pmwiki/pmwiki.php). It can generate 3D images manually or semi-automatically. DICOM format data from CT images can be imported into the ITK-Snap: click Open Main Images and Image Filename as prompted. The interface comprises four related Windows: axial, coronal, sagittal, and 3D view, quickly positioned by positioning tool and mouse. (Fig. A-2)

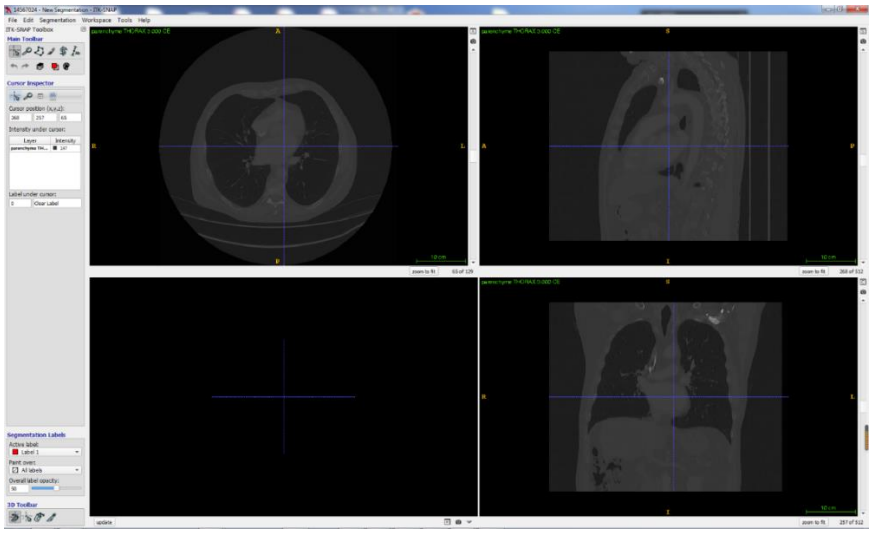

Figure A-2. The display of the axial, coronal, sagittal, and 3D view from ITK-Snap software.

Active the Segmentation Mode can be helpful for the semi-automatic aortic segmentation. The aortic mask was obtained using threshold selection, three-dimensional region growth, and cavity filling techniques. Since the aortic wall is thin and difficult to distinguish from the surrounding fat and spines, the contour of the reconstruction area is the edge of blood containing a high-density contrast agent in the aorta. The software threshold displacement is used to adjust the threshold range until the required tissue contour of the reconstruction model is extracted. In this case, the adjustment of the threshold should be noted. The interval under the threshold should not be set too low. Otherwise, much noise will be extracted. On the contrary, if the interval under the threshold is set too high, the vascular data we need will be lost. The threshold is about 63-917 Hounsfield Unit (HU) hu to locate the correct region. (Fig. A-3). The resulting image is similar to that of an intravascular contrast agent.

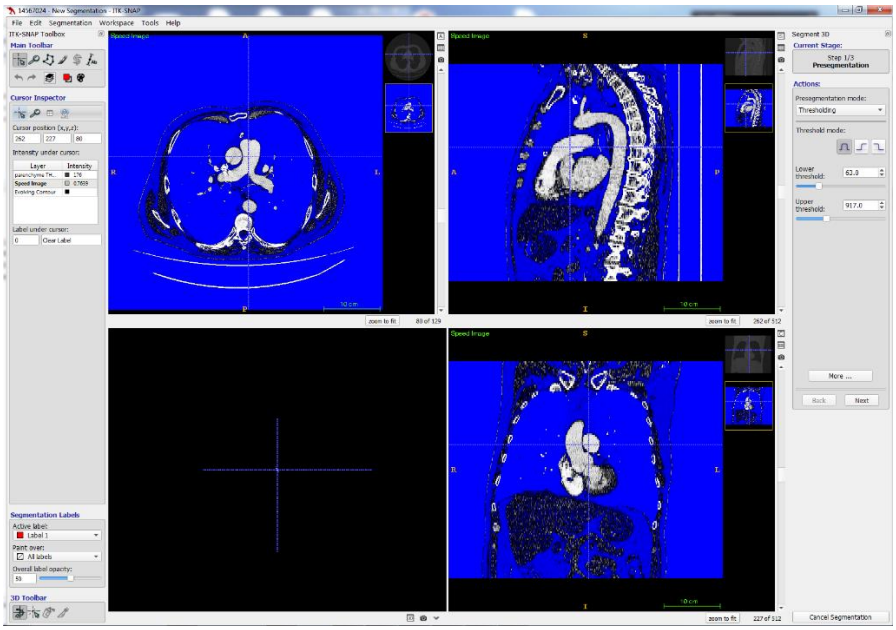

Figure A-3. The aortic zone selected with a specific threshold (63-917 HU).

At this point, select the automatic filling intravascular imaging function in ITK-Snap software. This function refers to the placement of "spheres" as Add Bubble at Cursor of different sizes in different areas within the aorta (Fig. A-4). Then the automatic filing process can be performed. The filling is making the sphere expand, similar to blowing up a balloon. The filling can be terminated according to the boundary position of the aorta. The difficulty of doing this is that the boundary area can be overflow or be missed due to the expansion of a spheroid process (Fig. A-5). Therefore, it is essential to manually remove spare parts and fill in missing parts by the Active Label - Clear Label function. This step is the key to 3D modeling and requires a lot of patience and time. Select Continue Version can help to follow the progress of changes in real-time. It is then exported in .stl format. The entire procedure can be processed in 2 hours. However, the duration can differ due to the image quality.

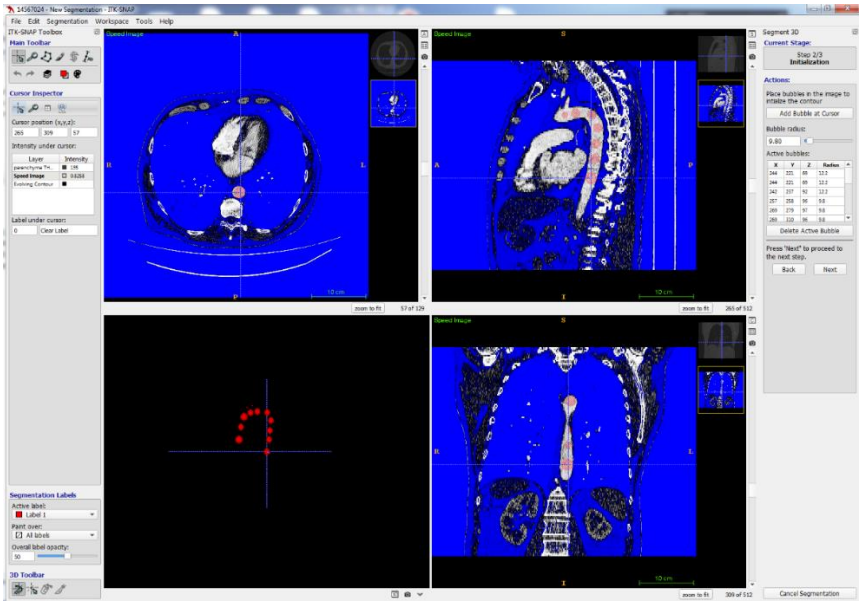

Figure A-4. Semi-automatic function of Add Bubble at Cursor in ITK-Snap.

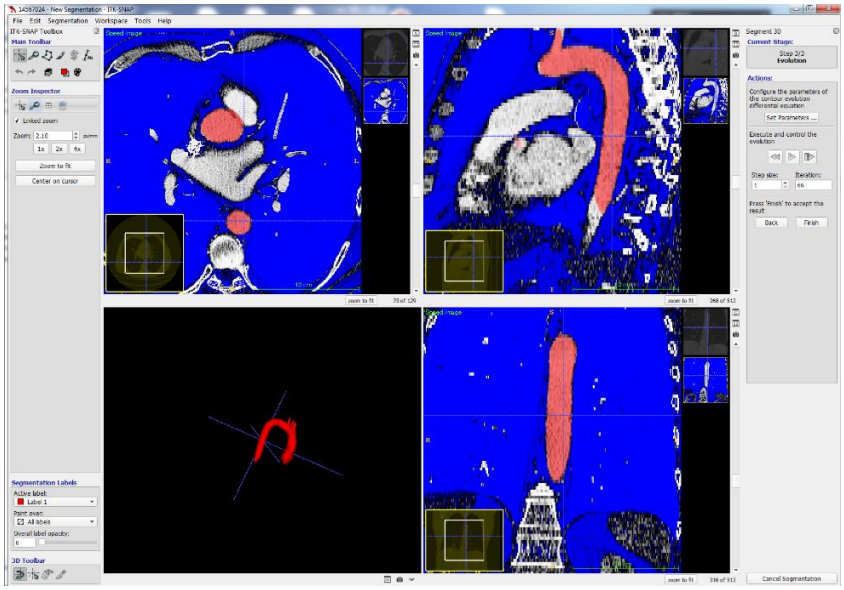

Figure A-5. Execute and control the evolution to fill the inner space of the aorta.

At this step, the geometry of generated aorta is rough and has many burrs, which need to be further corrected. Blender is a 3D design software, which can smooth rough masks (Fig. A-6).

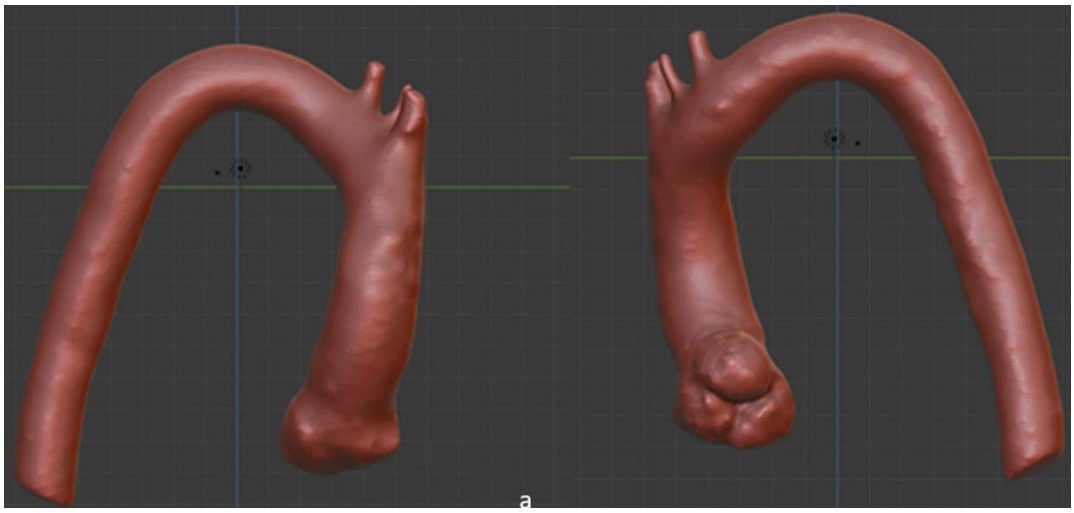

Figure A-6. The smoothed aortic geometry by Blender software. a) the aorta from the anterior view, b) the aorta from the posterior view.

This step requires careful attention to the degree of smoothness. Excessive smooth can reduce the size of the model and provocate distortion. The prominent burrs are then removed, and the .stl can be exported for 3D printing (Fig. A-7).

Figure A-7. The printed aorta is with normal plastic material.

Bibliography

1. Stein LH, Elefteriades JA. Epidemiology and Natural History of Thoraco-Abdominal Aortic Aneurysms. In: Chiesa R, Melissano G, Zangrillo A, eds. *Thoraco-Abdominal Aorta*. Springer Milan; 2011:25-32. doi:10.1007/978-88-470-1857-0_3

2. Booher AM, Eagle KA. Diagnosis and management issues in thoracic aortic aneurysm. *American Heart Journal*. 2011;162(1):38-46.e1. doi:10.1016/j.ahj.2011.04.010

3. Stoecker JB, Wang GJ. Epidemiology of thoracoabdominal aortic aneurysms. *Seminars in Vascular Surgery*. 2021;34(1):18-28. doi:10.1053/j.semvascsurg.2021.02.001

4. Pape LA, Awais M, Woznicki EM, et al. Presentation, Diagnosis, and Outcomes of Acute Aortic Dissection. *Journal of the American College of Cardiology*. 2015;66(4):350-358. doi:10.1016/j.jacc.2015.05.029

5. Hagan PG, Nienaber CA, Isselbacher EM, et al. The International Registry of Acute Aortic Dissection (IRAD): New Insights Into an Old Disease. *JAMA*. 2000;283(7):897. doi:10.1001/jama.283.7.897

6. 2014 ESC Guidelines on the diagnosis and treatment of aortic diseases: Document covering acute and chronic aortic diseases of the thoracic and abdominal aorta of the adultThe Task Force for the Diagnosis and Treatment of Aortic Diseases of the European Society of Cardiology (ESC). *Eur Heart J*. 2014;35(41):2873-2926. doi:10.1093/eurheartj/ehu281

7. Pape LA, Tsai TT, Isselbacher EM, et al. Aortic Diameter ≥5.5 cm Is Not a Good Predictor of Type A Aortic Dissection: Observations From the International Registry of Acute Aortic Dissection (IRAD). *Circulation*. 2007;116(10):1120-1127. doi:10.1161/CIRCULATIONAHA.107.702720

8. Tsai TT, Trimarchi S, Nienaber CA. Acute Aortic Dissection: Perspectives from the International Registry of Acute Aortic Dissection (IRAD). *European Journal of Vascular and Endovascular Surgery*. 2009;37(2):149-159. doi:10.1016/j.ejvs.2008.11.032

9. Di Martino ES, Bohra A, Vande Geest JP, Gupta N, Makaroun MS, Vorp DA. Biomechanical properties of ruptured versus electively repaired abdominal aortic aneurysm wall tissue. *Journal of Vascular Surgery*. 2006;43(3):570-576. doi:10.1016/j.jvs.2005.10.072

10. Pichamuthu JE, Phillippi JA, Cleary DA, et al. Differential Tensile Strength and Collagen Composition in Ascending Aortic Aneurysms by Aortic Valve Phenotype. *The Annals of Thoracic Surgery*. 2013;96(6):2147-2154. doi:10.1016/j.athoracsur.2013.07.001

11. Vorp DA, Schiro BJ, Ehrlich MP, Juvonen TS, Ergin MA, Griffith BP. Effect of aneurysm on the tensile strength and biomechanical behavior of the ascending thoracic aorta. *The Annals of Thoracic Surgery*. 2003;75(4):1210-1214. doi:10.1016/S0003-4975(02)04711-2

12. Iliopoulos DC, Deveja RP, Kritharis EP, et al. Regional and directional variations in the mechanical properties of ascending thoracic aortic aneurysms. *Medical Engineering & Physics*. 2009;31(1):1-9. doi:10.1016/j.medengphy.2008.03.002

13. Duprey A, Khanafer K, Schlicht M, Avril S, Williams D, Berguer R. In Vitro Characterisation of Physiological and Maximum Elastic Modulus of Ascending Thoracic Aortic Aneurysms Using Uniaxial Tensile Testing. *European Journal of Vascular and Endovascular Surgery*. 2010;39(6):700-707. doi:10.1016/j.ejvs.2010.02.015

14. Duprey A, Trabelsi O, Vola M, Favre JP, Avril S. Biaxial rupture properties of ascending thoracic aortic aneurysms. *Acta Biomaterialia*. 2016;42:273-285. doi:10.1016/j.actbio.2016.06.028

15. Di Giuseppe M, Alotta G, Agnese V, et al. Identification of circumferential regional heterogeneity of ascending thoracic aneurysmal aorta by biaxial mechanical testing. *Journal of Molecular and Cellular Cardiology*. 2019;130:205-215. doi:10.1016/j.yjmcc.2019.04.010

16. Sahu KN, Naidu CD, Satyam M, Sankar KJ. Study of RF Signal Attenuation of Human Heart. *Journal of Engineering*. 2015;2015:1-8. doi:10.1155/2015/484686

17. Naksuk N, Padmanabhan D, Yogeswaran V, Asirvatham SJ. Left Atrial Appendage. *JACC: Clinical Electrophysiology*. 2016;2(4):403-412. doi:10.1016/j.jacep.2016.06.006

18. Anderson RH, Razavi R, Taylor AM. Cardiac anatomy revisited. *J Anatomy*. 2004;205(3):159-177. doi:10.1111/j.0021-8782.2004.00330.x

19. Christian Cabrol, Raphael Vialle, Henry Guérin-Surville. *Anatomie Du Coeur Humain*.; 2002.

20. Mori S, Spicer DE, Anderson RH. Revisiting the Anatomy of the Living Heart. *Circ J*. 2016;80(1):24-33. doi:10.1253/circj.CJ-15-1147

21. Hurst JW, Alexander RW, eds. *Hurst's the Heart: Arteries and Veins*. McGraw-Hill; 1998.

22. Mori S, Tretter JT, Spicer DE, Bolender DL, Anderson RH. What is the real cardiac anatomy?: Living Cardiac Anatomy. *Clin Anat*. 2019;32(3):288-309. doi:10.1002/ca.23340

23. Anderson RH, Ho SY, Becker AE. Anatomy of the human atrioventricular junctions revisited. *Anat Rec*. 2000;260(1):81-91. doi:10.1002/1097-0185(20000901)260:1<81::AID-AR90>3.0.CO;2-3

24. Rawlins J, Bhan A, Sharma S. Left ventricular hypertrophy in athletes. *European Journal of Echocardiography*. 2009;10(3):350-356. doi:10.1093/ejechocard/jep017

25. De Paulis R, Salica A. Surgical anatomy of the aortic valve and root—implications for valve repair. *Ann Cardiothorac Surg*. 2019;8(3):313-321. doi:10.21037/acs.2019.04.16

26. Iaizzo PA, Hill, Alexander J., Martinsen, Brad J., et al. *Handbook of Cardiac Anatomy, Physiology, and Devices*. 3d edition. Springer; 2015.

27. Loukas M, Bilinsky E, Bilinsky S, Blaak C, Tubbs RS, Anderson RH. The anatomy of the aortic root: The Anatomy of the Aortic Root. *Clin Anat*. 2014;27(5):748-756. doi:10.1002/ca.22295

28. Misfeld M, Sievers HH. Heart valve macro- and microstructure. *Phil Trans R Soc B*. 2007;362(1484):1421-1436. doi:10.1098/rstb.2007.2125

29. Weind KL, Boughner DR, Rigutto L, Ellis CG. Oxygen diffusion and consumption of aortic valve cusps. *American Journal of Physiology-Heart and Circulatory Physiology*. 2001;281(6):H2604-H2611. doi:10.1152/ajpheart.2001.281.6.H2604

30. Rehman I, Rehman A. Anatomy, Thorax, Heart. In: *StatPearls*. StatPearls Publishing; 2021. Accessed August 4, 2021. http://www.ncbi.nlm.nih.gov/books/NBK470256/

31. El-Hamamsy I, Yacoub M, Chester A. Neuronal Regulation of Aortic Valve Cusps. *CVP*. 2009;7(1):40-46. doi:10.2174/157016109787354088

32. Chester AH, Kershaw JDB, Sarathchandra P, Yacoub MH. Localisation and function of nerves in the aortic root. *Journal of Molecular and Cellular Cardiology*. 2008;44(6):1045-1052. doi:10.1016/j.yjmcc.2008.03.014

33. Cozijnsen L, Braam RL, Waalewijn RA, et al. What Is New in Dilatation of the Ascending Aorta?: Review of Current Literature and Practical Advice for the Cardiologist. *Circulation*. 2011;123(8):924-928. doi:10.1161/CIRCULATIONAHA.110.949131

34. Piazza N, de Jaegere P, Schultz C, Becker AE, Serruys PW, Anderson RH. Anatomy of the Aortic Valvar Complex and Its Implications for Transcatheter Implantation of the Aortic Valve. *Circ Cardiovasc Interv*. 2008;1(1):74-81. doi:10.1161/CIRCINTERVENTIONS.108.780858

35. Shanewise JS, Cheung AT, Aronson S, et al. ASE/SCA Guidelines for Performing a Comprehensive Intraoperative Multiplane Transesophageal Echocardiography Examination: Recommendations of the American Society of Echocardiography Council for Intraoperative Echocardiography and the Society of Cardiovascular Anesthesiologists Task Force for Certification in Perioperative Transesophageal Echocardiography. *Journal of the American Society of Echocardiography*. 1999;12(10):884-900. doi:10.1016/S0894-7317(99)70199-9

36. Schiller NB. Gaining respect for echocardiographic volumetric quantitation: observations on a study of the baseline echocardiography data from the STICH echocardiography core laboratory. *J Am Soc Echocardiogr*. 2012;25(3):337-340. doi:10.1016/j.echo.2012.01.020

37. Abdeldayem EH, Ibrahim AS, Osman AM. CT aortic annulus parameters for pre-operative TAVI assessment: A comparative study between manual post processing and automated software tool. *The Egyptian Journal of Radiology and Nuclear Medicine*. 2018;49(2):352-357. doi:10.1016/j.ejrnm.2018.02.007

38. Marwan M, Achenbach S. Role of Cardiac CT Before Transcatheter Aortic Valve Implantation (TAVI). *Curr Cardiol Rep*. 2016;18(2):21. doi:10.1007/s11886-015-0696-3

39. Khoury GE, Glineur D, Rubay J, et al. Functional classification of aortic root/valve abnormalities and their correlation with etiologies and surgical procedures: *Current Opinion in Cardiology*. 2005;20(2):115-121. doi:10.1097/01.hco.0000153951.31887.a6

40. Silver MA, Roberts WC. Detailed anatomy of the normally functioning aortic valve in hearts of normal and increased weight. *The American Journal of Cardiology*. 1985;55(4):454-461. doi:10.1016/0002-9149(85)90393-5

41. Tamás E, Nylander E. Echocardiographic description of the anatomic relations within the normal aortic root. *J Heart Valve Dis*. 2007;16(3):240-246.

42. Collins JA, Munoz JV, Patel TR, Loukas M, Tubbs RS. The anatomy of the aging aorta: Anatomy of the Aging. *Clin Anat*. 2014;27(3):463-466. doi:10.1002/ca.22384

43. Komutrattananont P, Mahakkanukrauh P, Das S. Morphology of the human aorta and age-related changes: anatomical facts. *Anat Cell Biol*. 2019;52(2):109. doi:10.5115/acb.2019.52.2.109

44. Dagenais F. Anatomy of the Thoracic Aorta and of Its Branches. *Thoracic Surgery Clinics*. 2011;21(2):219-227. doi:10.1016/j.thorsurg.2010.12.004

45. Feller I, Woodburne RT. Surgical Anatomy of the Abdominal Aorta: *Annals of Surgery*. 1961;154(6):239-252. doi:10.1097/00000658-196112000-00033

46. Klabunde, R.E. *Cardiovascular Physiology Concepts*. second. Lippincott Williams & Wilkins; 2012. https://www.cvphysiology.com/

47. Erbel R, Aboyans V, Boileau C, et al. Corrigendum to: 2014 ESC Guidelines on the diagnosis and treatment of aortic diseases. *Eur Heart J*. 2015;36(41):2779-2779. doi:10.1093/eurheartj/ehv178

48. Tadros TM, Klein MD, Shapira OM. Ascending Aortic Dilatation Associated With Bicuspid Aortic Valve: Pathophysiology, Molecular Biology, and Clinical Implications. *Circulation*. 2009;119(6):880-890. doi:10.1161/CIRCULATIONAHA.108.795401

49. Robicsek F. Leonardo da Vinci and the sinuses of Valsalva. *The Annals of Thoracic Surgery*. 1991;52(2):328-335. doi:10.1016/0003-4975(91)91371-2

50. Brewer RJ, Deck JD, Capati B, Nolan SP. The dynamic aortic root. Its role in aortic valve function. *J Thorac Cardiovasc Surg*. 1976;72(3):413-417.

51. Thubrikar M, Piepgrass WC, Bosher LP, Nolan SP. The elastic modulus of canine aortic valve leaflets in vivo and in vitro. *Circ Res*. 1980;47(5):792-800. doi:10.1161/01.RES.47.5.792

52. Lansac E, Lim HS, Shomura Y, et al. Aortic valve opening and closure: the clover dynamics. *Ann Cardiothorac Surg*. 2019;8(3):351-361. doi:10.21037/acs.2019.05.03

53. Devereux RB, de Simone G, Arnett DK, et al. Normal Limits in Relation to Age, Body Size and Gender of Two-Dimensional Echocardiographic Aortic Root Dimensions in Persons ≥15 Years of Age. *The American Journal of Cardiology*. 2012;110(8):1189-1194. doi:10.1016/j.amjcard.2012.05.063

54. Bonow RO, Mann DL, Zipes DP, Libby P. *Braunwald's Heart Disease.* 9th ed. Elsevier Saunders; 2012.

55. Safar ME, Lévy BI. Resistance Vessels in Hypertension. In: *Comprehensive Hypertension*. Elsevier; 2007:145-150. doi:10.1016/B978-0-323-03961-1.50016-7

56. Bromley AB. Aortic Histology: What's 'Normal', Anyway? Published online 2015. http://www.aorta.ca/wp-content/uploads/2015/07/Aortic-Histology-062714.pdf

57. Kau T, Sinzig M, Gasser J, et al. Aortic Development and Anomalies. *Semin intervent Radiol*. 2007;24(2):141-152. doi:10.1055/s-2007-980040

58. Sano M, Unno N, Sasaki T, et al. Topologic distributions of vasa vasorum and lymphatic vasa vasorum in the aortic adventitia – Implications for the prevalence of aortic diseases. *Atherosclerosis*. 2016;247:127-134. doi:10.1016/j.atherosclerosis.2016.02.007

59. Beveridge TS, Johnson M, Power A, Power NE, Allman BL. Anatomy of the nerves and ganglia of the aortic plexus in males. *J Anat*. 2015;226(1):93-103. doi:10.1111/joa.12251

60. Vriz O, Driussi C, Bettio M, Ferrara F, D'Andrea A, Bossone E. Aortic Root Dimensions and Stiffness in Healthy Subjects. *The American Journal of Cardiology*. 2013;112(8):1224-1229. doi:10.1016/j.amjcard.2013.05.068

61. Celermajer DS, Sorensen KE, Spiegelhalter DJ, Georgakopoulos D, Robinson J, Deanfield JE. Aging is associated with endothelial dysfunction in healthy men years before the age-related decline in women. *Journal of the American College of Cardiology*. 1994;24(2):471-476. doi:10.1016/0735-1097(94)90305-0

62. Lakatta EG, Wang M, Najjar SS. Arterial Aging and Subclinical Arterial Disease are Fundamentally Intertwined at Macroscopic and Molecular Levels. *Medical Clinics of North America*. 2009;93(3):583-604. doi:10.1016/j.mcna.2009.02.008

63. Whitlock MC, Hundley WG. Noninvasive Imaging of Flow and Vascular Function in Disease of the Aorta. *JACC: Cardiovascular Imaging*. 2015;8(9):1094-1106. doi:10.1016/j.jcmg.2015.08.001

64. Saliba E, Sia Y, Dore A, El Hamamsy I. The ascending aortic aneurysm: When to intervene? *IJC Heart & Vasculature*. 2015;6:91-100. doi:10.1016/j.ijcha.2015.01.009

65. Clouse WD, Hallett, Jr JW, Schaff HV, Gayari MM, Ilstrup DM, Melton III LJ. Improved Prognosis of Thoracic Aortic Aneurysms: A Population-Based Study. *JAMA*. 1998;280(22):1926. doi:10.1001/jama.280.22.1926

66. Brooke BS, Habashi JP, Judge DP, Patel N, Loeys B, Dietz HC. Angiotensin II Blockade and Aortic-Root Dilation in Marfan's Syndrome. *N Engl J Med*. 2008;358(26):2787-2795. doi:10.1056/NEJMoa0706585

67. Kallenbach K, Karck M, Pak D, et al. Decade of Aortic Valve Sparing Reimplantation: Are We Pushing the Limits Too Far? *Circulation*. 2005;112(9_supplement). doi:10.1161/01.CIRCULATIONAHA.104.525907

68. Kroodsma C. LaPlace's law: Pathogenic relevance in diseases characterized by ectatic or dilated blood vessels. *Journal of the American Academy of Dermatology*. 2010;62(3):AB128. doi:10.1016/j.jaad.2009.11.490

69. Smart SJ, Kroodsma CT. Potential Relevance of LaPlace's Law to the Vascular Permeability Induced by Vasodilators such as Histamine and Bradykinin. *Journal of Allergy and Clinical Immunology*. 2009;123(2):S258-S258. doi:10.1016/j.jaci.2008.12.997

70. Hall AJ, Busse EFG, McCarville DJ, Burgess JJ. Aortic Wall Tension as a Predictive Factor for Abdominal Aortic Aneurysm Rupture: Improving the Selection of Patients for Abdominal Aortic Aneurysm Repair. *Annals of Vascular Surgery*. 2000;14(2):152-157. doi:10.1007/s100169910027

71. Raghavan ML, Vorp DA, Federle MP, Makaroun MS, Webster MW. Wall stress distribution on three-dimensionally reconstructed models of human abdominal aortic aneurysm. *Journal of Vascular Surgery*. 2000;31(4):760-769. doi:10.1067/mva.2000.103971

72. Raghavan ML, Kratzberg J, Castro de Tolosa EM, Hanaoka MM, Walker P, da Silva ES. Regional distribution of wall thickness and failure properties of human abdominal aortic aneurysm. *Journal of Biomechanics*. 2006;39(16):3010-3016. doi:10.1016/j.jbiomech.2005.10.021

73. Schaefer BM, Lewin MB, Stout KK, et al. The bicuspid aortic valve: an integrated phenotypic classification of leaflet morphology and aortic root shape. *Heart*. 2008;94(12):1634-1638. doi:10.1136/hrt.2007.132092

74. Walter MA, Melzer RA, Schindler C, Müller-Brand J, Tyndall A, Nitzsche EU. The value of [18F]FDG-PET in the diagnosis of large-vessel vasculitis and the assessment of activity and extent of disease. *Eur J Nucl Med Mol Imaging*. 2005;32(6):674-681. doi:10.1007/s00259-004-1757-9

75. Albornoz G, Coady MA, Roberts M, et al. Familial Thoracic Aortic Aneurysms and Dissections—Incidence, Modes of Inheritance, and Phenotypic Patterns. *The Annals of Thoracic Surgery*. 2006;82(4):1400-1405. doi:10.1016/j.athoracsur.2006.04.098

76. Kuzmik GA, Sang AX, Elefteriades JA. Natural history of thoracic aortic aneurysms. *Journal of Vascular Surgery*. 2012;56(2):565-571. doi:10.1016/j.jvs.2012.04.053

77. Detaint D, Michelena HI, Nkomo VT, Vahanian A, Jondeau G, Sarano ME. Aortic dilatation patterns and rates in adults with bicuspid aortic valves: a comparative study with Marfan syndrome and degenerative aortopathy. *Heart*. 2014;100(2):126-134. doi:10.1136/heartjnl-2013-304920

78. Pomerance A, Yacoub MH, Gula G. The surgical pathology of thoracic aortic aneurysms. *Histopathology*. 1977;1(4):257-276. doi:10.1111/j.1365-2559.1977.tb01665.x

79. Absi TS, Sundt TM, Tung WS, et al. Altered patterns of gene expression distinguishing ascending aortic aneurysms from abdominal aortic aneurysms: complementary DNA expression profiling in the molecular characterization of aortic disease. *The Journal of Thoracic and Cardiovascular Surgery*. 2003;126(2):344-357. doi:10.1016/S0022-5223(02)73576-9

80. Lansac E, Di Centa I, Raoux F, et al. A lesional classification to standardize surgical management of aortic insufficiency towards valve repair☆. *European Journal of Cardio-Thoracic Surgery*. 2008;33(5):872-878. doi:10.1016/j.ejcts.2007.12.033

81. Habashi JP, Doyle JJ, Holm TM, et al. Angiotensin II Type 2 Receptor Signaling Attenuates Aortic Aneurysm in Mice Through ERK Antagonism. *Science*. 2011;332(6027):361-365. doi:10.1126/science.1192152

82. WRITING GROUP MEMBERS, Hiratzka LF, Bakris GL, et al. 2010 ACCF/AHA/AATS/ACR/ASA/SCA/SCAI/SIR/STS/SVM Guidelines for the Diagnosis and Management of Patients With Thoracic Aortic Disease: A Report of the American College of Cardiology Foundation/American Heart Association Task Force on Practice Guidelines, American Association for Thoracic Surgery, American College of Radiology, American Stroke Association, Society of Cardiovascular Anesthesiologists, Society for Cardiovascular Angiography and Interventions, Society of Interventional Radiology, Society of Thoracic Surgeons, and Society for Vascular Medicine. *Circulation*. 2010;121(13). doi:10.1161/CIR.0b013e3181d4739e

83. Michelena HI, Khanna AD, Mahoney D, et al. Incidence of Aortic Complications in Patients With Bicuspid Aortic Valves. *JAMA*. 2011;306(10):1104. doi:10.1001/jama.2011.1286

84. Aydin A, Desai N, Bernhardt AMJ, et al. Ascending aortic aneurysm and aortic valve dysfunction in bicuspid aortic valve disease. *International Journal of Cardiology*. 2013;164(3):301-305. doi:10.1016/j.ijcard.2011.07.018

85. Judge DP, Dietz HC. Marfan's syndrome. *The Lancet*. 2005;366(9501):1965-1976. doi:10.1016/S0140-6736(05)67789-6

86. Arslan-Kirchner M, Kodolitsch Y von, Schmidtke J. The Importance of Genetic Testing in the Clinical Management of Patients With Marfan Syndrome and Related Disorders. *Deutsches Aerzteblatt Online*. Published online July 4, 2008. doi:10.3238/arztebl.2008.0483

87. Loeys BL, Dietz HC, Braverman AC, et al. The revised Ghent nosology for the Marfan syndrome. *Journal of Medical Genetics*. 2010;47(7):476-485. doi:10.1136/jmg.2009.072785

88. Silverman DI, Burton KJ, Gray J, et al. Life expectancy in the Marfan syndrome. *The American Journal of Cardiology*. 1995;75(2):157-160. doi:10.1016/S0002-9149(00)80066-1

89. Pepin M, Schwarze U, Superti-Furga A, Byers PH. Clinical and Genetic Features of Ehlers–Danlos Syndrome Type IV, the Vascular Type. *N Engl J Med*. 2000;342(10):673-680. doi:10.1056/NEJM200003093421001

90. Loeys BL, Schwarze U, Holm T, et al. Aneurysm Syndromes Caused by Mutations in the TGF-β Receptor. *N Engl J Med*. 2006;355(8):788-798. doi:10.1056/NEJMoa055695

91. Habashi JP. Losartan, an AT1 Antagonist, Prevents Aortic Aneurysm in a Mouse Model of Marfan Syndrome. *Science*. 2006;312(5770):117-121. doi:10.1126/science.1124287

92. Danyi P, Elefteriades JA, Jovin IS. Medical Therapy of Thoracic Aortic Aneurysms: Are We There Yet? *Circulation*. 2011;124(13):1469-1476. doi:10.1161/CIRCULATIONAHA.110.006486

93. Matura LA, Ho VB, Rosing DR, Bondy CA. Aortic Dilatation and Dissection in Turner Syndrome. *Circulation*. 2007;116(15):1663-1670. doi:10.1161/CIRCULATIONAHA.106.685487

94. Hjerrild BE, Mortensen KH, Sørensen KE, et al. Thoracic aortopathy in Turner syndrome and the influence of bicuspid aortic valves and blood pressure: a CMR study. *J Cardiovasc Magn Reson*. 2010;12(1):12. doi:10.1186/1532-429X-12-12

95. Elsheikh M, Casadei B, Conway GS, Wass JAH. Hypertension is a major risk factor for aortic root dilatation in women with Turner's syndrome: Hypertension and aortic root dilation in TS. *Clinical Endocrinology*. 2001;54(1):69-73. doi:10.1046/j.1365-2265.2001.01154.x

96. Mortensen KH, Hjerrild BE, Stochholm K, et al. Dilation of the ascending aorta in Turner syndrome - a prospective cardiovascular magnetic resonance study. *J Cardiovasc Magn Reson*. 2011;13(1):24. doi:10.1186/1532-429X-13-24

97. Davies RR, Kaple RK, Mandapati D, et al. Natural History of Ascending Aortic Aneurysms in the Setting of an Unreplaced Bicuspid Aortic Valve. *The Annals of Thoracic Surgery*. 2007;83(4):1338-1344. doi:10.1016/j.athoracsur.2006.10.074

98. LeMaire SA, McDonald MLN, Guo D chuan, et al. Genome-wide association study identifies a susceptibility locus for thoracic aortic aneurysms and aortic dissections spanning FBN1 at 15q21.1. *Nat Genet*. 2011;43(10):996-1000. doi:10.1038/ng.934

99. Erdheim J. Medionecrosis aortae idiopathica cystica. *Virchows Arch path Anat*. 1930;276(1):187-229. doi:10.1007/BF02275142

100. Koullias G, Modak R, Tranquilli M, Korkolis DP, Barash P, Elefteriades JA. Mechanical deterioration underlies malignant behavior of aneurysmal human ascending aorta. *The Journal of Thoracic and Cardiovascular Surgery*. 2005;130(3):677.e1-677.e9. doi:10.1016/j.jtcvs.2005.02.052

101. Tavora F, Burke A. Review of isolated ascending aortitis: differential diagnosis, including syphilitic, Takayasu's and giant cell aortitis. *Pathology*. 2006;38(4):302-308. doi:10.1080/00313020600820898

102. Hannuksela M, Lundqvist S, Carlberg B. Thoracic aorta – dilated or not? *Scandinavian Cardiovascular Journal*. 2006;40(3):175-178. doi:10.1080/14017430600565999

103. Svensson LG, Kim KH, Lytle BW, Cosgrove DM. Relationship of aortic cross-sectional area to height ratio and the risk of aortic dissection in patients with bicuspid aortic valves. *The Journal of Thoracic and Cardiovascular Surgery*. 2003;126(3):892-893. doi:10.1016/S0022-5223(03)00608-1

104. Svensson LG, Khitin L. Aortic cross-sectional area/height ratio timing of aortic surgery in asymptomatic patients with Marfan syndrome. *The Journal of Thoracic and Cardiovascular Surgery*. 2002;123(2):360-361. doi:10.1067/mtc.2002.118497

105. Roman MJ, Devereux RB, Kramer-Fox R, O'Loughlin J. Two-dimensional echocardiographic aortic root dimensions in normal children and adults. *The American Journal of Cardiology*. 1989;64(8):507-512. doi:10.1016/0002-9149(89)90430-X

106. Vahanian A, Baumgartner H, Bax J, et al. Guidelines on the management of valvular heart disease: The Task Force on the Management of Valvular Heart Disease of the European Society of Cardiology. *European Heart Journal*. 2006;28(2):230-268. doi:10.1093/eurheartj/ehl428

107. Coady MA, Rizzo JA, Hammond GL, et al. What is the appropriate size criterion for resection of thoracic aortic aneurysms? *The Journal of Thoracic and Cardiovascular Surgery*. 1997;113(3):476-491. doi:10.1016/S0022-5223(97)70360-X

108. Elefteriades JA. Thoracic aortic aneurysm: reading the enemy's playbook. *Yale J Biol Med*. 2008;81(4):175-186.

109. Gazoni LM, Speir AM, Kron IL, Fonner E, Crosby IK. Elective Thoracic Aortic Aneurysm Surgery: Better Outcomes from High-Volume Centers. *Journal of the American College of Surgeons*. 2010;210(5):855-859. doi:10.1016/j.jamcollsurg.2010.01.013

110. Ehrlich MP, Ergin MA, McCullough JN, et al. Predictors of adverse outcome and transient neurological dysfunction after ascending aorta/hemiarch replacement. *The Annals of Thoracic Surgery*. 2000;69(6):1755-1763. doi:10.1016/S0003-4975(00)01377-1

111. Cooley DA, Bloodwell RD, Beall AC, Hallman GL, De Bakey ME. Surgical Management of Aneurysms of the Ascending Aorta: Including Those Associated with Aortic Valvular Incompetence. *Surgical Clinics of North America*. 1966;46(4):1033-1044. doi:10.1016/S0039-6109(16)37945-2

112. Matthews AM. The development of the Starr-Edwards heart valve. *Tex Heart Inst J*. 1998;25(4):282-293.

113. Bentall H, De Bono A. A technique for complete replacement of the ascending aorta. *Thorax*. 1968;23(4):338-339. doi:10.1136/thx.23.4.338

114. Katselis C, Samanidis G, Papasotiriou A, et al. Long-Term Results after Modified Bentall Operation in 200 Patients. *J Heart Valve Dis*. 2017;26(6):639-645.

115. Guilmet D, Bonnet N, Saal JP, Le Houerou D, Ghorayeb G. Long term survival with the Bentall button operation in 150 patients. *Arch Mal Coeur Vaiss*. 2004;97(2):83-91.

116. Etz CD, Homann TM, Silovitz D, et al. Long-Term Survival After the Bentall Procedure in 206 Patients With Bicuspid Aortic Valve. *The Annals of Thoracic Surgery*. 2007;84(4):1186-1194. doi:10.1016/j.athoracsur.2007.03.057

117. Boccalini S, Swart LE, Bekkers JA, et al. CT angiography for depiction of complications after the Bentall procedure. *BJR*. Published online August 13, 2018:20180226. doi:10.1259/bjr.20180226

118. Yacoub MH, Gehle P, Chandrasekaran V, Birks EJ, Child A, Radley-Smith R. Late results of a valve-preserving operation in patients with aneurysms of the ascending aorta and root. *The Journal of Thoracic and Cardiovascular Surgery*. 1998;115(5):1080-1090. doi:10.1016/S0022-5223(98)70408-8

119. David TE, Feindel CM. An aortic valve-sparing operation for patients with aortic incompetence and aneurysm of the ascending aorta. *J Thorac Cardiovasc Surg*. 1992;103(4):617-621; discussion 622.

120. David TE, David CM, Feindel CM, Manlhiot C. Reimplantation of the aortic valve at 20 years. *The Journal of Thoracic and Cardiovascular Surgery*. 2017;153(2):232-238. doi:10.1016/j.jtcvs.2016.10.081

121. Lansac E, Di Centa I, Bonnet N, et al. Aortic prosthetic ring annuloplasty: a useful adjunct to a standardized aortic valve-sparing procedure?☆. *European Journal of Cardio-Thoracic Surgery*. 2006;29(4):537-544. doi:10.1016/j.ejcts.2005.12.055

122. Lansac E, Di Centa I, Sleilaty G, et al. Long-term results of external aortic ring annuloplasty for aortic valve repair. *Eur J Cardiothorac Surg*. 2016;50(2):350-360. doi:10.1093/ejcts/ezw070

123. Morgant M, Malapert G, Bernard C, et al. Aortic root remodeling with external annuloplasty for acute type A aortic dissection: Midterm results. *J Card Surg*. 2021;36(5):1770-1778. doi:10.1111/jocs.15095

124. Huntington K, Hunter AGW, Chan KL. A Prospective Study to Assess the Frequency of Familial Clustering of Congenital Bicuspid Aortic Valve. *Journal of the American College of Cardiology*. 1997;30(7):1809-1812. doi:10.1016/S0735-1097(97)00372-0

125. Clementi M, Notari L, Borghi A, Tenconi R. Familial congenital bicuspid aortic valve: a disorder of uncertain inheritance. *Am J Med Genet*. 1996;62(4):336-338. doi:10.1002/(SICI)1096-8628(19960424)62:4<336::AID-AJMG2>3.0.CO;2-P

126. Tutar E, Ekici F, Atalay S, Nacar N. The prevalence of bicuspid aortic valve in newborns by echocardiographic screening. *American Heart Journal*. 2005;150(3):513-515. doi:10.1016/j.ahj.2004.10.036

127. Nistri S, Basso C, Marzari C, Mormino P, Thiene G. Frequency of Bicuspid Aortic Valve in Young Male Conscripts by Echocardiogram. *The American Journal of Cardiology*. 2005;96(5):718-721. doi:10.1016/j.amjcard.2005.04.051

128. Sievers HH, Schmidtke C. A classification system for the bicuspid aortic valve from 304 surgical specimens. *The Journal of Thoracic and Cardiovascular Surgery*. 2007;133(5):1226-1233. doi:10.1016/j.jtcvs.2007.01.039

129. Singh S, Ghayal P, Mathur A, et al. Unicuspid Unicommissural Aortic Valve: An Extremely Rare Congenital Anomaly. *Texas Heart Institute Journal*. 2015;42(3):273-276. doi:10.14503/THIJ-13-3634

130. Reed CM, Richey PA, Pulliam DA, Somes GW, Alpert BS. Aortic dimensions in tall men and women. *The American Journal of Cardiology*. 1993;71(7):608-610. doi:10.1016/0002-9149(93)90523-F

131. Kinoshita N, Mimura J, Obayashi C, Katsukawa F, Onishi S, Yamazaki H. Aortic root dilatation among young competitive athletes: Echocardiographic screening of 1929 athletes between 15 and 34 years of age. *American Heart Journal*. 2000;139(4):723-728. doi:10.1016/S0002-8703(00)90055-3

132. van Kimmenade RRJ, Kempers M, de Boer MJ, Loeys BL, Timmermans J. A clinical appraisal of different Z-score equations for aortic root assessment in the diagnostic evaluation of Marfan syndrome. *Genet Med*. 2013;15(7):528-532. doi:10.1038/gim.2012.172

133. Chandra S, Lang RM, Nicolarsen J, et al. Bicuspid Aortic Valve: Inter-Racial Difference in Frequency and Aortic Dimensions. *JACC: Cardiovascular Imaging*. 2012;5(10):981-989. doi:10.1016/j.jcmg.2012.07.008

134. Fernandes SM, Sanders SP, Khairy P, et al. Morphology of bicuspid aortic valve in children and adolescents. *Journal of the American College of Cardiology*. 2004;44(8):1648-1651. doi:10.1016/j.jacc.2004.05.063

135. Fazel SS, Mallidi HR, Lee RS, et al. The aortopathy of bicuspid aortic valve disease has distinctive patterns and usually involves the transverse aortic arch. *The Journal of Thoracic and Cardiovascular Surgery*. 2008;135(4):901-907.e2. doi:10.1016/j.jtcvs.2008.01.022

136. Etz CD, Misfeld M, Borger MA, Luehr M, Strotdrees E, Mohr FW. Current Indications for Surgical Repair in Patients with Bicuspid Aortic Valve and Ascending Aortic Ectasia. *Cardiology Research and Practice*. 2012;2012:1-9. doi:10.1155/2012/313879

137. Siu SC, Silversides CK. Bicuspid Aortic Valve Disease. *Journal of the American College of Cardiology*. 2010;55(25):2789-2800. doi:10.1016/j.jacc.2009.12.068

138. Michelena HI, Desjardins VA, Avierinos JF, et al. Natural History of Asymptomatic Patients With Normally Functioning or Minimally Dysfunctional Bicuspid Aortic Valve in the Community. *Circulation*. 2008;117(21):2776-2784. doi:10.1161/CIRCULATIONAHA.107.740878

139. Etz CD, Zoli S, Brenner R, et al. When to Operate on the Bicuspid Valve Patient With a Modestly Dilated Ascending Aorta. *The Annals of Thoracic Surgery*. 2010;90(6):1884-1892. doi:10.1016/j.athoracsur.2010.06.115

140. Tzemos N. Outcomes in Adults With Bicuspid Aortic Valves. *JAMA*. 2008;300(11):1317. doi:10.1001/jama.300.11.1317

141. Borger MA, Preston M, Ivanov J, et al. Should the ascending aorta be replaced more frequently in patients with bicuspid aortic valve disease? *The Journal of Thoracic and Cardiovascular Surgery*. 2004;128(5):677-683. doi:10.1016/j.jtcvs.2004.07.009

142. Girdauskas E, Disha K, Borger MA, Kuntze T. Long-term prognosis of ascending aortic aneurysm after aortic valve replacement for bicuspid versus tricuspid aortic valve stenosis. *The Journal of Thoracic and Cardiovascular Surgery*. 2014;147(1):276-282. doi:10.1016/j.jtcvs.2012.11.004

143. Garg V, Muth AN, Ransom JF, et al. Mutations in NOTCH1 cause aortic valve disease. *Nature*. 2005;437(7056):270-274. doi:10.1038/nature03940

144. Fernández B, Durán AC, Fernández-Gallego T, et al. Bicuspid Aortic Valves With Different Spatial Orientations of the Leaflets Are Distinct Etiological Entities. *Journal of the American College of Cardiology*. 2009;54(24):2312-2318. doi:10.1016/j.jacc.2009.07.044

145. Loscalzo ML, Goh DL, Loeys B, Kent KC, Spevak PJ, Dietz HC. Familial thoracic aortic dilation and bicommissural aortic valve: A prospective analysis of natural history and inheritance. *Am J Med Genet*. 2007;143A(17):1960-1967. doi:10.1002/ajmg.a.31872

146. Bonow RO. Bicuspid Aortic Valves and Dilated Aortas: A Critical Review of the Critical Review of the ACC/AHA Practice Guidelines Recommendations. *The American Journal of Cardiology*. 2008;102(1):111-114. doi:10.1016/j.amjcard.2008.01.058

147. Girdauskas E, Borger MA, Secknus MA, Girdauskas G, Kuntze T. Is aortopathy in bicuspid aortic valve disease a congenital defect or a result of abnormal hemodynamics? A critical reappraisal of a one-sided argument. *European Journal of Cardio-Thoracic Surgery*. 2011;39(6):809-814. doi:10.1016/j.ejcts.2011.01.001

148. Hope MD, Meadows AK, Hope TA, et al. Evaluation of Bicuspid Aortic Valve and Aortic Coarctation With 4D Flow Magnetic Resonance Imaging. *Circulation*. 2008;117(21):2818-2819. doi:10.1161/CIRCULATIONAHA.107.760124

149. Cotrufo M, Corte AD, De Santo LS, et al. Different patterns of extracellular matrix protein expression in the convexity and the concavity of the dilated aorta with bicuspid aortic valve: Preliminary results. *The Journal of Thoracic and Cardiovascular Surgery*. 2005;130(2):504.e1-504.e9. doi:10.1016/j.jtcvs.2005.01.016

150. Holmes KW, Lehmann CU, Dalal D, et al. Progressive Dilation of the Ascending Aorta in Children With Isolated Bicuspid Aortic Valve. *The American Journal of Cardiology*. 2007;99(7):978-983. doi:10.1016/j.amjcard.2006.10.065

151. Nistri S, Sorbo MD, Marin M, Palisi M, Scognamiglio R, Thiene G. Aortic root dilatation in young men with normally functioning bicuspid aortic valves. *Heart*. 1999;82(1):19-22. doi:10.1136/hrt.82.1.19

152. Sabet HY, Edwards WD, Tazelaar HD, Daly RC. Congenitally Bicuspid Aortic Valves: A Surgical Pathology Study of 542 Cases (1991 Through 1996) and a Literature Review of 2,715 Additional Cases. *Mayo Clinic Proceedings*. 1999;74(1):14-26. doi:10.4065/74.1.14

153. Yuan SM. Quadricuspid Aortic Valve: A Comprehensive Review. *Brazilian Journal of Cardiovascular Surgery*. Published online 2016. doi:10.5935/1678-9741.20160090

154. Tsang MYC, Abudiab MM, Ammash NM, et al. Quadricuspid Aortic Valve: Characteristics, Associated Structural Cardiovascular Abnormalities, and Clinical Outcomes. *Circulation*. 2016;133(3):312-319. doi:10.1161/CIRCULATIONAHA.115.017743

155. Olson LJ, Subramanian R, Edwards WD. Surgical Pathology of Pure Aortic Insufficiency: A Study of 225 Gases. *Mayo Clinic Proceedings*. 1984;59(11-12):835-841. doi:10.1016/S0025-6196(12)65618-3

156. Pirundini PA, Balaguer JM, Lilly KJ, et al. Replacement of the Quadricuspid Aortic Valve: Strategy to Avoid Complete Heart Block. *The Annals of Thoracic Surgery*. 2006;81(6):2306-2308. doi:10.1016/j.athoracsur.2005.08.022

157. Malviya A, Jha PK, Ashwin, Mishra J, Srivastava P, Mishra A. Quadricuspid aortic valve – A case report and literature review. *The Egyptian Heart Journal*. 2016;68(4):271-275. doi:10.1016/j.ehj.2015.09.003

158. Savino K, Quintavalle E, Ambrosio G. Quadricuspid aortic valve: A case report and review of the literature. *J Cardiovasc Echography*. 2015;25(3):72. doi:10.4103/2211-4122.166077

159. Attaran RR, Habibzadeh MR, Baweja G, Slepian MJ. Quadricuspid aortic valve with ascending aortic aneurysm: report of a case and discussion of embryological mechanisms. *Cardiovascular Pathology*. 2009;18(1):49-52. doi:10.1016/j.carpath.2007.07.012

160. Hurwitz LE, Roberts WC. Quadricuspid semilunar valve. *The American Journal of Cardiology*. 1973;31(5):623-626. doi:10.1016/0002-9149(73)90332-9

161. Jagannath AD, Johri AM, Liberthson R, et al. Quadricuspid Aortic Valve: A Report of 12 Cases and a Review of the Literature: Quadricuspid Aortic Valve. *Echocardiography*. 2011;28(9):1035-1040. doi:10.1111/j.1540-8175.2011.01477.x

162. Nakamura Y, Taniguchi I, Saiki munehiro, Morimoto K, Yamaga T. Quadricuspid aortic valve associated with aortic stenosis and regurgitation. *Jpn J Thorac Cardiovasc Surg*. 2001;49(12):714-716. doi:10.1007/BF02913511

163. Godefroid O, Colles P, Vercauteren S, Louagie Y, Marchandise B. Quadricuspid aortic valve: A rare etiology of aortic regurgitation. *European Journal of Echocardiography*. 2006;7(2):168-170. doi:10.1016/j.euje.2005.03.011

164. Bauer F, Litzler P, Tabley A, Cribier A, Bessou J. Endocarditis complicating a congenital quadricuspid aortic valve. *European Journal of Echocardiography*. Published online February 21, 2007:S1525216706002769. doi:10.1016/j.euje.2006.12.001

165. Chow SCY, Wong RHL, Underwood MJ. Acute Aortic Syndrome. In: *New Approaches to Aortic Diseases from Valve to Abdominal Bifurcation*. Elsevier; 2018:479-489. doi:10.1016/B978-0-12-809979-7.00044-4

166. Pacini D, Di Marco L, Fortuna D, et al. Acute aortic dissection: Epidemiology and outcomes. *International Journal of Cardiology*. 2013;167(6):2806-2812. doi:10.1016/j.ijcard.2012.07.008

167. Nienaber CA, Clough RE, Sakalihasan N, et al. Aortic dissection. *Nat Rev Dis Primers*. 2016;2(1):16053. doi:10.1038/nrdp.2016.53

168. Lindholt JS, Juul S, Fasting H, Henneberg EW. Hospital Costs and Benefits of Screening for Abdominal Aortic Aneurysms. Results from a Randomised Population Screening Trial. *European Journal of Vascular and Endovascular Surgery*. 2002;23(1):55-60. doi:10.1053/ejvs.2001.1534

169. Mészáros I, Mórocz J, Szlávi J, et al. Epidemiology and Clinicopathology of Aortic Dissection. *Chest*. 2000;117(5):1271-1278. doi:10.1378/chest.117.5.1271

170. Rogers AM, Hermann LK, Booher AM, et al. Sensitivity of the Aortic Dissection Detection Risk Score, a Novel Guideline-Based Tool for Identification of Acute Aortic Dissection at Initial Presentation: Results From the International Registry of Acute Aortic Dissection. *Circulation*. 2011;123(20):2213-2218. doi:10.1161/CIRCULATIONAHA.110.988568

171. Nienaber CA, Fattori R, Mehta RH, et al. Gender-Related Differences in Acute Aortic Dissection. *Circulation*. 2004;109(24):3014-3021. doi:10.1161/01.CIR.0000130644.78677.2C

172. Braverman AC. Aortic dissection: Prompt diagnosis and emergency treatment are critical. *CCJM*. 2011;78(10):685-696. doi:10.3949/ccjm.78a.11053

173. Prêtre R, Von Segesser LK. Aortic dissection. *The Lancet*. 1997;349(9063):1461-1464. doi:10.1016/S0140-6736(96)09372-5

174. Homma S, Ishii T, Tsugane S, Hirose N. Different effects of hypertension and hypercholesterolemia on the natural history of aortic atherosclerosis by the stage of intimal lesions. *Atherosclerosis*. 1997;128(1):85-95. doi:10.1016/S0021-9150(96)05970-9

175. Giannakoulas G, Giannoglou G, Soulis J, et al. A computational model to predict aortic wall stresses in patients with systolic arterial hypertension. *Medical Hypotheses*. 2005;65(6):1191-1195. doi:10.1016/j.mehy.2005.06.017

176. De Bakey ME, Henly WS, Cooley DA, Morris GC, Crawford ES, Beall AC. SURGICAL MANAGEMENT OF DISSECTING ANEURYSMS OF THE AORTA. *The Journal of Thoracic and Cardiovascular Surgery*. 1965;49(1):130-149. doi:10.1016/S0022-5223(19)33323-9

177. Daily PO, Trueblood HW, Stinson EB, Wuerflein RD, Shumway NE. Management of acute aortic dissections. *Ann Thorac Surg*. 1970;10(3):237-247. doi:10.1016/s0003-4975(10)65594-4

178. Lempel JK, Frazier AA, Jeudy J, et al. Aortic Arch Dissection: A Controversy of Classification. *Radiology*. 2014;271(3):848-855. doi:10.1148/radiol.14131457

179. Karapanagiotidis GT, Antonitsis P, Charokopos N, et al. Serum levels of matrix metalloproteinases -1,-2,-3 and -9 in thoracic aortic diseases and acute myocardial ischemia. *J Cardiothorac Surg*. 2009;4(1):59. doi:10.1186/1749-8090-4-59

180. Golledge J, Eagle KA. Acute aortic dissection. *The Lancet*. 2008;372(9632):55-66. doi:10.1016/S0140-6736(08)60994-0

181. Sheikh AS, Ali K, Mazhar S. Acute Aortic Syndrome. *Circulation*. 2013;128(10):1122-1127. doi:10.1161/CIRCULATIONAHA.112.000170

182. Song C, Yu G, Feng X, et al. Impact of high blood pressure variability on the occurrence of acute type B aortic dissection. *Vascular*. 2020;28(4):413-420. doi:10.1177/1708538120902630

183. Zhang L, Tian W, Feng R, et al. Prognostic Impact of Blood Pressure Variability on Aortic Dissection Patients After Endovascular Therapy. *Medicine*. 2015;94(38):e1591. doi:10.1097/MD.0000000000001591

184. Alomari IB, Hamirani YS, Madera G, Tabe C, Akhtar N, Raizada V. Aortic Intramural Hematoma and Its Complications. *Circulation*. 2014;129(6):711-716. doi:10.1161/CIRCULATIONAHA.113.001809

185. Immer FF, Bansi AG, Immer-Bansi AS, et al. Aortic dissection in pregnancy: analysis of risk factors and outcome. *The Annals of Thoracic Surgery*. 2003;76(1):309-314. doi:10.1016/S0003-4975(03)00169-3

186. Yuan SM, Jing H. Cystic medial necrosis: pathological findings and clinical implications. *Rev Bras Cir Cardiovasc*. 2011;26(1):107-115. doi:10.1590/S0102-76382011000100019

187. Mussa FF, Horton JD, Moridzadeh R, Nicholson J, Trimarchi S, Eagle KA. Acute Aortic Dissection and Intramural Hematoma: A Systematic Review. *JAMA*. 2016;316(7):754. doi:10.1001/jama.2016.10026

188. Iskandrian AE, Garcia EV, eds. *Atlas of Nuclear Cardiology: Imaging Companion to Braunwald' s Heart Disease*. Elsevier, Saunders; 2012.

189. Nienaber CA, Eagle KA. Aortic Dissection: New Frontiers in Diagnosis and Management: Part II: Therapeutic Management and Follow-Up. *Circulation*. 2003;108(6):772-778. doi:10.1161/01.CIR.0000087400.48663.19

190. JCS Joint Working Group. Guidelines for Diagnosis and Treatment of Aortic Aneurysm and Aortic Dissection (JCS 2011): – Digest Version –. *Circ J*. 2013;77(3):789-828. doi:10.1253/circj.CJ-66-0057

191. Roy CS. The Elastic Properties of the Arterial Wall. *The Journal of Physiology*. 1881;3(2):125-159. doi:10.1113/jphysiol.1881.sp000088

192. Liu M, Liang L, Sulejmani F, et al. Identification of in vivo nonlinear anisotropic mechanical properties of ascending thoracic aortic aneurysm from patient-specific CT scans. *Sci Rep*. 2019;9(1):12983. doi:10.1038/s41598-019-49438-w

193. Carew TE, Vaishnav RN, Patel DJ. Compressibility of the Arterial Wall. *Circulation Research*. 1968;23(1):61-68. doi:10.1161/01.RES.23.1.61

194. Holzapfel GA, Gasser TC, Ogden RW. A New Constitutive Framework for Arterial Wall Mechanics and a Comparative Study of Material Models. *Journal of Elasticity*. 2000;61(1/3):1-48. doi:10.1023/A:1010835316564

195. Fung YC. What are the residual stresses doing in our blood vessels? *Ann Biomed Eng*. 1991;19(3):237-249. doi:10.1007/BF02584301

196. Azeloglu EU, Albro MB, Thimmappa VA, Ateshian GA, Costa KD. Heterogeneous transmural proteoglycan distribution provides a mechanism for regulating residual stresses in the aorta. *American Journal of Physiology-Heart and Circulatory Physiology*. 2008;294(3):H1197-H1205. doi:10.1152/ajpheart.01027.2007

197. Mohan D, Melvin JW. Failure properties of passive human aortic tissue. I—Uniaxial tension tests. *Journal of Biomechanics*. 1982;15(11):887-902. doi:10.1016/0021-9290(82)90055-0

198. Li WC, Yu MH, Zhang HM, et al. Biomechanical properties of ascending aorta and pulmonary trunk in pigs and humans. *Xenotransplantation*. 2008;15(6):384-389. doi:10.1111/j.1399-3089.2008.00498.x

199. Vera L, Muylle S, Van Steenkiste G, et al. Histological and biomechanical properties of systemic arteries in young and old Warmblood horses. Vogel J, ed. *PLoS ONE*. 2021;16(7):e0253730. doi:10.1371/journal.pone.0253730

200. Saey V, Famaey N, Smoljkic M, et al. Biomechanical and biochemical properties of the thoracic aorta in warmblood horses, Friesian horses, and Friesians with aortic rupture. *BMC Vet Res*. 2015;11(1):285. doi:10.1186/s12917-015-0597-0

201. Han W qing, Chen J, Wu L yun, Zhu D liang, Gao P jin. Different biomechanical properties of medial and adventitial layers of thoracic aorta in Wistar-Kyoto and spontaneously hypertensive rats. *Acta Pharmacol Sin*. 2010;31(10):1319-1323. doi:10.1038/aps.2010.121

202. Gamero LG, Armentano RL, Barra JG, Simon A, Levenson J. Identification of Arterial Wall Dynamics in Conscious Dogs. *Experimental Physiology*. 2001;86(4):519-528. doi:10.1113/eph8602172

203. de Gelidi S, Tozzi G, Bucchi A. The Role of Pre-Conditioning Frequency in the Experimental Characterization of Hyper-Elastic Materials as Models for Soft Tissue Applications. *Int J Appl Mechanics*. 2016;08(05):1650066. doi:10.1142/S1758825116500666

204. Raghavan ML, Webster MW, Vorp DA. Ex vivo biomechanical behavior of abdominal aortic aneurysm: Assessment using a new mathematical model. *Ann Biomed Eng*. 1996;24(5):573-582. doi:10.1007/BF02684226

205. Okamoto RJ, Wagenseil JE, DeLong WR, Peterson SJ, Kouchoukos NT, Sundt, III TM. Mechanical Properties of Dilated Human Ascending Aorta. *Annals of Biomedical Engineering*. 2002;30(5):624-635. doi:10.1114/1.1484220

206. García-Herrera CM, Atienza JM, Rojo FJ, et al. Mechanical behaviour and rupture of normal and pathological human ascending aortic wall. *Med Biol Eng Comput*. 2012;50(6):559-566. doi:10.1007/s11517-012-0876-x

207. Khanafer K, Schlicht MS, Berguer R. How Should We Measure and Report Elasticity in Aortic Tissue? *European Journal of Vascular and Endovascular Surgery*. 2013;45(4):332-339. doi:10.1016/j.ejvs.2012.12.015

208. Forsell C, Björck HM, Eriksson P, Franco-Cereceda A, Gasser TC. Biomechanical Properties of the Thoracic Aneurysmal Wall: Differences Between Bicuspid Aortic Valve and Tricuspid Aortic Valve Patients. *The Annals of Thoracic Surgery*. 2014;98(1):65-71. doi:10.1016/j.athoracsur.2014.04.042

209. Ferrara A, Totaro P, Morganti S, Auricchio F. Effects of clinico-pathological risk factors on in-vitro mechanical properties of human dilated ascending aorta. *Journal of the Mechanical Behavior of Biomedical Materials*. 2018;77:1-11. doi:10.1016/j.jmbbm.2017.08.032

210. Sherifova S, Sommer G, Viertler C, et al. Failure properties and microstructure of healthy and aneurysmatic human thoracic aortas subjected to uniaxial extension with a focus on the media. *Acta Biomaterialia*. 2019;99:443-456. doi:10.1016/j.actbio.2019.08.038

211. Amabili M, Asgari M, Breslavsky ID, Franchini G, Giovanniello F, Holzapfel GA. MICROSTRUCTURAL AND MECHANICAL CHARACTERIZATION OF THE LAYERS OF HUMAN DESCENDING THORACIC AORTAS. *Acta Biomaterialia*. Published online July 2021:S1742706121004748. doi:10.1016/j.actbio.2021.07.036

212. Ferrara A, Morganti S, Totaro P, Mazzola A, Auricchio F. Human dilated ascending aorta: Mechanical characterization via uniaxial tensile tests. *Journal of the Mechanical Behavior of Biomedical Materials*. 2016;53:257-271. doi:10.1016/j.jmbbm.2015.08.021

213. Sherifova S, Holzapfel GA. Biomechanics of aortic wall failure with a focus on dissection and aneurysm: A review. *Acta Biomaterialia*. 2019;99:1-17. doi:10.1016/j.actbio.2019.08.017

214. Lim H, Hoag SW. Plasticizer Effects on Physical–Mechanical Properties of Solvent Cast Soluplus® Films. *AAPS PharmSciTech*. 2013;14(3):903-910. doi:10.1208/s12249-013-9971-z

215. Seibert H, Scheffer T, Diebels S. Biaxial Testing of Elastomers - Experimental Setup, Measurement and Experimental Optimisation of Specimen's Shape. *Technische Mechanik; 34; 2; 72-89; ISSN 2199-9244*. Published online 2014:2,26 MB. doi:10.24352/UB.OVGU-2017-054

216. Deplano V, Boufi M, Boiron O, Guivier-Curien C, Alimi Y, Bertrand E. Biaxial tensile tests of the porcine ascending aorta. *Journal of Biomechanics*. 2016;49(10):2031-2037. doi:10.1016/j.jbiomech.2016.05.005

217. Nicosia MA, Kasalko JS, Cochran RP, Einstein DR, Kunzelman KS. Biaxial mechanical properties of porcine ascending aortic wall tissue. *J Heart Valve Dis*. 2002;11(5):680-686; discussion 686-687.

218. Tremblay D, Cartier R, Mongrain R, Leask RL. Regional dependency of the vascular smooth muscle cell contribution to the mechanical properties of the pig ascending aortic tissue. *Journal of Biomechanics*. 2010;43(12):2448-2451. doi:10.1016/j.jbiomech.2010.04.018

219. Vande Geest JP, Sacks MS, Vorp DA. The effects of aneurysm on the biaxial mechanical behavior of human abdominal aorta. *Journal of Biomechanics*. 2006;39(7):1324-1334. doi:10.1016/j.jbiomech.2005.03.003

220. Choudhury N, Bouchot O, Rouleau L, et al. Local mechanical and structural properties of healthy and diseased human ascending aorta tissue. *Cardiovascular Pathology*. 2009;18(2):83-91. doi:10.1016/j.carpath.2008.01.001

221. Haskett D, Johnson G, Zhou A, Utzinger U, Vande Geest J. Microstructural and biomechanical alterations of the human aorta as a function of age and location. *Biomech Model Mechanobiol*. 2010;9(6):725-736. doi:10.1007/s10237-010-0209-7

222. Azadani AN, Chitsaz S, Mannion A, et al. Biomechanical Properties of Human Ascending Thoracic Aortic Aneurysms. *The Annals of Thoracic Surgery*. 2013;96(1):50-58. doi:10.1016/j.athoracsur.2013.03.094

223. Azadani AN, Chitsaz S, Matthews PB, et al. Comparison of Mechanical Properties of Human Ascending Aorta and Aortic Sinuses. *The Annals of Thoracic Surgery*. 2012;93(1):87-94. doi:10.1016/j.athoracsur.2011.08.002

224. Pham T, Martin C, Elefteriades J, Sun W. Biomechanical characterization of ascending aortic aneurysm with concomitant bicuspid aortic valve and bovine aortic arch. *Acta Biomaterialia*. 2013;9(8):7927-7936. doi:10.1016/j.actbio.2013.04.021

225. Deplano V, Boufi M, Gariboldi V, et al. Mechanical characterisation of human ascending aorta dissection. *Journal of Biomechanics*. 2019;94:138-146. doi:10.1016/j.jbiomech.2019.07.028

226. Kim JH, Avril S, Duprey A, Favre JP. Experimental characterization of rupture in human aortic aneurysms using a full-field measurement technique. *Biomech Model Mechanobiol*. 2012;11(6):841-853. doi:10.1007/s10237-011-0356-5

227. Kim J, Baek S. Circumferential variations of mechanical behavior of the porcine thoracic aorta during the inflation test. *Journal of Biomechanics*. 2011;44(10):1941-1947. doi:10.1016/j.jbiomech.2011.04.022

228. Howard DPJ, Banerjee A, Fairhead JF, Handa A, Silver LE, Rothwell PM. Age-specific incidence, risk factors and outcome of acute abdominal aortic aneurysms in a defined population. *British Journal of Surgery*. 2015;102(8):907-915. doi:10.1002/bjs.9838

229. Martin C, Pham T, Sun W. Significant differences in the material properties between aged human and porcine aortic tissues. *European Journal of Cardio-Thoracic Surgery*. 2011;40(1):28-34. doi:10.1016/j.ejcts.2010.08.056

230. Caro-Bretelle AS, Gountsop PN, Ienny P, et al. Effect of sample preservation on stress softening and permanent set of porcine skin. *Journal of Biomechanics*. 2015;48(12):3135-3141. doi:10.1016/j.jbiomech.2015.07.014

231. Caro-Bretelle AS, Ienny P, Leger R, Corn S, Bazin I, Bretelle F. Constitutive modeling of stress softening and permanent set in a porcine skin tissue: Impact of the storage preservation. *Journal of Biomechanics*. 2016;49(13):2863-2869. doi:10.1016/j.jbiomech.2016.06.026

232. Spyder. Anaconda Inc.; 2020. https://docs.anaconda.com/

233. Van Rossum G, Drake FL. *Python 3 Reference Manual.* Scotts Valley, CA: CreateSpace; 2009.

234. Szczesny SE, Peloquin JM, Cortes DH, Kadlowec JA, Soslowsky LJ, Elliott DM. Biaxial Tensile Testing and Constitutive Modeling of Human Supraspinatus Tendon. *Journal of Biomechanical Engineering*. 2012;134(2):021004. doi:10.1115/1.4005852

235. Anssari-Benam A, Tseng YT, Holzapfel GA, Bucchi A. Rate-dependency of the mechanical behaviour of semilunar heart valves under biaxial deformation. *Acta Biomaterialia*. 2019;88:120-130. doi:10.1016/j.actbio.2019.02.008

236. Holmes MWR, Howarth SJ, Callaghan JP, Keir PJ. Biomechanical properties of the transverse carpal ligament under biaxial strain: BIOMECHANICAL PROPERTIES OF THE TCL. *J Orthop Res*. 2012;30(5):757-763. doi:10.1002/jor.21583

237. Lafrance H, Yahia L, Germain L, Guillot M, Auger FA. Study of the Tensile Properties of Living Skin Equivalents. *Bio-Medical Materials and Engineering*. 1995;5(4):195-208. doi:10.3233/BME-1995-5401

238. Schneider DC, Davidson TM, Nahum AM. In Vitro Biaxial Stress-Strain Response of Human Skin. *Archives of Otolaryngology - Head and Neck Surgery*. 1984;110(5):329-333. doi:10.1001/archotol.1984.00800310053012

239. Dabiri Y, Paulson K, Tyberg J, et al. Design of Bioprosthetic Aortic Valves using biaxial test data. In: *2015 37th Annual International Conference of the IEEE Engineering in Medicine and Biology Society (EMBC)*. IEEE; 2015:3319-3322. doi:10.1109/EMBC.2015.7319102

240. Murr LE. Frontiers of 3D Printing/Additive Manufacturing: from Human Organs to Aircraft Fabrication†. *Journal of Materials Science & Technology*. 2016;32(10):987-995. doi:10.1016/j.jmst.2016.08.011

241. Sames WJ, List FA, Pannala S, Dehoff RR, Babu SS. The metallurgy and processing science of metal additive manufacturing. *International Materials Reviews*. 2016;61(5):315-360. doi:10.1080/09506608.2015.1116649

242. Bedarf P, Dutto A, Zanini M, Dillenburger B. Foam 3D printing for construction: A review of applications, materials, and processes. *Automation in Construction*. 2021;130:103861. doi:10.1016/j.autcon.2021.103861

243. Shi D, Liu K, Zhang X, Liao H, Chen X. Applications of three-dimensional printing technology in the cardiovascular field. *Intern Emerg Med*. 2015;10(7):769-780. doi:10.1007/s11739-015-1282-9

244. Silva K, Rand S, Cancel D, Chen Y, Kathirithamby R, Stern M. Three-Dimensional (3-D) Printing: A Cost-Effective Solution for Improving Global Accessibility to Prostheses. *PM&R*. 2015;7(12):1312-1314. doi:10.1016/j.pmrj.2015.06.438

245. Dodziuk H. Applications of 3D printing in healthcare. *kitp*. 2016;3:283-293. doi:10.5114/kitp.2016.62625

246. Witek L, Tovar N. Trends in the 3D-Printing Parts for Medical and Dental Implant Technologies. In: *Reference Module in Materials Science and Materials Engineering*. Elsevier; 2021:B9780128203521001000. doi:10.1016/B978-0-12-820352-1.00092-4

247. Xu T, Shen W, Lin X, Xie YM. Mechanical Properties of Additively Manufactured Thermoplastic Polyurethane (TPU) Material Affected by Various Processing Parameters. *Polymers*. 2020;12(12):3010. doi:10.3390/polym12123010

248. Ho D, Squelch A, Sun Z. Modelling of aortic aneurysm and aortic dissection through 3D printing. *J Med Radiat Sci*. 2017;64(1):10-17. doi:10.1002/jmrs.212

249. Levin D, Mackensen GB, Reisman M, McCabe JM, Dvir D, Ripley B. 3D Printing Applications for Transcatheter Aortic Valve Replacement. *Curr Cardiol Rep*. 2020;22(4):23. doi:10.1007/s11886-020-1276-8

250. Anwar S, Singh GK, Miller J, et al. 3D Printing is a Transformative Technology in Congenital Heart Disease. *JACC: Basic to Translational Science*. 2018;3(2):294-312. doi:10.1016/j.jacbts.2017.10.003

251. Vranicar M, Gregory W, Douglas WI, Di Sessa P, Di Sessa TG. The use of stereolithographic hand held models for evaluation of congenital anomalies of the great arteries. *Stud Health Technol Inform*. 2008;132:538-543.

252. Schmauss D, Haeberle S, Hagl C, Sodian R. Three-dimensional printing in cardiac surgery and interventional cardiology: a single-centre experience. *European Journal of Cardio-Thoracic Surgery*. 2015;47(6):1044-1052. doi:10.1093/ejcts/ezu310

253. Kurenov SN, Ionita C, Sammons D, Demmy TL. Three-dimensional printing to facilitate anatomic study, device development, simulation, and planning in thoracic surgery. *The Journal of Thoracic and Cardiovascular Surgery*. 2015;149(4):973-979.e1. doi:10.1016/j.jtcvs.2014.12.059

254. Geisbüsch S, Kuehnl A, Salvermoser M, Reutersberg B, Trenner M, Eckstein HH. Editor's Choice – Hospital Incidence, Treatment, and In Hospital Mortality Following Open and Endovascular Surgery for Thoraco-abdominal Aortic Aneurysms in Germany from 2005 to 2014: Secondary Data Analysis of the Nationwide German DRG Microdata. *European Journal of Vascular and Endovascular Surgery*. 2019;57(4):488-498. doi:10.1016/j.ejvs.2018.10.030

255. Davies RR, Goldstein LJ, Coady MA, et al. Yearly rupture or dissection rates for thoracic aortic aneurysms: simple prediction based on size. *The Annals of Thoracic Surgery*. 2002;73(1):17-28. doi:10.1016/S0003-4975(01)03236-2

256. Isselbacher EM. Thoracic and Abdominal Aortic Aneurysms. *Circulation*. 2005;111(6):816-828. doi:10.1161/01.CIR.0000154569.08857.7A

257. Kent KC, Zwolak RM, Egorova NN, et al. Analysis of risk factors for abdominal aortic aneurysm in a cohort of more than 3 million individuals. *Journal of Vascular Surgery*. 2010;52(3):539-548. doi:10.1016/j.jvs.2010.05.090

258. Bugan B, Cekirdekci EI, Cekirdekci A. Is the size criterion for surgery decision of ascending aortic aneurysm changed? Left shift of the aortic diameter. *The Journal of Thoracic and Cardiovascular Surgery*. 2020;159(1):e19-e20. doi:10.1016/j.jtcvs.2019.05.054

259. Schoenhoff FS, Carrel T. Commentary: Decision making in thoracic aortic surgery: One size fits all? *The Journal of Thoracic and Cardiovascular Surgery*. 2019;157(5):1748-1749. doi:10.1016/j.jtcvs.2018.09.104

260. Papakonstantinou NA, Rorris FP. Elective replacement of the ascending aorta: is the 5.5-cm threshold appropriate? The insidious, small aorta. *European Journal of Cardio-Thoracic Surgery*. 2021;59(3):554-561. doi:10.1093/ejcts/ezaa387

261. Raaz U, Zöllner AM, Schellinger IN, et al. Segmental Aortic Stiffening Contributes to Experimental Abdominal Aortic Aneurysm Development. *Circulation*. 2015;131(20):1783-1795. doi:10.1161/CIRCULATIONAHA.114.012377

262. Ito S, Akutsu K, Tamori Y, et al. Differences in Atherosclerotic Profiles Between Patients With Thoracic and Abdominal Aortic Aneurysms. *The American Journal of Cardiology*. 2008;101(5):696-699. doi:10.1016/j.amjcard.2007.10.039

263. Toghill BJ, Saratzis A, Bown MJ. Abdominal aortic aneurysm—an independent disease to atherosclerosis? *Cardiovascular Pathology*. 2017;27:71-75. doi:10.1016/j.carpath.2017.01.008

264. Sigaeva T, Polzer S, Vitásek R, Di Martino ES. Effect of testing conditions on the mechanical response of aortic tissues from planar biaxial experiments: Loading protocol and specimen side. *Journal of the Mechanical Behavior of Biomedical Materials*. 2020;111:103882. doi:10.1016/j.jmbbm.2020.103882

265. Stata. *Stata Statistical Software: Release 15*. StataCorp, LLC; 2017.

266. Brown H. *Applied Mixed Models in Medicine.* Wiley; 2015. Accessed September 30, 2021. http://www.myilibrary.com?id=683342

267. Mickey RM, Greenland S. The impact of confounder selection criteria on effect estimation. *American Journal of Epidemiology*. 1989;129(1):125-137. doi:10.1093/oxfordjournals.aje.a115101

268. Vach W. *Regression Models as a Tool in Medical Research*. CRC Press; 2013.

269. Harrell FE. *Regression Modeling Strategies: With Applications to Linear Models, Logistic and Ordinal Regression, and Survival Analysis*. 2nd edition. Springer; 2015.

270. Liu CY, Chen D, Bluemke DA, et al. Evolution of Aortic Wall Thickness and Stiffness With Atherosclerosis: Long-Term Follow Up From the Multi-Ethnic Study of Atherosclerosis. *Hypertension*. 2015;65(5):1015-1019. doi:10.1161/HYPERTENSIONAHA.114.05080

271. Mensel B, Kühn JP, Schneider T, Quadrat A, Hegenscheid K. Mean Thoracic Aortic Wall Thickness Determination by Cine MRI with Steady-State Free Precession. *Academic Radiology*. 2013;20(8):1004-1008. doi:10.1016/j.acra.2013.03.014

272. Van Puyvelde J, Verbeken E, Verbrugghe P, Herijgers P, Meuris B. Aortic wall thickness in patients with ascending aortic aneurysm versus acute aortic dissection. *Eur J Cardiothorac Surg*. 2016;49(3):756-762. doi:10.1093/ejcts/ezv197

273. Pignoli P, Tremoli E, Poli A, Oreste P, Paoletti R. Intimal plus medial thickness of the arterial wall: a direct measurement with ultrasound imaging. *Circulation*. 1986;74(6):1399-1406. doi:10.1161/01.CIR.74.6.1399

274. Kamenskiy AV, Dzenis YA, Kazmi SAJ, et al. Biaxial mechanical properties of the human thoracic and abdominal aorta, common carotid, subclavian, renal and common iliac arteries. *Biomech Model Mechanobiol*. 2014;13(6):1341-1359. doi:10.1007/s10237-014-0576-6

275. Labrosse MR, Beller CJ, Mesana T, Veinot JP. Mechanical behavior of human aortas: Experiments, material constants and 3-D finite element modeling including residual stress. *Journal of Biomechanics*. 2009;42(8):996-1004. doi:10.1016/j.jbiomech.2009.02.009

276. Taghizadeh H, Tafazzoli-Shadpour M, Shadmehr M, Fatouraee N. Evaluation of Biaxial Mechanical Properties of Aortic Media Based on the Lamellar Microstructure. *Materials*. 2015;8(1):302-316. doi:10.3390/ma8010302

277. Matsumoto T, Fukui T, Tanaka T, et al. Biaxial Tensile Properties of Thoracic Aortic Aneurysm Tissues. *JBSE*. 2009;4(4):518-529. doi:10.1299/jbse.4.518

278. Hosoda Y, Kawano K, Yamasawa F, Ishii T, Shibata T, Inayama S. Age-Dependent Changes of Collagen and Elastin Content in Human Aorta and Pulmonary Artery. *Angiology*. 1984;35(10):615-621. doi:10.1177/000331978403501001

279. Fritze O, Romero B, Schleicher M, et al. Age-Related Changes in the Elastic Tissue of the Human Aorta. *J Vasc Res*. 2012;49(1):77-86. doi:10.1159/000331278

280. Lakatta EG. Arterial and Cardiac Aging: Major Shareholders in Cardiovascular Disease Enterprises: Part III: Cellular and Molecular Clues to Heart and Arterial Aging. *Circulation*. 2003;107(3):490-497. doi:10.1161/01.CIR.0000048894.99865.02

281. Schlatmann TJM, Becker AE. Histologic changes in the normal aging aorta: Implications for dissecting aortic aneurysm. *The American Journal of Cardiology*. 1977;39(1):13-20. doi:10.1016/S0002-9149(77)80004-0

282. Groenink M. The influence of aging and aortic stiffness on permanent dilation and breaking stress of the thoracic descending aorta. *Cardiovascular Research*. 1999;43(2):471-480. doi:10.1016/S0008-6363(99)00095-4

283. Qiu H, Depre C, Ghosh K, et al. Mechanism of Gender-Specific Differences in Aortic Stiffness With Aging in Nonhuman Primates. *Circulation*. 2007;116(6):669-676. doi:10.1161/CIRCULATIONAHA.107.689208

284. Gomes VC, Fernando da Silva L, Zyngier SP, et al. Left Common Carotid Artery Biomechanical Properties in Individuals over 80 years: Women Have Stiffer Vessels. *Annals of Vascular Surgery*. 2020;67:461-467. doi:10.1016/j.avsg.2020.01.107

285. Wanga S, Hibender S, Ridwan Y, et al. Aortic microcalcification is associated with elastin fragmentation in Marfan syndrome: Microcalcification and elastin fragmentation in Marfan syndrome. *J Pathol*. 2017;243(3):294-306. doi:10.1002/path.4949

286. Szabo Z. Aortic aneurysmal disease and cutis laxa caused by defects in the elastin gene. *Journal of Medical Genetics*. 2005;43(3):255-258. doi:10.1136/jmg.2005.034157

287. Chung J, Lachapelle K, Wener E, et al. Energy loss, a novel biomechanical parameter, correlates with aortic aneurysm size and histopathologic findings. *The Journal of Thoracic and Cardiovascular Surgery*. 2014;148(3):1082-1089. doi:10.1016/j.jtcvs.2014.06.021

288. Allison MA, Kwan K, DiTomasso D, Wright CM, Criqui MH. The epidemiology of abdominal aortic diameter. *Journal of Vascular Surgery*. 2008;48(1):121-127. doi:10.1016/j.jvs.2008.02.031

289. Aune D, Schlesinger S, Norat T, Riboli E. Tobacco smoking and the risk of abdominal aortic aneurysm: a systematic review and meta-analysis of prospective studies. *Sci Rep*. 2018;8(1):14786. doi:10.1038/s41598-018-32100-2

290. Boodhwani M, de Kerchove L, Glineur D, et al. Repair-oriented classification of aortic insufficiency: Impact on surgical techniques and clinical outcomes. *The Journal of Thoracic and Cardiovascular Surgery*. 2009;137(2):286-294. doi:10.1016/j.jtcvs.2008.08.054

291. Ho SY. Structure and anatomy of the aortic root. *European Journal of Echocardiography*. 2009;10(1):i3-i10. doi:10.1093/ejechocard/jen243

292. Cosentino F, Giuseppe MD, Agnese V, et al. On the severity of aortic stenosis in ascending aortic aneurysm: A computational tool to examine ventricular-arterial interaction and aortic wall stress. *Mechanics Research Communications*. 2020;110:103621. doi:10.1016/j.mechrescom.2020.103621

293. Campobasso R, Condemi F, Viallon M, Croisille P, Campisi S, Avril S. Evaluation of Peak Wall Stress in an Ascending Thoracic Aortic Aneurysm Using FSI Simulations: Effects of Aortic Stiffness and Peripheral Resistance. *Cardiovasc Eng Tech*. 2018;9(4):707-722. doi:10.1007/s13239-018-00385-z

294. Wilton E, Jahangiri M. Post-stenotic aortic dilatation. *J Cardiothorac Surg*. 2006;1(1):7. doi:10.1186/1749-8090-1-7

295. Borger MA, Fedak PWM, Stephens EH, et al. The American Association for Thoracic Surgery consensus guidelines on bicuspid aortic valve–related aortopathy: Full online-only version. *The Journal of Thoracic and Cardiovascular Surgery*. 2018;156(2):e41-e74. doi:10.1016/j.jtcvs.2018.02.115

296. Forsell C, Björck HM, Eriksson P, Franco-Cereceda A, Gasser TC. Biomechanical Properties of the Thoracic Aneurysmal Wall: Differences Between Bicuspid Aortic Valve and Tricuspid Aortic Valve Patients. *The Annals of Thoracic Surgery*. 2014;98(1):65-71. doi:10.1016/j.athoracsur.2014.04.042

297. Chung JC -Y., Wong E, Tang M, et al. Biomechanics of Aortic Dissection: A Comparison of Aortas Associated With Bicuspid and Tricuspid Aortic Valves. *JAHA*. Published online July 28, 2020. doi:10.1161/JAHA.120.016715

298. Shim CY, Cho IJ, Yang WI, et al. Central Aortic Stiffness and Its Association with Ascending Aorta Dilation in Subjects with a Bicuspid Aortic Valve. *Journal of the American Society of Echocardiography*. 2011;24(8):847-852. doi:10.1016/j.echo.2011.04.017

299. Sode BF, Nordestgaard BG, Grønbæk M, Dahl M. Tobacco smoking and aortic aneurysm: Two population-based studies. *International Journal of Cardiology*. 2013;167(5):2271-2277. doi:10.1016/j.ijcard.2012.06.003

300. Verma S, Siu SC. Aortic Dilatation in Patients with Bicuspid Aortic Valve. *N Engl J Med*. 2014;370(20):1920-1929. doi:10.1056/NEJMra1207059

301. Attaran RR, Habibzadeh MR, Baweja G, Slepian MJ. Quadricuspid aortic valve with ascending aortic aneurysm: report of a case and discussion of embryological mechanisms. *Cardiovascular Pathology*. 2009;18(1):49-52. doi:10.1016/j.carpath.2007.07.012

302. Naito K, Ohteki H, Yunoki J, Hisajima K, Sato H, Narita Y. Aortic valve repair for quadricuspid aortic valve associated with aortic regurgitation and ascending aortic aneurysm. *The Journal of Thoracic and Cardiovascular Surgery*. 2004;128(5):759-760. doi:10.1016/j.jtcvs.2004.03.038

303. Bankhead P, Loughrey MB, Fernández JA, et al. QuPath: Open source software for digital pathology image analysis. *Sci Rep*. 2017;7(1):16878. doi:10.1038/s41598-017-17204-5

304. Bersi MR, Bellini C, Humphrey JD, Avril S. Local variations in material and structural properties characterize murine thoracic aortic aneurysm mechanics. *Biomech Model Mechanobiol*. 2019;18(1):203-218. doi:10.1007/s10237-018-1077-9

305. Shahmansouri N, Alreshidan M, Emmott A, et al. Investigation on the Regional Loss Factor and Its Anisotropy for Aortic Aneurysms. *Materials*. 2016;9(11):867. doi:10.3390/ma9110867

306. Tsamis A, Krawiec JT, Vorp DA. Elastin and collagen fibre microstructure of the human aorta in ageing and disease: a review. *Journal of The Royal Society Interface*. 2013;10(83):20121004. doi:10.1098/rsif.2012.1004

307. Evangelista A, Isselbacher EM, Bossone E, et al. Insights From the International Registry of Acute Aortic Dissection: A 20-Year Experience of Collaborative Clinical Research. *Circulation*. 2018;137(17):1846-1860. doi:10.1161/CIRCULATIONAHA.117.031264

308. Guo D chuan, Regalado ES, Gong L, et al. LOX Mutations Predispose to Thoracic Aortic Aneurysms and Dissections. *Circ Res*. 2016;118(6):928-934. doi:10.1161/CIRCRESAHA.115.307130

309. Lee VS, Halabi CM, Hoffman EP, et al. Loss of function mutation in *LOX* causes thoracic aortic aneurysm and dissection in humans. *Proc Natl Acad Sci USA*. 2016;113(31):8759-8764. doi:10.1073/pnas.1601442113

310. Renard M, Francis C, Ghosh R, et al. Clinical Validity of Genes for Heritable Thoracic Aortic Aneurysm and Dissection. *Journal of the American College of Cardiology*. 2018;72(6):605-615. doi:10.1016/j.jacc.2018.04.089

311. Jondeau G, Ropers J, Regalado E, et al. International Registry of Patients Carrying TGFBR1 or TGFBR2 Mutations: Results of the MAC (Montalcino Aortic Consortium). *Circ Cardiovasc Genet*. 2016;9(6):548-558. doi:10.1161/CIRCGENETICS.116.001485

312. Januzzi JL, Isselbacher EM, Fattori R, et al. Characterizing the young patient with aortic dissection: results from the international registry of aortic dissection (IRAD). *Journal of the American College of Cardiology*. 2004;43(4):665-669. doi:10.1016/j.jacc.2003.08.054

313. David Levy, Amandeep Goyal, Yulia Grigorova, Fabiola Farci, Jacqueline K. Le. *Aortic Dissection*. StatPearls; 2021. https://www-ncbi-nlm-nih-gov/books/NBK441963/

314. Di Achille P, Tellides G, Humphrey JD. Hemodynamics-driven deposition of intraluminal thrombus in abdominal aortic aneurysms. *Int J Numer Meth Biomed Engng*. 2017;33(5). doi:10.1002/cnm.2828

315. Menichini C, Cheng Z, Gibbs RGJ, Xu XY. A computational model for false lumen thrombosis in type B aortic dissection following thoracic endovascular repair. *Journal of Biomechanics*. 2018;66:36-43. doi:10.1016/j.jbiomech.2017.10.029

316. Menichini C, Cheng Z, Gibbs RGJ, Xu XY. Predicting false lumen thrombosis in patient-specific models of aortic dissection. *J R Soc Interface*. 2016;13(124):20160759. doi:10.1098/rsif.2016.0759

317. Karmonik C, Partovi S, Müller-Eschner M, et al. Longitudinal computational fluid dynamics study of aneurysmal dilatation in a chronic DeBakey type III aortic dissection. *Journal of Vascular Surgery*. 2012;56(1):260-263.e1. doi:10.1016/j.jvs.2012.02.064

318. Long Ko JK, Liu RW, Ma D, Shi L, Ho Yu SC, Wang D. Pulsatile hemodynamics in patient-specific thoracic aortic dissection models constructed from computed tomography angiography. Wong KKL, Fong S, Wang D, eds. *XST*. 2017;25(2):233-245. doi:10.3233/XST-17256

319. Manopoulos C, Karathanasis I, Kouerinis I, et al. Identification of regional/layer differences in failure properties and thickness as important biomechanical factors responsible for the initiation of aortic dissections. *Journal of Biomechanics*. 2018;80:102-110. doi:10.1016/j.jbiomech.2018.08.024

320. Fanari Z, Hammami S, Hammami MB, Hammami S, Eze-Nliam C, Weintraub WS. Using The Descending Aortic Wall Thickness Measured In Transesophageal Echocardiography As A Risk Marker For Aortic Dissection. *Eur J Cardiovasc Med*. 2015;3(1):448-451. doi:10.5083/ejcm.20424884.136

321. Sokolis DP, Kritharis EP, Iliopoulos DC. Effect of layer heterogeneity on the biomechanical properties of ascending thoracic aortic aneurysms. *Med Biol Eng Comput*. 2012;50(12):1227-1237. doi:10.1007/s11517-012-0949-x

322. Pasta S, Phillippi JA, Gleason TG, Vorp DA. Effect of aneurysm on the mechanical dissection properties of the human ascending thoracic aorta. *The Journal of Thoracic and Cardiovascular Surgery*. 2012;143(2):460-467. doi:10.1016/j.jtcvs.2011.07.058

323. Bäck M, Gasser TC, Michel JB, Caligiuri G. Biomechanical factors in the biology of aortic wall and aortic valve diseases. *Cardiovascular Research*. 2013;99(2):232-241. doi:10.1093/cvr/cvt040

324. Doyle JM, Dobrin PB. Finite deformation analysis of the relaxed and contracted dog carotid artery. *Microvascular Research*. 1971;3(4):400-415. doi:10.1016/0026-2862(71)90042-2

325. Ploch CC, Mansi CSSA, Jayamohan J, Kuhl E. Using 3D Printing to Create Personalized Brain Models for Neurosurgical Training and Preoperative Planning. *World Neurosurgery*. 2016;90:668-674. doi:10.1016/j.wneu.2016.02.081

326. Hochman JB, Rhodes C, Wong D, Kraut J, Pisa J, Unger B. Comparison of cadaveric and isomorphic three-dimensional printed models in temporal bone education. *The Laryngoscope*. 2015;125(10):2353-2357. doi:10.1002/lary.24919

327. Ogden KM, Aslan C, Ordway N, Diallo D, Tillapaugh-Fay G, Soman P. Factors Affecting Dimensional Accuracy of 3-D Printed Anatomical Structures Derived from CT Data. *J Digit Imaging*. 2015;28(6):654-663. doi:10.1007/s10278-015-9803-7

328. Matsumoto JS, Morris JM, Foley TA, et al. Factors Affecting Dimensional Accuracy of 3-D Printed Anatomical Structures Derived from CT Data. *RadioGraphics*. 2015;35(7):1989-2006. doi:10.1148/rg.2015140260

329. Friedman T, Michalski M, Goodman TR, Brown JE. Factors Affecting Dimensional Accuracy of 3-D Printed Anatomical Structures Derived from CT Data. *Skeletal Radiol*. 2016;45(3):307-321. doi:10.1007/s00256-015-2282-6

330. Negi S, Dhiman S, Kumar Sharma R. Basics and applications of rapid prototyping medical models. *Rapid Prototyping Journal*. 2014;20(3):256-267. doi:10.1108/RPJ-07-2012-0065

331. Brantner P, Madaffari A, Fahrni G, Zellweger MJ, Haaf P. 3D-Printed Visualization of a Complex Coronary-Venous Fistula With Additional Feeders From the Descending Aorta. *JACC: Case Reports*. 2020;2(11):1736-1738. doi:10.1016/j.jaccas.2020.06.028

332. Santoro G, Pizzuto A, Rizza A, et al. Transcatheter Treatment of "Complex" Aortic Coarctation Guided by Printed 3D Model. *JACC: Case Reports*. 2021;3(6):900-904. doi:10.1016/j.jaccas.2021.04.036

333. Kim WK, Kim T, Lee S, et al. 3D-Printing-Based Open Repair of Extensive Thoracoabdominal Aorta in Severe Scoliosis. *Seminars in Thoracic and Cardiovascular Surgery*. 2019;31(1):61-63. doi:10.1053/j.semtcvs.2018.09.017

334. Ooms JF, Wang DD, Rajani R, et al. Computed Tomography–Derived 3D Modeling to Guide Sizing and Planning of Transcatheter Mitral Valve Interventions. *JACC: Cardiovascular Imaging*. 2021;14(8):1644-1658. doi:10.1016/j.jcmg.2020.12.034

335. Vukicevic M, Puperi DS, Grande-Allen KJ, Little SH. Erratum to: 3D Printed Modeling of the Mitral Valve for Catheter-Based Structural Interventions. *Ann Biomed Eng*. 2016;44(11):3432-3432. doi:10.1007/s10439-016-1690-7

336. Wang K, Wu C, Qian Z, Zhang C, Wang B, Vannan MA. Dual-material 3D printed metamaterials with tunable mechanical properties for patient-specific tissue-mimicking phantoms. *Additive Manufacturing*. 2016;12:31-37. doi:10.1016/j.addma.2016.06.006

337. Biglino G, Verschueren P, Zegels R, Taylor AM, Schievano S. Rapid prototyping compliant arterial phantoms for in-vitro studies and device testing. *J Cardiovasc Magn Reson*. 2013;15(1):2. doi:10.1186/1532-429X-15-2

338. Yushkevich PA, Pashchinskiy A, Oguz I, et al. User-Guided Segmentation of Multi-modality Medical Imaging Datasets with ITK-SNAP. *Neuroinform*. 2019;17(1):83-102. doi:10.1007/s12021-018-9385-x

339. Hess, R. *Blender Foundations: The Essential Guide to Learning Blender 2.6.* Focal Press.; 2010. http://www.blender.org